Characterization of Hydraulic Properties in Fractured Aquifers Using Slug Test-based Hydraulic Tomography and Thermal Tracer Tomography

Dissertation

for the award of the degree
„Doctor rerum naturalium“ (Dr.rer.nat.)
of the Georg-August-Universität Göttingen

within the doctoral program Geoscience
of the Georg-August University School of Science (GAUSS)

submitted by

Quan Liu

from Hubei, China

Göttingen, 2022

Thesis Committee

Prof. Dr. Thomas Ptak-Fix

Department of Applied Geology, Georg-August-Universität Göttingen

Prof. Dr. Rui Hu

School of Earth Sciences and Engineering, Hohai University

Members of the Examination Board

Reviewer: Prof. Dr. Thomas Ptak-Fix

Department of Applied Geology, Georg-August-Universität Göttingen

Second reviewer: Prof. Dr. Rui Hu

School of Earth Sciences and Engineering, Hohai University

Further members of the Examination Board

Prof. Dr. Peter Bayer

Department of Applied Geology, Martin Luther University of Halle-Wittenberg (MLU)

Prof. Dr. Ekkehard Holzbecher

Department of Earth Sciences, German University of Technology in Oman (GUtech)

Dr. Jannes Kordilla

Department of Applied Geology, Georg-August-Universität Göttingen

Dr. Linwei Hu

Department of Geoscience, Christian-Albrechts-Universität zu Kiel (CAU)

Date of the oral examination: 05 September, 2022

Link: http://dx.doi.org/10.53846/goediss-9495

Abstract

Fractured aquifers are widely distributed on the earth's surface and are frequently encountered in many underground projects, such as groundwater resource evaluation, contaminants remediation, and geothermal energy exploration. Hydraulic properties such as fracture locations, fracture permeability, and hydraulic connectivity, generally play essential roles in these projects, which dominate the fluid flow, solute migration, and heat transport processes in fractured aquifers. Compared to porous media, these processes in fractured aquifers are more complicated due to the complex fracture geometry, highly hydraulic contrast between fractures and rock matrix, and complex hydraulic connectivity. Characterizing hydraulic properties of fractured aquifers is therefore quite challenging. Over the past decades, numerous studies have been devoted to the development of the relevant theory, testing techniques, modeling methods, and characterization methods at laboratory and field scales. In this thesis, the purpose is to characterize the hydraulic properties of fractured aquifers at field scales by using slug test-based hydraulic tomography (HTs) and thermal tracer tomography (TT). These two tomographic methods are firstly modified considering the features of the fractured aquifer, validated in synthetic cases, and further applied in a fractured rock experimental site located at Göttingen, Germany.

For the HTs method, wellbore effects including inertial effects and wellbore storage can have considerable impacts on slug test responses, especially in deep wells or highly permeable fractured aquifers. To take into account wellbore effects and even the possible skin effects, a three-dimensional forward slug test model (3DHIM) was first developed, considering the inertial effects in a heterogeneous aquifer. Groundwater flow in the wellbore is described by the Navier-Stokes equation and coupled with the Darcian flow in the heterogeneous aquifer by using some specific boundary conditions on the screen interface. To trace the water level movement in the wellbore, a moving boundary defined by the arbitrary Lagrangian-Eulerian method is assigned. After verified by some analytical methods, the proposed slug test model is applied to simulate a series of multilevel cross-well slug tests in a highly heterogeneous aquifer analogue to investigate the influence of wellbore effects on slug test responses. Results indicate that the influence of wellbore effects on hydraulic travel time can be linearly related to the water column height, and the influence on the head attenuation in the observation well is not obvious.

To accurately characterize the hydraulic parameters, the influence of wellbore effects on slug test responses needs to be removed, otherwise, estimation errors will be introduced. Therefore, two correction methods with respect to the hydraulic travel time and head attenuation in the test well are then proposed. Hydraulic travel time delay caused by wellbore effects is assumed to be linear with the water column length, and head attenuation in test well caused by wellbore effects can be analytically derived by the measured water level

of test well. These methods are then verified by successfully reconstructing the hydraulic parameters (i.e., hydraulic diffusivity and specific storage) of an aquifer analogue using the travel time inversion and attenuation inversion.

Thermal tracer tomography equipped with distributed temperature sensing (DTS) has been shown to improve the accuracy and resolution in characterizing hydraulic properties of porous media. To apply this method in fractured aquifers, some modifications to the TT inversion framework are made considering the hydraulic properties of fractured aquifers. Considering the spatially sparse temperature response induced by the complex fracture geometry and highly hydraulic contrast between fractures and rock matrix, a regularization term and an irregular triangular mesh are introduced. Regarding the possible annular wall flow at an observation well, a specific well zone in the inversion model is assigned to eliminate the distortion of thermal travel times. The performance of the modified TT inversion framework in characterizing hydraulic properties of fractured aquifers was firstly tested through numerical experiments. Features of fractured aquifers, such as different hydraulic connectivity patterns, highly hydraulic contrast between fracture and rock matrix, and some practical issues were investigated. Inversion results indicate that the TT method can efficiently identify directly connected or interconnected fractures, even with the presence of some practical issues.

The HTs and TT methods were finally applied at the fractured rock experimental site to investigate the hydraulic properties. A total of 96 cross-well slug tests and 96 cross-well thermal tracer tests were conducted. Using the HTs and TT inversion methods, both results revealed three connected fractures at depths about 19 m, 28 m, and 35 m. By combining the results revealed by the two tomographic methods, the uncertainty and non-uniqueness issues of the single inversion method are reduced. By comparing these two tomographic methods, results indicate that the TT method can provide a more accurate and higher-resolution characterization of high-conductive fractures due to the DTS device, and the HTs method based on the fast hydraulic diffusion process can offer more hydraulic information about the medium-k fractures and rock matrix. Both of the proposed inversion frameworks are proved to be efficient and robust and show broad application prospects in the hydraulic characterization of fractured aquifers.

Acknowledgements

I would like to express my deepest gratitude to my principal supervisor Prof. Dr.-Ing. Thomas Ptak. Not only his rigor in academics but also his persistence in scientific research have deeply admired me. At each group meeting, he cared about the details of my research and always gave me constructive guidance and advice. He encouraged me to boldly stick to my ideas and meanwhile guided me in scientific thinking, which benefits me a lot. Pleasant study in Göttingen was inseparable from the caring supervision of my supervisor Prof. Dr. Rui Hu. Unphased by geographical and temporal separation, he was always truly supportive and provided a lot of help both in my studies and in my life. His enthusiasm both on the football pitch or in every academic discussion will continue to inspire me. Further, I would like to extend my thanks to the committee members, Prof. Dr. Peter Bayer, Prof. Dr. Ekkehard Holzbecher, Dr. Jannes Kordilla, and Dr. Linwei Hu, for their careful and constructive reviews and for taking time out of their busy schedules to attend my defense.

I am also thankful to collaborators in field experiments. I gratefully acknowledge Steffen Fischer for his tireless work throughout my experiments and provided me with excellent equipment and technical assistance, especially during the pandemic. Thanks should also go to Dr. Pengxiang Qiu, Huichen Yang, Ran Tao, Junjie Qi, and Mingyuan Wang. Without their support, the fieldwork would not be possible. I am also thankful to Dr. Linwei Hu for her creative ideas on the development of methodology and Prof. Honggbiao Gu as well for fruitful contributions to our discussions. And many thanks to Dr. Bernd Leiss, who taught me a lot about the geological background at our research site.

I am grateful to all my friends and colleagues at the Department of Applied Geology. Among many, I am thankful to Dr. Graciela Sosa, Mrs. Ines Ringel, and Mrs. Heckeroth, for their kindly help whenever I needed it. I am also grateful to Prof. Dr. Martin Sauter, Dr. Chicgoua Noubactep, Dr. Shigorina Elena, and Maria Pinheiro, for their constructive discussions on my research. Special thanks go to my friends Dr. Taherdangkoo Reza, Dr. Huhao Gao, and Dr. Dejian Zhou.

Last but not least, my deepest thanks go to my Family, my parents, and all the teachers I have met throughout my study. I could not be more grateful to my wife Yixuan, she has been a great comfort to me on countless days and nights when I struggled in my research. Words are powerless to express my love to them.

Finally, I specially dedicate my thanks to Prof. Thomas Ptak again for the financial support by offering research assistant contract.

Contents

1

Introduction

Contents

This chapter firstly introduces the motivation and scope of this thesis. After reviewing the common methods for characterizing the hydraulic properties of fractured aquifers, the slug test-based hydraulic tomography and thermal tracer tomography are reviewed. Finally, the objectives and structure of this thesis are outlined. The aim of this introduction is to give a basic background for the individual papers comprised in this cumulative thesis.

1.1 Motivation and scope

Fractured aquifers are widely distributed on the earth's surface, to be precise, about 75% of the surface area of continents is composed of fractured or karstic fractured aquifers (Dietrich et al., 2005). With the increase in engineering, geotechnical, and hydrogeological practice, fractured aquifers are frequently encountered and extensively discussed. Fractures that act as hydraulic conductors in low-permeability rocks can form preferential flow paths for fluid flow, solute migration, and heat transfer. Due to the complex fracture geometry, highly hydraulic contrast between fractures and rock matrix, and complex hydraulic connectivity, flow and transport in fractured aquifers are much more complicated than those in porous media and thus require more attention. As shown in Figure 1.1, fractures can exert evident influences both on the resource supply (e.g. petroleum, gas, and water), on environment safety (e.g. contamination remediation, nuclear waste disposal, and CO_2 sequestration), and on the production of geothermal energy (e.g. aquifer thermal energy storage (ATES), ground source heat pump (GSHP), and enhanced geothermal system (EGS)). Therefore, the characterization of fractured rock, especially the hydraulic properties of fractures, has gained increasing interest and has been motivated by the aforementioned projects over the past few decades.

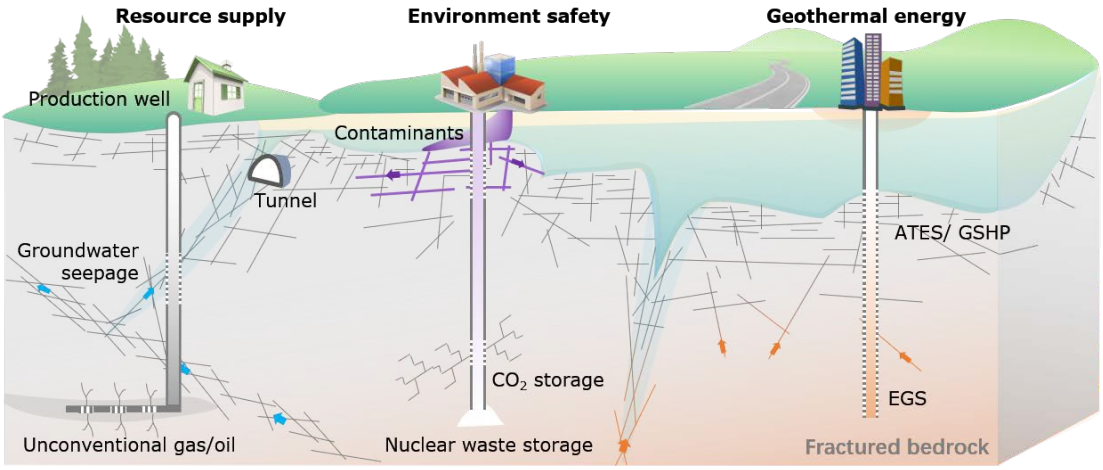

Figure 1.1: Sketch of underground projects for resource supply, environment safety, and geothermal energy exploration, which can be impacted by fractured bedrock aquifers.

In nature, fractures exist over a broad range of scales, from the scale of rock grains to the scale of tectonic plates, in response to different types of stress (National Research Council, 1996). Recent studies on the characterization of hydraulic properties of fractures mainly focus on two types of scales, the field scale and core/bench scale (Day-Lewis et al., 2017). A range of practical problems in the projects listed above is normally field-scale. In practice, addressing filed-scale problems is often expensive incurred by drilling and sampling, and investigation results are usually uncertain due to many uncontrollable conditions. By contrast, core/bench-scale experiments can perform under fully controlled conditions and can economically provide the basic knowledge of characterization methods and modeling approaches from individual fractures to

overall sample properties. Figure 1.2 illustrates the characterization methods of hydraulic properties at the two different scales and their main purposes. At the core/bench scale, fracture geometry can be directly measured by magnetic resonance imaging or resin casting methods, the hydraulic parameters of all fractures will receive full attention through the use of some flow/transport tests with complicated arrangements. However, only hydraulically dominant and connective fractures can play crucial roles in engineering practices. At the field scale, the characterization methods, like the hydrogeological tests or geophysical survey, are thus be majorly focused on the identification of fracture locations and hydraulic parameters of hydraulically dominant fractures in order to meet engineering needs. But the current understanding of fluid flow and solute transport in large-scale fracture sites needs to be further improved, due to the geometrical complexity of the natural fractured system. To sum up, one can benefit from the obtained knowledge at a core/bench-scale for the characterization of fractured aquifers at large scales. Although much work has been done to study the relationship between core/bench-scale experimental results and the practical field-scale problems, further validation and improvement at field scales are still necessary due to the possible difference in approach and purpose.

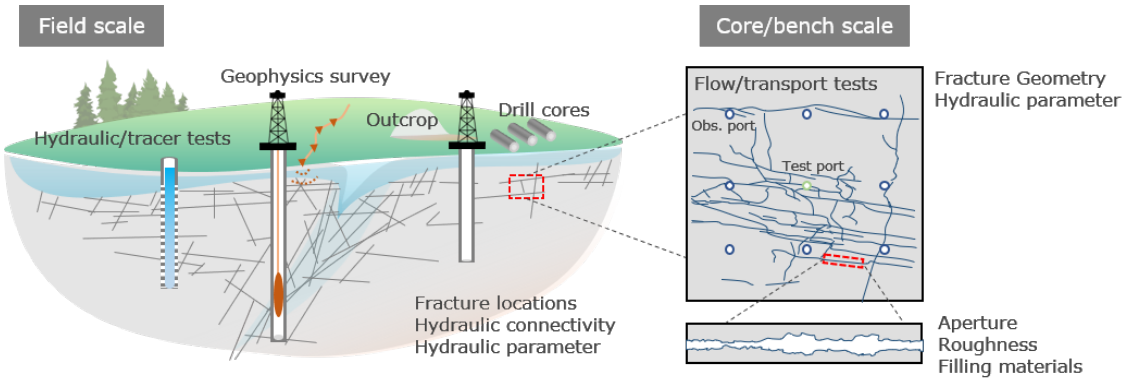

Figure 1.2: Methods for characterizing the hydraulic properties of fractured media at the field and core/bench scales and their main purposes (not to scale).

In this thesis, the scope is to characterize the hydraulic properties of fractured aquifers at field scales, including fracture locations, cross-well hydraulic connectivity, and hydraulic parameters. Hydraulic properties of the rock mass are also taken into account due to potential impacts on hydraulic diffusion and heat transfer when using temperature as a tracer. The investigation of hydraulic properties in vadose zones is beyond the scope of this study. Also, the coupling between fluid pressure and rock stress is not covered.

1.2 Hydraulic characterization methods

Characterizing the hydraulic properties of fractured aquifers at a field scale is probably one of the most challenging problems that hydrogeologists and petroleum geologists have to face. Numerous studies have

been devoted to this field in the past decades (Illman, 2014; Le Borgne et al., 2006; Maréchal et al., 2004; Tsoflias et al., 2001). Typically, fracture system formed by a large number of interconnected fractures has a very complex geometry, and only conductive fractures that may account for a small proportion of total fractures, are conduits for fluid flow. The identification and location of such conductive fractures is thus a fundamental step in hydraulic characterization of fractured aquifers. Also, hydraulic parameters of fractures usually exhibit strong heterogeneity, which is controlled by the fracture aperture, filling materials, and stress. In order to quantitatively estimate flow and transport behavior in the fracture system, characterizing hydraulic parameters such as permeability and hydraulic diffusivity, as well as cross-well connectivity is crucial. Methods on how conductive fractures can be identified, located, and characterized are reviewed in the following.

1.2.1 Conventional methods

Geophysical methods

Characterization of hydraulic properties by geophysical methods is achieved by detecting fracture locations and their physical properties. In geophysics, fractures can be considered as zones of anomalous physical properties and detected remotely by various means. According to the different detection scales of target sites, geophysical methods can be majorly divided into three types (National Research Council, 1996). The first is the large-scale method associated with surface soundings, including seismic reflection, electrical and electromagnetic methods (Brodic et al., 2017; Munoz, 2014; Schmelzbach et al., 2007). The second type is the intermediate scale method associated with cross-hole soundings, such as cross-hole transmission tomography. Compared to surface surveys, cross-hole methods typically employ compact sensors to observe the response to disturbances in the test borehole, and can therefore have a better ability to spatially resolve the locations of fractures. Over the past decades, cross-hole seismic tomography and ground-penetrating radar (GPR) tomography have been intensively studied and widely used to map fracture zones with high resolution (Doetsch et al., 2020; Dorn et al., 2012; Ellefsen et al., 2002; Grasmueck, 1996; Robinson et al., 2016) The third type is the small-scale method associated with measurements made adjacent to a borehole. All single-bole methods can be classified into this type, for instance, the core inspection and conventional well logs. These methods can straightforwardly observe in-situ fracture attributes along the borehole, including fracture locations, orientations, and densities, and even allow for extrapolating the fracture geometry to some extent based on statistical fracture information (Massiot et al., 2017). Compared to borehole imaging methods and other geophysical logs, flowmeter logging can additionally provide high-resolution information about connections between fractures and larger-scale groundwater flow systems. Many studies on the theory and testing techniques of flow logging have been reported over the past decades (Basiricò et al., 2015; Díaz-Curiel et al., 2022; Lo et al., 2014; Pehme et al., 2007).

Although geophysical methods can characterize fractures at multiple scales, the focus is mainly on fracture identification and the characterization of physical properties. The relationship bridging the physical properties and hydraulic properties can be influenced by many factors, such as infillings and stress, which limits application prospects. Some studies have pointed out that it is quite challenging to quantitatively characterize the hydraulic parameters and connectivity of fractures merely using geophysical observations, especially for complex mineral-filled fracture systems (Somogyvári & Bayer, 2017; Zha et al., 2015). Therefore, some integrated methods combining the geophysical data with additional measurements are popularly developed in recent years (Castagna et al., 2011; Chen et al., 2006; Commer et al., 2020; Day-Lewis et al., 2006), for instance, the combined interpretation of the hydraulic properties using GPR, hydraulic, and tracer data.

Hydraulic and tracer testing

Hydraulic and tracer tests are field methods that can directly estimate the hydraulic parameters of fractured aquifers. They are generally implemented by artificially inducing perturbations into the subsurface and measuring the resulting responses. Hydraulic and tracer tests can be combined with packer systems when testing specific fractures, such as those detected by geophysical logs. An advantage of using a packer system is that it allows testing to focus only on the more permeable portions of the borehole. To investigate fracture connectivity and hydraulic heterogeneity in complex fractured aquifers, hydraulic and tracer tests can be also performed between multiple boreholes and combined with multi-packer systems. Quinn et al. (2015) obtained high-resolution estimates of fracture location and hydraulic conductivity by the synergistic use of liner profiling and packer testing.

To extract hydraulic properties from the measurements during pumping tests or slug tests., a number of fractured aquifer models were developed over the past decades (Audouin & Bodin, 2008; Le Borgne et al., 2004; Moench, 1984). Some models were developed for taking into account wellbore effects and skin effects, which can have significant influences on parameter estimation when testing low-permeability rocks or significant changes that occur in permeability of the borehole wall as a result of drilling. However, many common models assume that the tested fractured aquifer can be approximated as an isotropic homogeneous porous medium. Especially for slug tests, few models can account for highly heterogeneous fractured media. This shortcoming limits the application of conventional hydraulic tests in characterizing the hydraulic properties of fractured aquifers to a certain extent.

Tracer tests are primarily used to explore the hydraulic connectivity and transport properties in fractured aquifers. When the advection process is dominated during testing, hydraulic properties of fractured media can be approximately estimated by the observation data. Among the commonly used tracers, thermal tracer

is naturally present within the groundwater, can be easily measured, and with less disturbance to the environment (Bodvarsson, 1969; Keys & Brown, 1978; Michalski & Klepp, 1990). In recent years, using heat as a tracer to characterize the hydraulic properties of fractured aquifers has become increasingly popular (Coleman et al., 2015; Maldaner et al., 2019; Read et al., 2013). Particularly, the application of distributed temperature sensing system (DTS) greatly improves the temperature measurement efficiency and its resolution in time and space, thereby improving the ability to identify fractures.. Read et al. (2014) improved the identification and characterization of the conductive fractures by recording heat movement and rate of heat dissipation using the active-DTS device. At present, most studies regarding thermal tracer tests mainly focus on the single-well scale. Although complex testing settings at large scales are developed, like a cross-hole and multilevel arrangement, the development of corresponding inversion procedures to interpret test data was relatively delayed.

1.2.2 Hydraulic tomography

Compared to conventional characterization methods, hydraulic tomography (HT) is a method for characterizing aquifer heterogeneity whereby the spatial distribution of hydraulic parameters (e.g. hydraulic conductivity k, specific storage S_s, etc.) can be estimated by the inversion of head responses from cross-well multilevel pumping tests or slug tests. For fractured aquifers, the hydraulic properties of fractures can be identified and characterized according to the inverted high k and low S_s zones (National Research Council, 1996). Recently, Tiedeman and Barrash (2020) performed a hydraulic tomography in a fractured mudstone site, and characterized hydraulic properties of the fracture network according to the estimated 3D hydraulic conductivity distribution. Ringel et al. (2021) characterized the geometric and hydraulic parameters of a 3D discrete fracture network using the HT method.

Hydraulic tomography consists of two basic processes, i.e. field testing and parameter estimation, as demonstrated in Figure 1.3. In the field testing process, pumping test and slug test are the two traditional ways to stimulate hydraulic interference in the subsurface. Compared to the pumping test, slug test-based HT method for fractured aquifers was rarely reported so far. The reason, on the one hand, could be that the modeling research on slug tests is relatively lagging behind. On the other hand, it is due to the influence of wellbore effects that complicate the interpretation of slug test responses, especially in deep wells or in highly permeable fractured aquifers. Although the slug test-based hydraulic tomography is currently not widely applied, it is still worth promoting it due to the unique advantages of slug tests. For instance, a slug test has considerable logistic and economic advantages, especially for testing at contaminated sites, and it can resolve a higher degree of aquifer heterogeneity due to its small sampling scale (i.e., the tested volume of the subsurface). For the parameter estimation process, many inversion methods regarding pumping-test responses have been developed, such as the sequential successive linear estimator (SSLE), quasi-linear

geostatistical approach, Kalman filter approach, trajectory-based travel time approach, etc. (Brauchler et al., 2003; Cardiff et al., 2013; Fienen et al., 2008; Schöniger et al., 2012; Zhu & Yeh, 2005). Different from the other imaging approaches, trajectory-based travel time inversion only utilizes the travel time characteristics instead of the entire hydraulic signal. It implies that the travel time inversion is not only faster in computation than other imaging approaches, but also much less time-consuming in field testing (travel time in a minute even in seconds, which leads to much less time in head recovery and greatly enhances the repeatability of the tests. Additionally, the inversion problem for travel times is quasi-linear, its solution can be much less sensitive to the initial model compared to non-linear inversion problems, such as the full-wave inversion (Vasco et al., 2019).

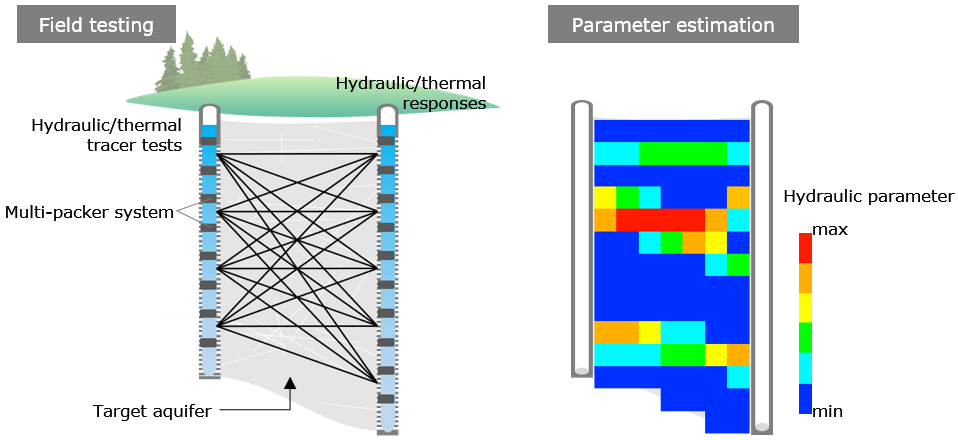

Figure 1.3: Sketch of the basic implementation processes of hydraulic tomography and thermal tracer tomography, taking 2D testing as an example (not to scale).

1.2.3 Thermal tracer tomography

Thermal tracer tomography (TT) is another method for characterizing aquifer heterogeneity based on thermal signals (Figure 1.3). It combines a series of thermal tracer tests arranged in a tomographic manner with imaging methods, and it has been extensively promoted over the past few years (Doro et al., 2015; Schwede et al., 2014; Somogyvári & Bayer, 2017; Somogyvári et al., 2016; Wagner et al., 2014). In order to investigate aquifer heterogeneity in the field, Doro et al. (2015) improved the field-scale experimental design for thermal tracer tomography. Somogyvári and Bayer (2017) successfully estimated hydraulic conductivity profiles in alluvial sediments using travel time-based thermal tracer tomography.

To date, thermal tracer tomography has primarily been applied in porous media (Lee et al., 2018; Ringel et al., 2019; Schwede et al., 2014; Somogyvári et al., 2016; Somogyvári et al., 2019). However, given the advantages of conventional thermal tracer tests in fracture identification introduced in Section 1.2.1, e.g. easy to measure and high-resolution measurements when equipped with the DTS, thermal tracer tomography should have a broad prospect in characterizing the geometric and hydraulic parameters of fractured aquifers.

Once combining the TT method with the DTS device, the high-resolution temperature data can greatly improve the capability in capturing the potential conductive fractures and reduce the uncertainty of the inversion results (Maldaner et al., 2019; Pehme et al., 2010). Therefore, a study to extend thermal tracer tomography to fractured aquifers is quite necessary.

1.3 Objectives and structure

The cutting-edge underground engineering projects put forward higher requirements for the characterization accuracy and resolution of fractured aquifers. Benefiting from the development of inversion algorithms, testing techniques, and equipment over the past few decades, hydraulic tomography and thermal tomography offer the possibility to fulfill these higher requirements. With logistic and economic advantages of slug test, hydraulic tomography based on slug test responses gains increasing attention. Although the two tomography methods have been well-established in porous media, their validation and application in fractured aquifers are not straightforward. In detail, this thesis addresses the following main questions:

1. *How to consider the influence of wellbore effects when using slug test-based hydraulic tomography to characterize the hydraulic properties of fractured aquifers, and how to improve the characterization accuracy?*

   Slug tests have some special advantages in characterizing the hydraulic heterogeneity of fractured aquifers. However, the influence of wellbore effects on slug test responses can be significant when testing in deep wells or in highly permeable fractured aquifers. To apply the slug test-based hydraulic tomography in field investigations, a fundamental step is to study the influence of wellbore effects on slug test responses in a highly heterogeneous media through numerical modeling, which has been rarely reported before. In the field testing, the influence of wellbore effects is also collected by the measured slug test responses, which needs to be excluded. Otherwise, estimation errors will be introduced during the hydraulic tomography inversion process.

2. *Can thermal tracer tomography be applied in fractured aquifers to characterize their hydraulic properties, and how to improve the characterization resolution?*

   Compared to porous media, heat transfer in fractured aquifers is more complicated due to the complex fracture geometry, highly hydraulic contrast between fractures and rock matrix, and

complex hydraulic connectivity. Thermal tracer tomography, originally developed for porous media, should be modified to take into account the hydraulic characteristics of fractures and needs to be validated before it applies to field investigations. To improve the characterization resolution, DTS has been widely used in field tests. To interpret the measured high-resolution data by the DTS, a robust and efficient inversion method is required. Additionally, the influence of some practical issues on the characterization results also needs to be investigated.

3. *How well do these two tomography methods perform in characterizing the hydraulic properties of fractured aquifers at field scales?*

   These two tomography methods have certain differences in physical process and testing technology. Compared to heat transfer processes of TT methods, hydraulic diffusion processes can spread much faster and are relatively less sensitive to low permeability rock mass. In contrast, with the DTS, the temperature measurements have higher resolution and measurement efficiency than hydraulic head observations. The above differences may have evident impacts on the inversion results.

If these questions are addressed, slug test-based hydraulic tomography and thermal tracer tomography hold a better promise for the field-scale characterization of the hydraulic properties of fractured aquifers. Hereby, this study attempts to provide some new insights into the application of these two methods in the hydraulic characterization of fractured media through numerical modeling, synthetic studies, and field tests. This thesis is structured according to the three questions outlined above:

Chapter 2 details the fractured experimental site in Göttingen, including the well arrangement, testing device, geological background, previous work, and the area selected to investigate in the following studies. In order to verify the feasibility of the slug test-based hydraulic tomography for highly heterogeneous aquifers, a heterogeneous slug test model considering wellbore effects is developed. The modeling methodology and the influences of aquifer heterogeneity and wellbore effects on slug test responses are introduced in Chapter 3. According to this numerical study, a method for removing the impacts of wellbore effects from the observed slug test responses is further proposed in Chapter 4. And combined with travel time inversion and attenuation inversion, a highly heterogeneous aquifer analogue is well reconstructed and the hydraulic properties of the fractured experimental site are investigated.

Considering the features of the fractured aquifer and some practical issues, some modifications are made to the original thermal tracer tomography. In order to improve the characterization resolution, DTS is employed in thermal tracer tomography. Chapter 5 illustrates the performance of this modified method in a synthetic fractured aquifer, and enables a high-resolution characterization of the hydraulic properties of the Göttingen site using the modified thermal tracer tomography.

In Chapter 6 the performance of the two tomographic methods is compared based on the results tested at the Göttingen site with respect to their theories, test configurations, and inversion results. Finally, a summary of conclusions and outlook of this whole study are given in Chapter 7. Supplementary information for site conditions, forward numerical modeling approaches, parameter settings, inversion results, and field test data can be found in the Appendices.

2

Fractured experimental site in Göttingen

Contents

This chapter introduces the basic information about the fractured experimental site and summarizes the relevant previous studies. Previous tests provide a preliminary understanding of geological and hydrogeological conditions at this site. Considering the testing devices and hydrogeological background, an investigation area between well M, O, and S above 40 m was finally selected.

2.1 Site description

2.1.1 Location and well arrangement

A fractured experimental site located at the north campus of the University of Göttingen, Germany, is selected and investigated in this study. As shown in Figure 2.1, this site settles several hundred meters west of the Geoscience Center of the University of Göttingen (GZG, Universität Göttingen). Five groundwater wells (well M, O, S, N, and W) with depth of 80 m are installed. The well W was first drilled in 2007 to study the usage of shallow geothermal energy. As an extension research, the other four wells with the same structure and depth as well W were built up from June 2012 to July 2013. The five wells form a spatially-splayed experimental site in a cross-shaped arrangement, which provides an ideal condition to study the hydraulic properties between the wells. The horizontal distance on the ground from the middle well M to the others is 3 m, except that to the well O, which is 1.9 m. The borehole vertical deviations of the wells M, O, and S were measured and displayed in Appendix A1.

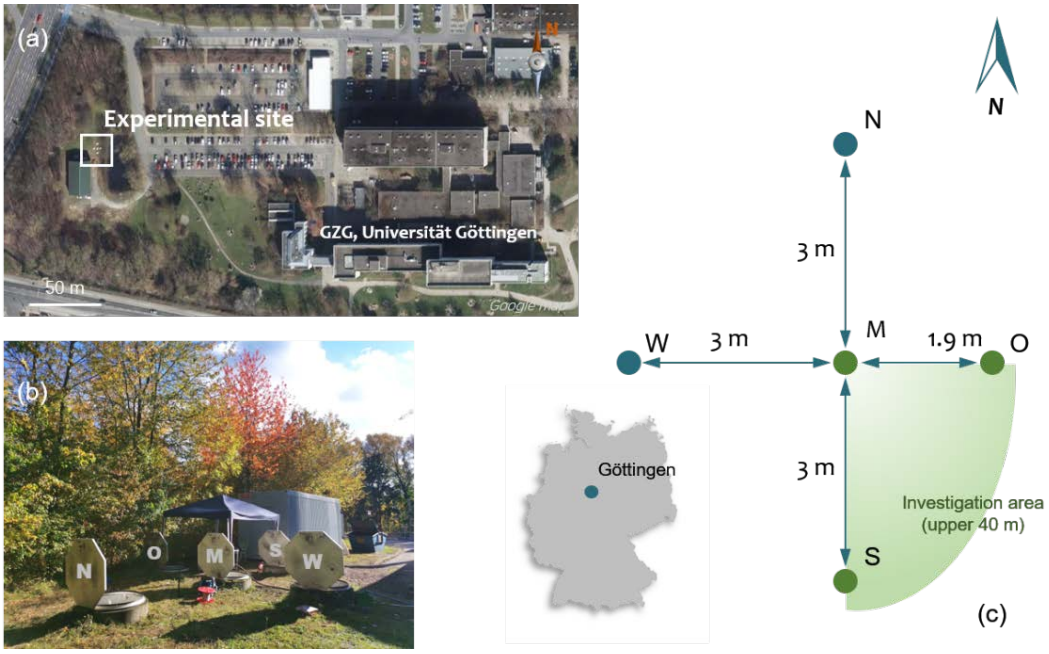

Figure 2.1: Site location (left top), the field photo taken during the thermal tracer test (left bottom), and the arrangement of groundwater wells (right).

To enable a reconstruction of the hydraulic parameter distributions spatially, each well was fitted with 9 separate filter sections, which can be individually hydraulically connected to the surrounding formations by an appropriate packer. Each filter screen was 5m long and installed alternately with 3m impermeable screens, in addition to the top 8m well casing (Figure 2.3). Therefore, there are 36 possible observation intervals available for each hydraulic or thermal tracer test, providing a dense monitoring network. Due to the unique well construction and small distances between the wells (from 1.9 m to 6 m), as well as due to the advanced

thermometers, this site is especially suitable for the application of tomographic methods. It offers the opportunity to investigate groundwater flow and heat transport in a relatively short time period at a high resolution.

2.1.2 Geological background

Geologically, this test site is located at the eastern shoulder of the Leinetalgraben, which is a distinctive zone of subsidence in the southern part of Lower Saxony, Germany. Its geological structure is very complicated due to polyphase tectonic development under various tension forces (Leiss, 2011) as shown in Figure 2.2. Two strike-slip zones (i.e. BN and BS) located at the north and south of Göttingen. Following Werner (2013), especially in the eastern shoulder including this site, it is dominated by NNE-striking faults with high offsets and a number of folds. Fractures have also well developed. The acoustic and optic televiewer data delivers three trends of the dip angle and azimuth of inserted fractures: 351/06, 221/37 and 045/59 (Werner, 2013). Lithologically, this area is located in the Lower and Middle Keuper which mainly consists of clay sequences and silt-sandstone layers. The main lithology exposed by the drill cores mainly includes limestone, siltstone and claystone. The geophysical loggings show that the bedding planes dip of rock formation is constantly with approximately 75° towards SE.

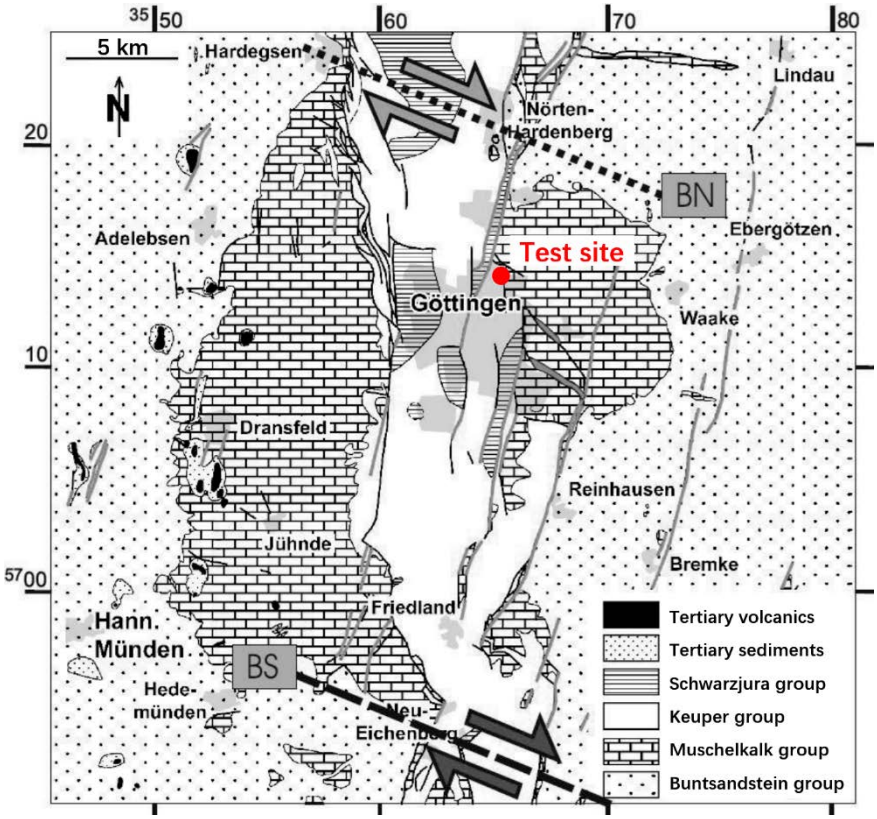

Figure 2.2: Regional geological map of the Leinetalgraben modified from Vollbrecht and Tanner (2011) and the location of the test site.

2.1.3 Testing devices

The main testing methods employed in the following chapters can be divided into two categories, thermal tracer tests, and slug tests. The related devices are highlighted in the field photos illustrated in Figure 2.3. In thermal tracer tests, warm water with a temperature of 20 °C is injected into the well with a double packer system utilized to isolate each filter section. The accompanying hydraulic propagation and heat transfer processes were monitored by three systems. The first is the inlet mass flow and injection temperature which were measured by the flowmeter and a high-precision thermal sensor embedded at the warm water supply port, respectively. Secondly, the water level changes were recorded by the pressure transducers placed in all wells. Last, the temperature evolution is documented by the fiber-optical distributed temperature sensors system (DTS) and a total of 27 resistance thermometers (PT1000) installed along each new wells (M, O, S, and N), and the distance between the adjacent sensors is 2.5 m. The DTS has a higher resolution in space, whereas the PT1000 can provide more accurate temperature measurements. The detailed technical parameters of the main devices are listed in Table 2.1.

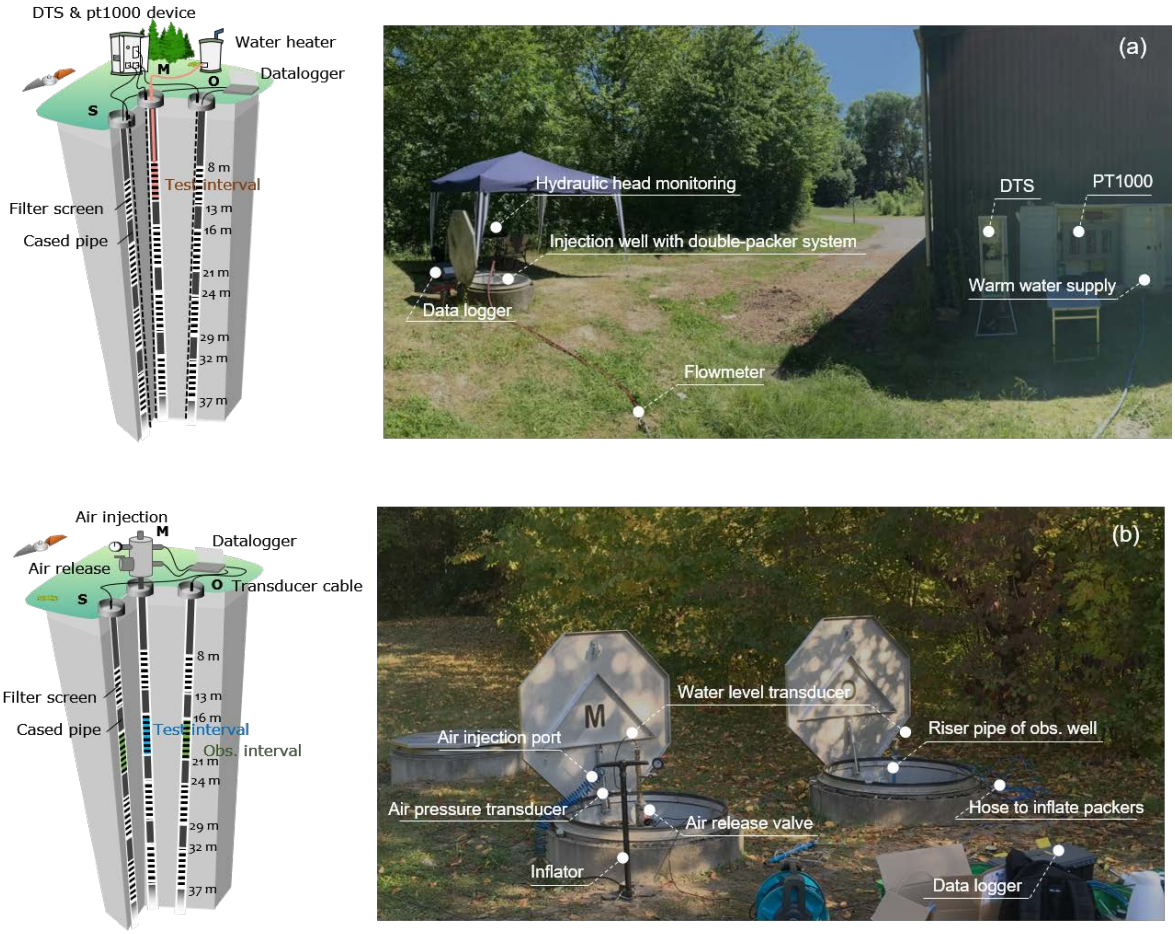

Figure 2.3: 3d schematics, field photos and main devices employed in (a) thermal tracer tests and (b) slug tests.

A pneumatic setup is adopted in the slug tests (Figure 2.3b). After injecting a certain amount of gas into the riser pipe by the inflator, the slug test was initiated by instantaneously releasing the injected gas into the test well. The water level response was then observed by the pressure transducer placed in each well just under the water level. For the detailed setup of cross-well slug tests please refer to Figure 4.1. To separate the hydraulic connection in the wells, the double packer system is employed in the test and observation wells. Please refer to Table 2.1 for the detailed technical parameters of the related devices.

Table 2.1: Technical parameters of the main testing devices.

	Brand	*Range*	Accuracy	*Resolution*[*]
DTS	Ap Sensing	-10~60 °C	±1 °C	0.1 °C, 0.5 (spatially)
PT1000	/	-50~200 °C	±0.25 °C	0.002°C, 2.5 m (spatially)
Flowmeter	Kobold	0.3~300 GPM	2% full scale	/
Datalogger (CR3000)	CAMPELL	/	0.04% of reading	< 100 Hz
Pressure transducer	Druck	1~900 psi	0.06% full scale	> 10 ms (temporally)
Spinner flowmeter	Mount Sopris	0~3000 rpm	Better than 1%	256 ppr

[*] Spatial resolution just refers to the vertical sensor resolution used in this study.

2.2 Previous work

2.2.1 Borehole geophysics

Since the experimental site was built, different studies have already been carried out at this site, not only by the Göttingen group but also by the Leibniz Institute for Applied Geophysics (LIAG) in Hannover. A series of geophysical logging was performed, including the gamma-ray logs, optical and acoustic televiewers, and caliper logs, etc.. Part of the geophysical logging results measured majorly in well O are summarized in Figure 2.4. Based on these geophysical measurements, several bachelors' and masters' students in Göttingen have written their theses related to this test site regarding different topics. Werner (2013) has set up a 3-D structure geological model of this site based on the acoustic televiewer data. According to the results of gamma-ray and ultrasonic logging, Schuster (2015) obtained the density and porosity profiles along the well N (Figure 2.4). Combining the geophysical measurements with information on the dip angle and azimuth of the bedding system, it was identified that at this site, the bedding planes' dip was constantly at approximately 75° towards SE. The reorientation of the drilling core samples, together with the acoustic and optic televiewer data, indicates different trends in the dip angle and azimuth of calcite-mineralized veins with different types of calcites. The paleo stress field analyses show two different orientations: NW-SE and NE-SW. The caliper log and optical televiewer (OTV) results revealed that the upper 40 m was more fractured than that from the bottom.

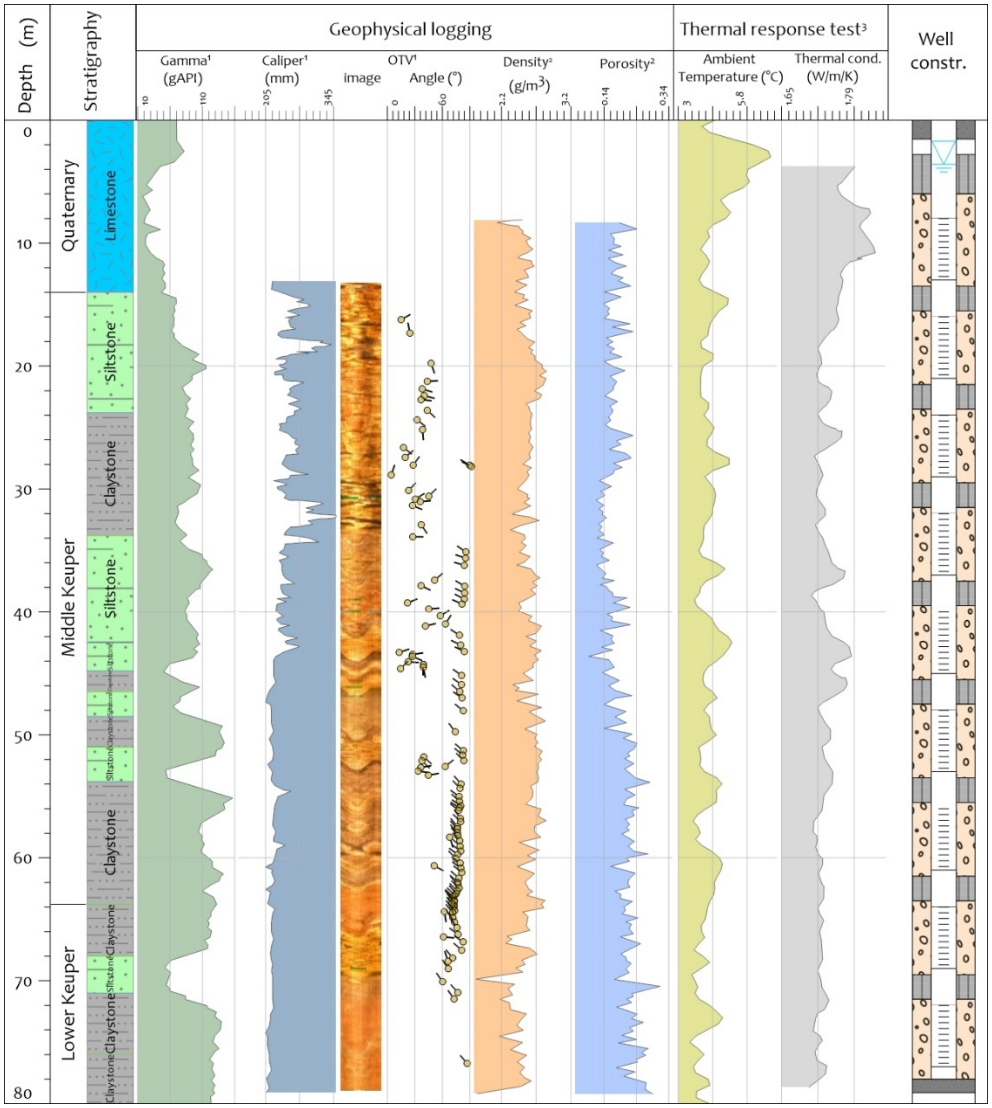

Figure 2.4: Borehole geophysics, thermal response test results, and groundwater well construction. The superscript 1, 2, and 3 represent the results were measured in well O, N, and W, respectively. Dataset is cited from Werner (2013)

2.2.2 Hydraulic and thermal tracer tests

Besides the geophysical surveys, some hydraulic investigations, such as hydrogeological and thermal tracer tests, were conducted at this site as well. Oberdorfer et al. (2013) firstly carried out a pumping test within the first filter sections between five wells, and preliminary estimated the hydraulic parameters of this site. Schuster (2015) performed a series of laboratory permeability tests on the drill cores of well N. A fully penetrating pumping test and tomographic pumping tests were performed by Qiu (2020) at this site. The inverted hydraulic diffusivity between well M and O above 40 m varied from 0.01 to 199 m^2/s and three high diffusivity layers (> 5 m^2/s) were revealed in his work. And the hydraulic parameters of this site were estimated by the conventional pumping test in well M, in which the hydraulic conductivity and specific storage were 1.46×10^{-5} m/s and 3.75×10^{-5} 1/m, respectively. In addition, the thermal tracer tests conducted

at this site also deliver some hydraulic information about the conductive fractures. Baetzel (2017a) performed a full-well-length heat injection test in well M for more than 15 days, and the temperature evolution along the wells was measured by the DTS and PT1000 system. Several obvious temperature responses above 40 m in wells O and W were observed, which can be inferred as the locations of hydraulically connected fractures. The relevant testing results are depicted in Figure 2.5.

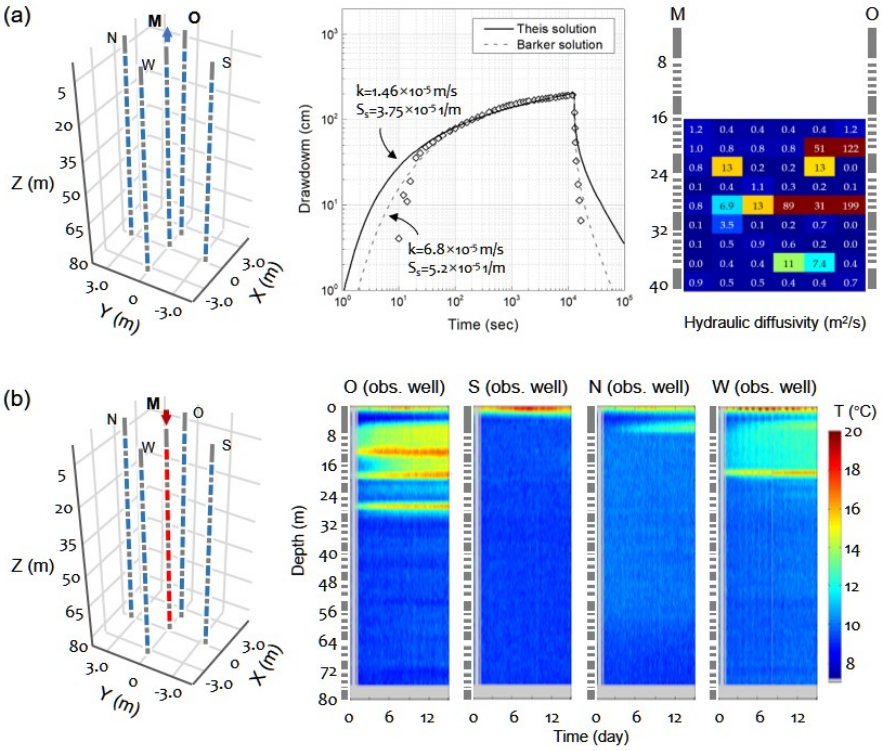

Figure 2.5: Results of the previous hydraulic and thermal tracer tests. (a) the results of the fully penetrating pumping test and inverted hydraulic diffusivity tomogram between well M and O, which are modified from Qiu (2020), and (b) the temperature responses observed by the DTS during the heat injection test, modified from Baetzel (2017a).

Some thermal properties of this site were measured by Piecha (2008). A thermal response test was performed in well W, and obtained thermal conductivity varies from 1.62 to 1.95 W/m/K. The thermal conductivity profile along well W is plotted in Figure 2.4.

All collected information indicates a highly hydraulic heterogeneity at this fractured site, especially at the upper 40 m. However, although the previous studies revealed some heterogeneous information, such as the inverted hydraulic diffusivity tomogram from the hydraulic tomography and the potential fracture locations by thermal tracer tests, it is still challenging to comprehensively investigate the spatially hydraulic heterogeneity of this site, especially the hydraulic connectivity and conductivity of the fractures that are crucial for groundwater flow, solute migration and heat transfer.

2.2.3 Supplementary flowmeter logging

In order to reveal more information about the transmissive fractures, a supplementary flowmeter logging in well M and O was performed in 2020, which can provide the accurate locations of the transmissive fractures exposed along the wellbore. In this test, a spinner flowmeter was employed to measure the vertical flow rate during the pumping process with a rate of 4.35 l/s. The related technical parameters of the spinner flowmeter are listed in Table 2.1. The flowmeter logs are plotted in Figure 2.6.

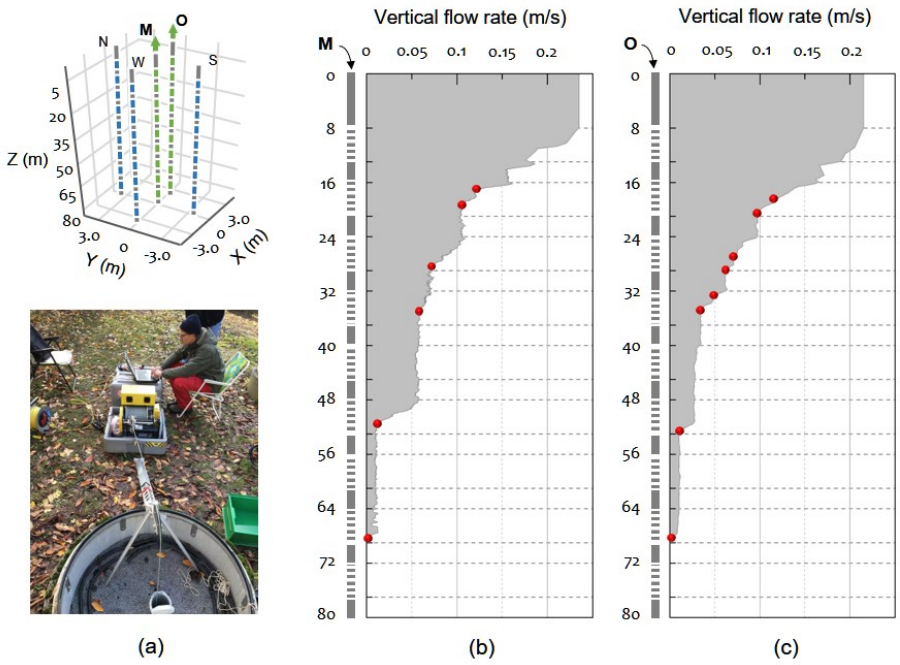

Figure 2.6: Flowmeter loggings measured in well M and O. (a) Field photo of the flowmeter logging and the vertical flow rate logs in well (b) M and (c) O during pumping. The red dots represent the identified locations of transmissive fractures exposed along the wellbore. It is worth noting that only the fractures exposed at the permeable screen can be identified.

The location of the transmissive fractures can be figured out through a sudden increase in the vertical flow rate curve. In Figure 2.6, serval fracture locations were accordingly identified, which are marked by the red dots. No fracture was identified above 14 m, because the formations at this depth were Quaternary sediments as shown in Figure 2.4. The flowmeter logs indicate that most fractures are developed at the upper 40 m at this site, which agrees with geophysical measurements.

2.3 Investigation area

According to the previous work, the hydraulic heterogeneity at the upper 40 m of this site is more pronounced. Since the high-dense monitoring network was installed only in the four new wells (M, O, S, and N), the area at the upper 40 m between wells M, O, and S, is determined as a three-dimensional investigation area, as

illustrated in Figure 2.1. The hydraulic properties of this investigation area were characterized using thermal tracer tomography and slug test-based hydraulic tomography in the following chapters.

3

Heterogeneous slug test model

Contents

This Chapter has been published as:

Liu, Q., Hu, L., Bayer, P., Xing, Y., Qiu, P., Ptak, T., & Hu, R. (2020). A numerical study of slug tests in a three dimensional heterogeneous porous aquifer considering well inertial effects. Water Resources Research, 56(11), DOI: 10.1029/2020WR027155

Abstract

The slug test is a common field technique for obtaining local hydraulic parameters near wells, applied for example for the hydrogeological investigation at contaminated sites. Although many slug test models have been developed for interpretation of measurements, only a few of them have considered heterogeneous conditions, and water column inertial effects are usually neglected. In this paper, we propose a novel three-dimensional slug test model (3DHIM) for application in heterogeneous aquifers, considering inertial effects associated with skin effects and linear friction forces. After comparison with existing analytical and numerical solutions of slug tests, the model is applied to an aquifer analog to simulate a series of slug tests. The results from single-well slug tests show that the well geometry (i.e. the well radius, well depth and screen length) has an impact on the water level response. For cross-well slug tests, the results indicate that the water level fluctuations not only include information on the hydraulic signal propagation process in the aquifer but also on well characteristics, such as wellbore storage and inertial effects. These effects cause a phase shift and amplitude change of the water level fluctuation. As the observation and test wells have a good hydraulic connection and similar well geometry, the water level amplitude could be amplified relative to aquifer pressure at the measured position. Therefore, we suggest considering wellbore storage and in-well inertial effects in slug test based subsurface investigations, otherwise the parameter estimates based on well water levels may include errors, particularly in highly permeable layers.

3.1 Introduction

Heterogeneity of aquifer hydraulic properties has a crucial impact on groundwater flow and solute transport. To characterize this heterogeneity, some innovative aquifer testing configurations have been developed, such as multilevel, and cross-well tomographical hydraulic tests. The slug test is one of the most common approaches for obtaining local hydraulic parameters. It is based on recording the recovery of the water level in a well after an instantaneous extraction (or injection) of a certain amount of water or gas. The recovery curve contains information about the hydraulic properties of the aquifer, such as hydraulic conductivity and specific storage, which can be obtained by some inversion methods. Recently, this method has been widely used for contaminated site surveys as it requires no additional water injection or extraction. Moreover, compared to other approaches, such as those based on pumping tests, a slug test has considerable logistic and economic advantages, and it can resolve a higher degree of aquifer heterogeneity due to its small sampling scale (i.e., the volume of the subsurface sampled by a slug test). In the last decades, variants of slug test configurations for the characterization of aquifer heterogeneity have been studied (Brauchler et al., 2010; Cardiff et al., 2011; Wang et al., 2018; Widdowson et al., 1990; Zlotnik & McGuire, 1998). Tomographic slug tests, for instance, measure hydraulic head responses in the testing and observation intervals at different depths to estimate the spatial heterogeneity of the hydraulic properties between two or more wells.

In order to resolve the spatial heterogeneity of hydraulic parameters, a slug test model is usually required to establish mathematical relationships between the field test data and the parameters sought. Based on different types of slug tests, the basic options for aquifer characterization are as shown in Figure 3.1.

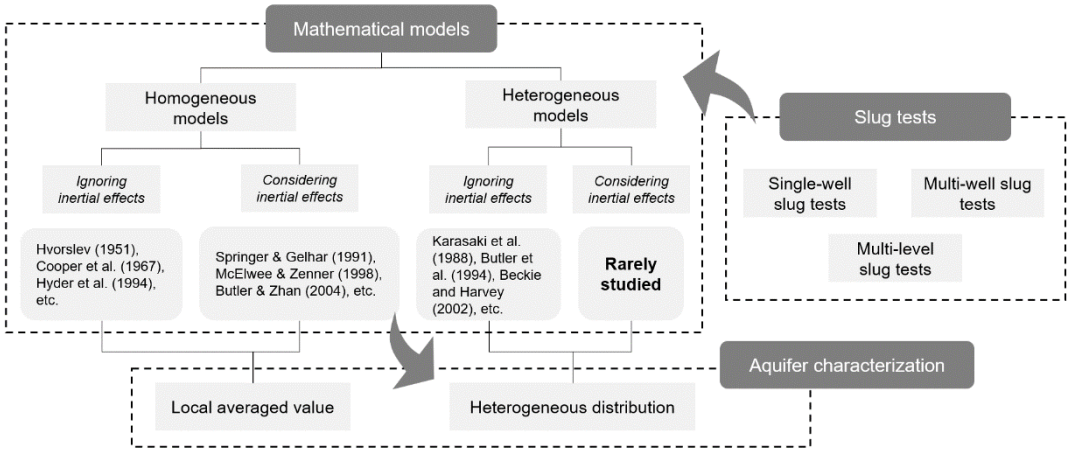

Figure 3.1: The basic options of aquifer characterization based on slug tests.

Among the presented slug test models, however, only a few consider heterogeneity. Karasaki et al. (1988) examined slug-induced flow in a two-layer aquifer by using an analytical model. Shapiro and Hsieh (1998)

extended the Karasaki model to *n* layers. Some numerical models were also developed to study some more complicated situations, such as multilevel slug tests. Originally, numerical models were used to analyze the tests results to obtain information on the heterogeneity of hydraulic conductivity in vertical direction (Braester & Thunvik, 1984; Butler et al., 1994; Melville et al., 1991; Widdowson et al., 1990). In these models, aquifers are conceptualized as a series of regular homogeneous layers. To establish a more realistic representation, also models with more complicated spatial heterogeneity description were proposed. Beckie and Harvey (2002) used a randomly generated transmissivity field to assess the impact of hydraulic parameter heterogeneity on the slug test results. Brauchler et al. (2007) and Paradis et al. (2015) simulated a series of synthetic tomographic slug tests by using the heterogeneous models and evaluated their inversion algorithms. All these numerical models consider hydraulic conductivity variations in horizontal or vertical directions. However, most of them focus merely on the groundwater flow in the aquifer and ignore the hydrodynamic processes inside the well.

In fact, inertia-induced oscillations of the water level in a well are not uncommon during slug tests, especially in highly permeable aquifers. This phenomenon has been extensively studied in homogeneous aquifers. Some researches point out that the magnitude of the oscillation will increase as the hydraulic conductivity of the aquifer and the water column height increase (Bredehoeft et al., 1966; Butler & Zhan, 2004). Since Bredehoeft et al. (1966) discussed the role of water-column inertia in hydraulic tests, many researchers also considered inertial effects in their analytical slug test models to interpret the oscillatory head (Butler & Zhan, 2004; Kabala et al., 1985; Kipp, 1985; Malama et al., 2011; Malama et al., 2016; McElwee & Zenner, 1998; Springer & Gelhar, 1991; Zurbuchen et al., 2002). Butler and Zhan (2004) presented a homogeneous slug test model for confined aquifers which considers inertial mechanisms both in the observation and test wells. Malama et al. (2016) further developed the model for unconfined aquifers. Considering the inertial effects in both wells makes their model more adequate for interpreting cross-well slug tests. Given the often rapid oscillatory nature of water level response, the pressure transducer measured head in an accelerating water column cannot be directly related to the water level by the standard equations for calculating the height of water above the measurement point, since it involves significant accelerations in the water column. To handle this, several correction models that reduce the error between actual water level and the measured head have been proposed (McElwee, 2002; Zurbuchen et al., 2002).

To date, few studies have incorporated inertial effects into a heterogeneous slug test model. A major hurdle is the limited applicability of analytical models to represent heterogeneity. In contrast, for the common numerical methods, such as finite element and finite difference methods, a fixed solution domain is required. With these, it is challenging to simulate the oscillatory water level in the well, because it is a deforming domain problem. As remedy, the arbitrary Lagrangian-Eulerian (ALE) method was proposed (Brindt & Wallach, 2017; Jin et al., 2014). The ALE method combines the advantages of Eulerian and Lagrangian

descriptions, which allows the computational mesh to move arbitrarily inside the domain to optimize the shapes, and which precisely tracks the material interface on the boundaries of the domain. Except for the deforming domain, interface conditions between the well and the aquifer are also not readily specifiable. Because the water flow in the well and in the aquifer is commonly represented by different physical equations, the dependent variables from different governing equations require specific continuous conditions for coupling. This coupling issue has been widely explored in many fields, such as geoscience, applied mathematics and chemical engineering (Alazmi & Vafai, 2001; Cimolin & Discacciati, 2013; Cooper et al., 1965; Hanspal et al., 2009). Here, constraints of normal stress, normal velocity or some other specific conditions are employed to ensure the continuity of variables between different physical equations. Obviously, it is challenging, but necessary to establish a coupled numerical slug test model that accounts for both inertial effects and aquifer heterogeneity. The objective of our work is to establish a fully coupled model considering aquifer heterogeneity and inertia-controlled water level oscillations in wells.

In this study, we introduce a new three-dimensional numerical slug test model (3DHIM) considering the inertial effects in a heterogeneous aquifer. In the following, model validation is addressed by comparing simulation results with some existing solutions. Furthermore, we examine the performance of the model by implementing an aquifer outcrop analogue with a high resolution of heterogeneity. A series of single-well slug tests with different well geometry and cross-well slug tests are simulated to examine the influence of inertial effects on the slug test results.

3.2 Slug test modeling in a heterogeneous aquifer

3.2.1 Slug test processes in the well-aquifer system

Figure 3.2a shows the principle of a commonly used pneumatic slug test setup. After a certain amount of gas is injected into the well pipe, the water level in the riser pipe moves down until it is stable. The air pressure is then instantaneously released by opening the venting valve of the injection unit, and the air pressure is recorded by the upper pressure transducer. The recovery of the water level is recorded by the lower pressure transducer placed at a predefined depth of the water column. In fact, fluctuation of the water level can be akin to a damped simple harmonic motion (Kabala et al., 1985; Marschall & Barczewski, 1989). The main difference is that the damping effect in slug tests is controlled by the interaction of the well and the aquifer. In shallow formations of a low hydraulic conductivity, the recovery curve of the water level typically shows an overdamped behavior. That is, the water monotonically recharges to the well (or discharges to the aquifer). On the contrary, in deep and highly permeable aquifers, the recovery curve can show oscillations with an underdamped behavior. In the latter case, the groundwater exchanges alternatively between the well and the aquifer. However, in both cases, the hydrodynamic process is always controlled by two mechanisms. One is the groundwater flow inside the well, and the other one is the groundwater flow in the aquifer. A conceptual

model with the boundary types of a slug test is shown in Figure 3.2b. In this model, a two-dimensional (2-D) axisymmetric wellbore (Ω_f) with a moving water level boundary (Γ_f) is embedded in a 3-D heterogeneous aquifer (Ω_a), and the skin (Ω_s) is also included. The interface boundary (Γ_s) between the fluid flow and porous media flow, i.e. the well screen, is identified by certain coupling boundary conditions. No-flow boundary conditions are imposed to the aquifer top and bottom ($\Gamma_{top}$and Γ_{bom}). The outer edge of the entire model (Γ_{out}) is represented by a constant-head boundary. An observation well can be also considered, model settings of the test well and the observation well are the same. Packers are commonly used in both the test and the observation wells for multi-well slug tests. In the 3DHIM model, the wells with a double packer system (Figure 3.2a) are simplified to a setup only containing a corresponding screen interval and the riser pipe.

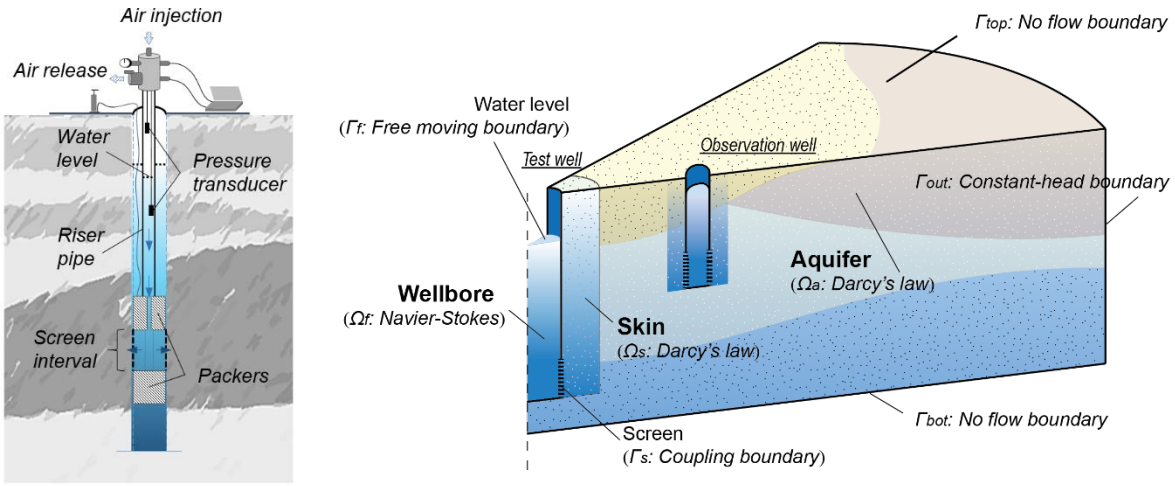

(a) (b)

Figure 3.2: Schematic sketch of (a) the setup of a pneumatic slug test, and (b) a conceptual model of a slug test in 3-D heterogeneous porous formations including skin. Model settings of the test well and the observation well are the same.

3.2.2 Well-aquifer coupling slug test model

The hydrodynamic processes in the well include water exchange between the well and the aquifer, momentum dynamics of the water column in the riser pipe, and head losses due to friction within the well screen and riser pipes (Clemo, 2010; Houben, 2015; Quinn et al., 2018; Zurbuchen et al., 2002). Among them, the former two are the main processes affecting the water level fluctuation. In heterogeneous formations, a double-packer system is often utilized to isolate the well into several test intervals, which leads to a diameter change from the screen interval to the riser pipe (Figure 3.2a). Narrowing and enlargement of the pipe diameter at the connections between the screen interval and the riser pipe make the momentum dynamics of the water column more complicated (Zenner, 2008; Zlotnik & McGuire, 1998).

The model presented in this paper considers the above-mentioned issues through a well-aquifer coupling.

Besides, we also include the head losses caused by linear friction forces in the well screen and riser pipe in this model.

Groundwater movement inside the well

The movement of groundwater inside a well is affected by inertial effects. To describe this nonlinear hydrodynamic process, many different forms of momentum conservation equations were developed (Butler & Zhan, 2004; Cooper et al., 1965; McElwee & Zenner, 1998; Van der Kamp, 1976). In slug tests, the vertical motion of the water column is also significant. Accounting for the hydrodynamic behavior caused by variable well diameters, radial flow also needs to be considered. Assuming that the tangential velocity is negligible, groundwater flow in the well can be treated as 2-D axisymmetric. In some studies, the incompressible Navier-Stokes (NS) equation was adopted to describe the motion of the water column in the wellbore (Kim, 2003; McElwee & Zenner, 1998), and the friction force in the well screen and riser pipes is assumed to be linearly proportional to the vertical velocity of the water column following the Poiseuille law (Butler, 2002; Butler & Zhan, 2004; Quinn et al., 2018). Accordingly, the fluid flow rate $\boldsymbol{v_f}(r,z)$ and pressure p_f should satisfy the NS momentum and the continuity equations, reading as,

$$\rho\left[\frac{\partial \boldsymbol{v_f}}{\partial t}+(\boldsymbol{v_f}\cdot\nabla)\boldsymbol{v_f}\right]=-\nabla\cdot T(\boldsymbol{v_f},p_f)+\rho g k+\boldsymbol{f}_{fric} \tag{3.1}$$

$$\nabla\cdot\boldsymbol{v_f}=0 \tag{3.2}$$

where $T(\boldsymbol{v_f},p_f)=-p_f\boldsymbol{I}+\mu(\nabla\boldsymbol{v_f}+(\nabla\boldsymbol{v_f})^T)$ is the Cauchy stress tensor, $\boldsymbol{I}$ is the identity tensor, and μ denotes the fluid dynamic viscosity. ρ is the fluid density, g is gravitational acceleration, and k is the unit vector in z-direction. ∇ and $\nabla\cdot$ are the gradient and divergence operators with respect to the coordinate system. $\boldsymbol{f}_{fric}$ represents the Poiseuille friction term, which is defined as $8\mu\boldsymbol{v}_z/r^2$. $\boldsymbol{v}_z$ is the vertical component of the fluid flow rate $\boldsymbol{v_f}$, and r is the pipe radius. For detailed derivation of Eq.(3.1), please see the Appendix A2.

Groundwater flow in a heterogeneous aquifer

Darcy's law and a mass conservation equation are usually used to describe groundwater flow through an aquifer and skin. In a 3-D heterogeneous media, this can be written as

$$\mathbb{S}_\mathbb{S}\frac{\partial h}{\partial t}+\nabla\cdot\boldsymbol{v_p}=Q_m \tag{3.3}$$

$$\boldsymbol{v_p}=-\mathbb{K}\nabla h \tag{3.4}$$

where $\boldsymbol{v_p}$ is the Darcy velocity. h denotes the hydraulic head, which is defined as $h=z+p_m/\rho g$. p_m is the pressure in the aquifer, and Q_m is a source/sink term. $\mathbb{K}$ and $\mathbb{S}_\mathbb{S}$, which are spatially dependent, represent the hydraulic conductivity tensor and specific storage of the porous media, respectively.

Previous slug test studies revealed that the head in the test well is much less sensitive to aquifer storativity than to transmissivity, and the storativity estimated by single-well slug tests usually has questionable values (Beckie & Harvey, 2002; Bredehoeft et al., 1966; McElwee et al., 1995a). To reduce the impact of uncertainty caused by storativity, we thus assume a spatially uniform value for the specific storage in the model.

Free water surface boundary in the well

Ignoring the effect of atmospheric pressure changes, the free water surface boundary in the well can be defined as

$$T(\boldsymbol{v_f}, p_f) = 0 \qquad on\ \Gamma_f \tag{3.5}$$

$$u = \boldsymbol{v_f} \cdot \boldsymbol{n} \qquad on\ \Gamma_f \tag{3.6}$$

where u is the moving velocity of the water level. $\boldsymbol{n}$ denotes a unit vector outward and normal to the boundary of the fluid domain (Γ_f).

Navier Stokes-Darcy interfacial boundary at the well screen

During slug tests, when water is exchanging at the screen interval, the near-normal flow is dominant. To describe the mass and momentum transfer at the screen, the continuity conditions of normal velocity and normal stress are adopted, where $\emptyset$ is the porosity,

$$\boldsymbol{v_f} \cdot \boldsymbol{n} = -\frac{1}{\emptyset}\boldsymbol{v_p} \cdot \boldsymbol{n} \qquad \text{on } \Gamma_s \tag{3.7}$$

$$-n^T T(\boldsymbol{v_f}, p_f) n = p_m \qquad \text{on } \Gamma_s \tag{3.8}$$

No-flow boundaries

The no-flow boundaries are defined as,

$$(\mathbb{K}\nabla\varphi) \cdot \boldsymbol{n} = 0 \qquad \text{on } \Gamma_{bot} \tag{3.9}$$

$$(\mathbb{K}\nabla\varphi) \cdot \boldsymbol{n} = 0 \qquad \text{on } \Gamma_{top} \tag{3.10}$$

The top boundary for an unconfined aquifer can be described by specific moving water table methods. A comprehensive evaluation of this boundary is beyond the scope of this paper, and more details can be found in the work of Brindt and Wallach (2017), Jin et al. (2014), and Malama et al. (2011). In this model, the well casing is also set as no flow boundary, which means groundwater in the well and aquifer can only exchange through the well screen.

Constant-head boundary

For the constant-head boundary we have,

$$\varphi = h_{out} \qquad \text{on } \Gamma_{out} \tag{3.11}$$

The sampling scale of the slug tests is usually smaller than that of pumping tests. Previous studies indicated that this scale is inversely proportional to the storage coefficient and can be well approximated by $r_c/\sqrt{S}$ (Beckie & Harvey, 2002; Dai et al., 2015; Karasaki et al., 1988), where r_c is the radius of well casing. Therefore, the observation well should be located within the zone of influence and the scale of the numerical slug test model can be determined by such relationship to minimize the influence of the constant-head boundary on the simulation results.

Initial conditions

Before the slug test is initiated, the groundwater in the well and the aquifer maintains a hydrostatic condition. Upon starting the test, the pressure equivalent to a certain height of the water column is applied rapidly on the water level boundary to induce the initial head difference. The initial conditions including the pressure, the flow rate in the well and the head difference can be defined as follows:

$$p_f = p_m = \rho g \psi \qquad \text{at } t = 0 \tag{3.12}$$

$$\boldsymbol{v_f} = 0 \qquad \text{at } t = 0 \tag{3.13}$$

$$H = H_0 \qquad \text{at } t = 0 \tag{3.14}$$

where ψ is the pressure head, which is measured relative to the static groundwater level. H denotes the head difference between the well and the aquifer, which means that the geometric height of the well will be reduced by H in our model.

3.2.3 Numerical technique

The arbitrary Lagrangian-Eulerian method

The ALE method is a numerical technique for solving free-surface problems (Donea et al., 2004; Duarte et al., 2004; Jin et al., 2014). By introducing referential coordinates, it redefines the node position of the calculation units which are originally defined in a spatial domain (pure Eulerian description) or material domain (pure Lagrangian description). Hence it combines the advantages of both Lagrangian and Eulerian algorithms for the kinematic description. During a slug test, the Lagrangian method is ideal for tracking the water level fluctuation and the Eulerian method is suitable for calculating the internal pressure change. Because the motion of the free water surface boundary is mainly in to normal direction, this boundary can be assigned a Lagrangian description in the normal direction and a Eulerian description in the tangential direction. Through this method, the mesh on this boundary can adaptively move along with materials to precisely track the water level fluctuations. This fluctuation Δw is expressed as a line integration in the time domain of the flow velocity of the water in the well,

$$\Delta w = \int_0^t u dt \tag{3.15}$$

In our 3DHIM model, after the mesh is initialized by Eqs. (3.13) and (3.14), the mesh deformation is forced to fit the pressure condition at the top boundary of the domain (Γ_f) which is defined by Eqs. (3.5) and (3.6). Finally, the updated mesh is delivered into the spatial coordinates to solve Eq. (3.1).

Coordinate transformation

Simplifying the well flow into a 2-D axisymmetric problem is reasonable in slug tests and can considerably reduce the computational cost compared to a full 3-D pipe flow model. As the coordinate systems used in the well and the aquifer are different (well: cylindrical coordinates, aquifer: Cartesian coordinates), transformation and coupling of the two coordinate systems is required. The variables on the NS-Darcy interfacial boundary (well screen boundary) can be connected by using a coordinate projection from 3-D to 2-D, and transferred back by using the coordinate extrusion. These two kinds of coordinate transformation procedures can be expressed as,

Coordinate projection: $g(r,z)|_{r=r_s} = \frac{(\int_{-\pi}^{\pi} f(X,Y,Z)\sqrt{X^2+Y^2}d\theta)|_{X^2+Y^2=r_s{}^2}}{2\pi\sqrt{X^2+Y^2}}$

Coordinate extrusion: $f(X,Y,Z)|_{X^2+Y^2=r_s{}^2} = g(r,z)|_{r=r_s}$

Here $\theta = atan2(y,x)$ is the arc tangent of the two variables x and y. It is similar to calculating the arc tangent of y/x, except that the signs of both arguments are used to determine the quadrant of the result, which lies in the range $[-\pi,\pi]$. r_s is the radius of the screen.

The numerical implementation of this model is realized by using the finite element software COMSOL (2012) (Cardenas & Gooseff, 2008; Hu, Rui et al., 2018; Liang et al., 2018), which is an ideal tool for coupling variables of different physical fields. Concretely, the “Darcy’s Law” mode and “Free and Porous Media Flow” mode are employed to simulate groundwater movement within the aquifer and inside the well, respectively. And they are coupled by the interfacial boundary conditions. The “ALE” mode is also implemented within the wellbore domain to track the water level fluctuation.

3.3 Model tests and applications

3.3.1 Model tests considering inertial effects and multilayered aquifers

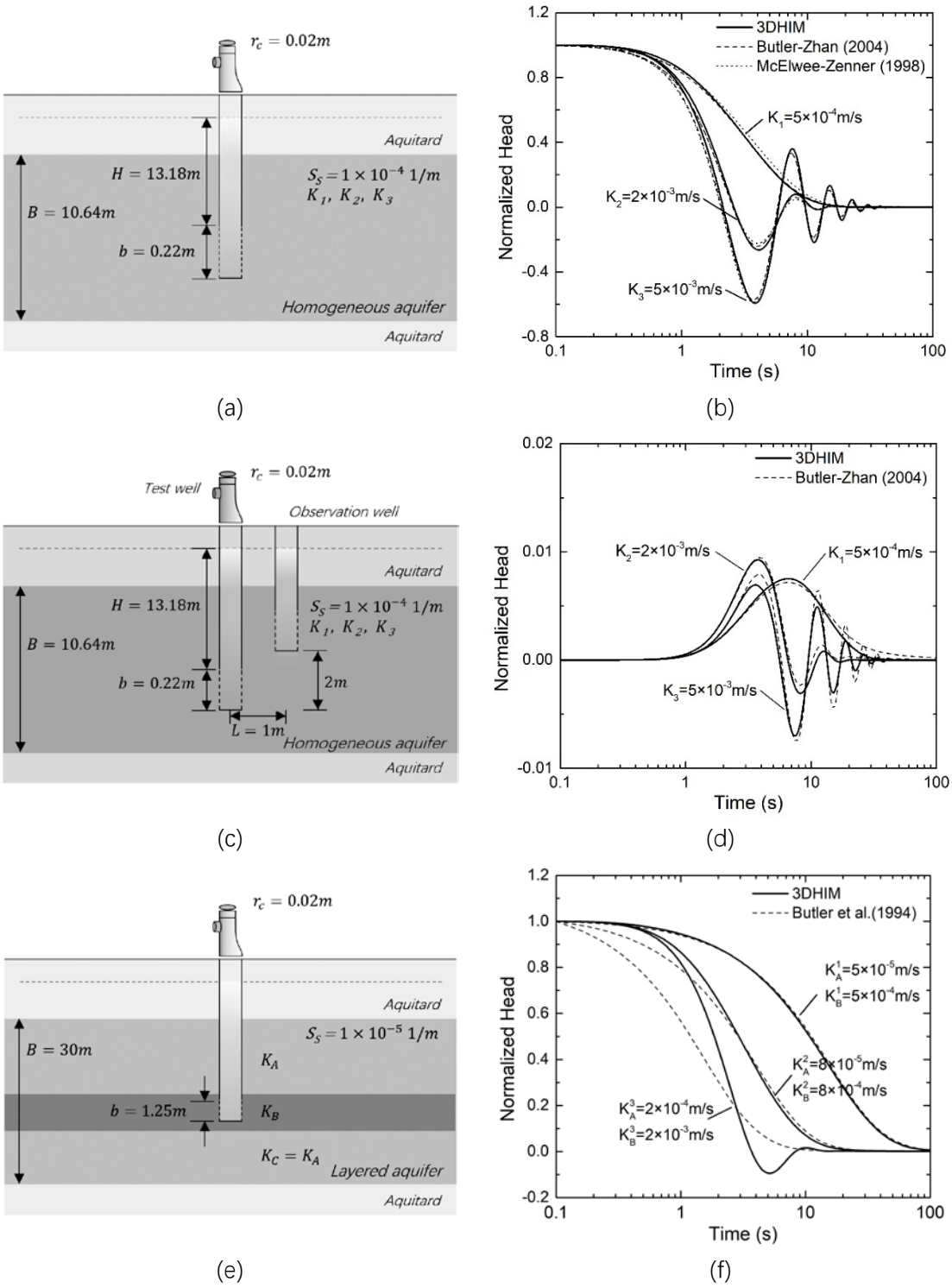

Figure 3.3: Validation of the 3DHIM model in a homogeneous aquifer with (a) a single well and (c) a cross-well setup, and (e) in a layered aquifer, note that the size is not to scale. The corresponding normalized head curves calculated by the analytical models (Butler & Zhan, 2004; McElwee & Zenner, 1998), a numerical model of Butler et al. (1994) and the new numerical model (3DHIM) are shown in (b), (d) and (f), respectively.

The validation procedure of the 3DHIM model is divided into two steps. First, we compare the simulation results from 3DHIM with those from analytical solutions of a homogeneous case for testing the inertial effects. Second, this 3DHIM model is tested in a multilayered heterogeneous aquifer by comparing the results from another numerical solution which does not consider inertial effects in the well.

Figure 3.3a shows the conceptual model of a single well slug test for a homogeneous case and the model parameters used in Butler and Zhan (2004). A partially penetrating well is embedded in a homogeneous confined aquifer with a thickness (B) of 10.64 m. The well has a radius of r_c = 0.02 m and a screen length of b = 0.22 m. The water column height from the top of the screen to the water level is 13.18 m. Two analytical solutions proposed by McElwee and Zenner (1998) and Butler and Zhan (2004) are chosen for the validation. The two analytical solutions are merely for homogeneous conditions while accounting for inertial effects in the well. Combined with the 3DHIM model, these three are all applied into a series of slug tests in a homogeneous confined aquifer (Figure 3.3a) with variable hydraulic conductivities, k. The simulation results are plotted in Figure 3.3b. It shows that the curves are very close to the analytical solution and the oscillation becomes more obvious as the value of k increases. For the multi-well slug test, we also need to assess the 3DHIM model responses at the observation well by comparison with the analytical solution of Butler and Zhan (2004). In Figure 3.3c, an observation well, with the same layout except the screen installed 2 m higher than the test well, is placed into the previous homogeneous aquifer. The horizontal distance between these two wells is 1 m. The simulated head responses at the observation well are shown in Figure 3.3d. Comparing to the analytical results for various k values shows that the 3DHIM model accurately simulates these oscillations and properly reproduces the analytical solutions. Small differences between the two types of curves can be found when k equals to 5×10^{-3} m/s, which could be due to interference of the perturbation at the observation well with the water level fluctuation in the test well. This mechanism is not included in Butler and Zhan model.

Figure 3.3e shows another conceptual model for validating the performance of 3DHIM in a multilayered heterogeneous aquifer. The thickness of the three-layer confined aquifer is 30 m. A 5 m thick highly permeable layer is sandwiched in the middle, which is 15 m below the aquifer top. In this layer, a partially penetrating well is installed with a screen length of 1.25 m. A numerical model presented in Butler et al. (1994) which was developed for the case of multi-level slug tests in layered aquifers is selected. Based on the layered conceptual model (Figure 3.3e), a series of slug tests with different sets of hydraulic conductivities are simulated by using the 3DHIM model and the model proposed by Butler et al. (1994), assuming that the top and bottom layers have the same hydraulic conductivity. The simulated results are shown in Figure 3.3f, which indicates that two curves simulated by the different models are almost the same when the conductivity is low. As the k_B value of the middle layer increases, the difference between these two results first appears at early time, and then expresses in the two distinct fluctuation forms, such as

overdamped or underdamped. Considering that the model of Butler et al. (1994) does not account for groundwater flow in the well, these differences are reasonable. The absence of a groundwater well means a faster response and no inertia-induced oscillations. In summary, the comparison result shows that the 3DHIM model has a good performance when simulating inertial effects in a simple heterogeneous aquifer.

3.3.2 Model application to an outcrop analogue

Aquifer analogue study

To test the model performance in a highly heterogeneous formation, an outcrop analogue is adopted. The outcrop analogue approach is originally derived from mapping outcrops in the petroleum industry. It is also of special interest in hydrogeology due to the realistic representation of aquifer heterogeneity. It can serve as a surrogate to construct models of heterogeneous hydraulic parameter distribution. Using such analogs, with the fully known parameter distribution, the quality of simulated slug test result interpretation can be assessed. The 3DHIM model is applied in the following to an analog outcrop study to simulate slug tests.

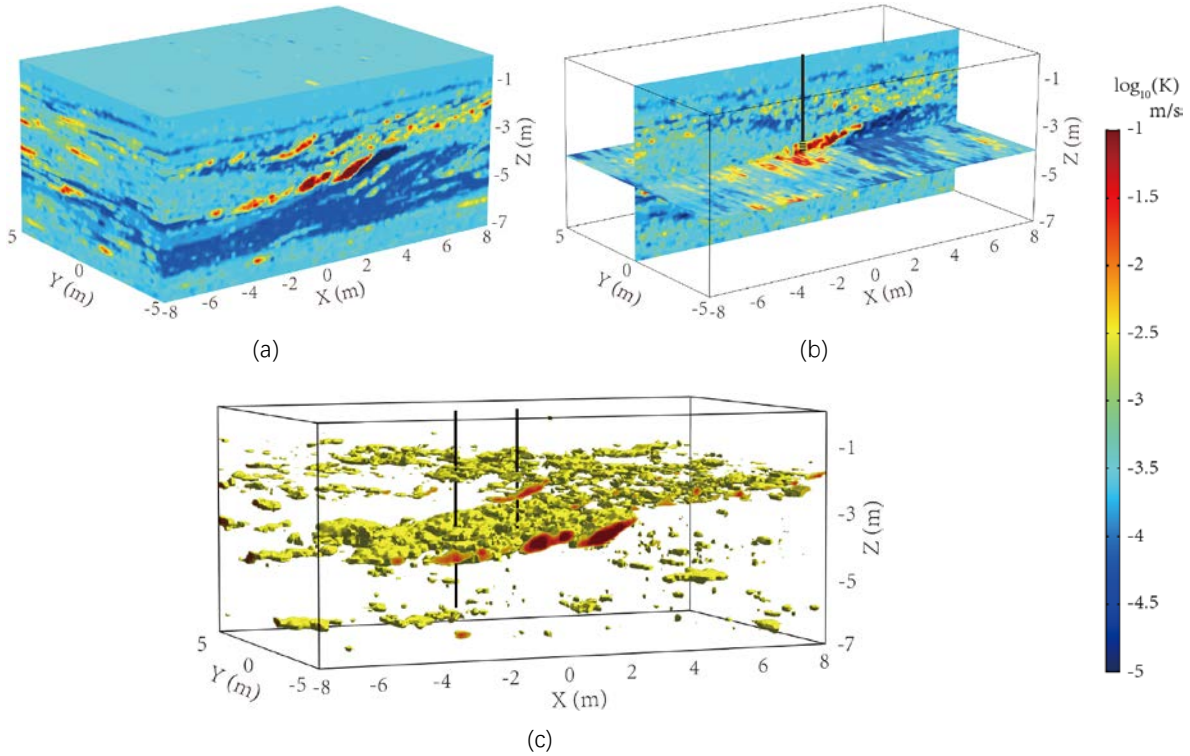

Figure 3.4: The reference log(k) field of the outcrop analogue in (a) 3D view, (b) cross-section view of XY-plane at z = -4 m and of XZ-plane at y = 0 m, and (c) the spatial distribution of high k zone (log(k) > -2.5). The black lines represent the wells with a screen installed at the bottom.

The aquifer outcrop analogue adopted in the following numerical investigations is developed by Bayer (2000), and it represents unconsolidated fluvial sediments near the town of Herten in southwest Germany.

By digital mapping during the ongoing excavation of the sediment body in a gravel pit, vertical facies mosaics of lithology were mapped. Based on laboratory measurements of hydraulic properties, the lithology description served as basis for a hydrofacies description with dm-scale resolution of hydraulic conductivity and porosity. Maji and Sudicky (2008) further translated the gathered information into a 3-D hydraulic parameter distribution using a transition probability/Markov chain-based procedure. This outcrop analogue has already been utilized in further studies, and more details can be found in Bayer et al. (2011) and Hu, R et al. (2011). The size of this analogue is 16 m × 10 m × 7 m, and the original numerical resolution of hydrogeological parameters is 5 cm × 5 cm × 5 cm. The k value varies from 6×10^{-7} to 1 m/s. The mean value of this database is 2.11×10^{-3} m/s and its standard deviation is 0.0274 m/s. Figure 3.4 shows the $\log_{10}$-hydraulic conductivity field in 3-D and cross-section views, and the spatial distribution of a relatively high k zone in which k is above ca. 3×10^{-3} m/s ($\log_{10}(k) > -2.5$).

Single-well slug tests with various well geometries

The single-well slug test is the most common way to obtain the local hydraulic parameters near the well. Combined with multiple packer systems, depth orientated single-well multilevel slug tests can be used to resolve the vertical change of hydraulic conductivity around the well. In a homogeneous model, due to the inertial effects, the water level response in the well is not only affected by the aquifer hydraulic conductivity, but also by the well geometry, including the pipe radius r, screen length b and water column height H. A smaller well radius, a longer screen length, or a larger water column height can result in a more significant water level oscillation in a highly permeable aquifer. Therefore, interpretation of the water level response of the test well in a heterogeneous aquifer should also consider the impact of well geometries. To investigate these factors, based on the outcrop analogue, a series of single-well slug tests with different well radii, water column heights and screen lengths are simulated. The test well is located at the center of the analogue, and three levels are selected for each well parameter (r: 0.01, 0.03, 0.05 m; b: 0.1, 0.2, 0.5 m; H: 1.8, 3.8, 5.8 m).

Figure 3.5 shows the curves of the normalized head in the test wells with various well radii, screen lengths and water column heights. The results in Figure 3.5a indicate that the water level oscillation is intensified as the well radius decreases. This trend is consistent with that in the homogeneous aquifers. However, as shown in Figure 3.5b and c, the oscillation of the curves is no longer intensified as the screen length and water column height increases, which is distinct from the homogeneous cases. This is because the results from the various screen lengths and water column heights are heavily affected by the heterogeneous conductivity distribution. When b = 0.1 m or H = 3.8 m, the water level curve has the largest oscillation amplitude, because there is a thin and highly permeable layer near the depth of -4.0 m at the well location (Figure 3.5c). When the screen length or water column height is changed, the position of the screened interval is also

changed. These simulation results indicate that the water level response in the test well shows the combined effect of well geometry and heterogeneous conductivity.

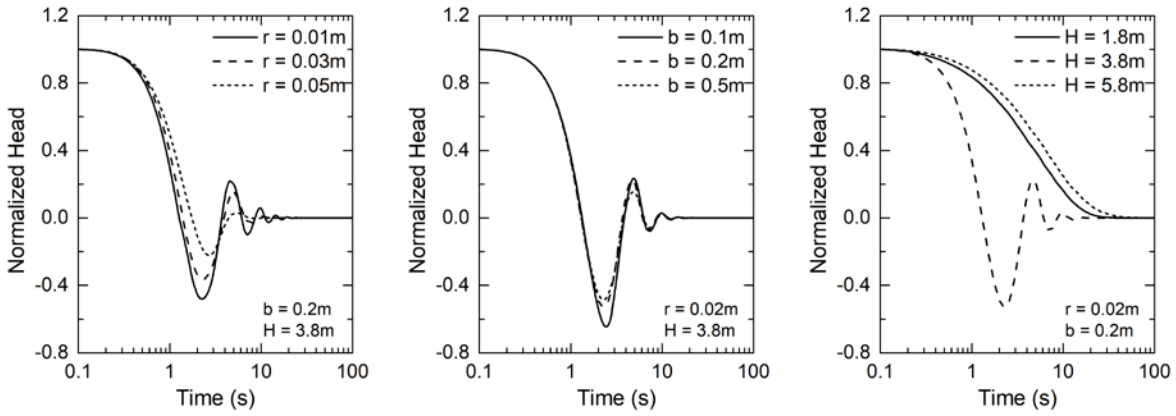

(a) (b) (c)

Figure 3.5: The curves of the normalized head in single-well slug tests with various (a) well radii, (b) screen lengths, and (c) water column heights.

Cross-well slug tests considering inertial and skin effects

The cross-well slug test is another way to obtain hydraulic parameters, which can vastly improve parameter estimation in space(McElwee et al., 1995b). Specifically, a cross-well tomographic slug test can provide spatial heterogeneity of hydraulic parameters. In addition to the influence of well geometry, the oscillating water level is also affected by the inertia of the water column, which is often ignored in heterogeneous models, and by skin effects. In order to investigate the influence of in-well inertial and skin effects around the wells in heterogeneous aquifers on test results, based on the Herten analogue, four numerical cases of cross-well slug tests are designed:

Case 1: a test well and three observation points with the depths of 2 m, 4 m and 6 m, respectively;

Case 2: a test well and a 2 m deep observation well;

Case 3: a test well and a 4 m deep observation well;

Case 4: a test well and a 6 m deep observation well.

In fact, Case 1 can serve as a control case to compare pressure changes with or without observation wells. The other three cases are used to compare water level changes in observation wells at different depths considering inertial and skin effects. Firstly, to facilitate a comparison of the results impacted by the inertial effects between different cases and to distinguish the pressure diffusion process in aquifers and wells, three types of head changes at observation points, midpoints of the screen and water levels in the wells are monitored. Subsequently, a certain thickness of skin is added around both wells in each case. The water levels in each well are also recorded.

The settings of all cases are shown in Figure 3.6. The bottom of the test well is 4 m below the aquifer top. The radius of the riser pipe and screen are 0.017 m and 0.03 m, respectively. The screen length is 0.2 m. The horizontal distance between the test well and observation points or wells is 2 m. As mentioned in Section 3.2, the specific storage is defined as a spatially uniform value, which is set here 1×10^{-4} 1/m. We assume an initial head of zero everywhere in the aquifer with an initial displacement of the water level in the test well by 1 m.

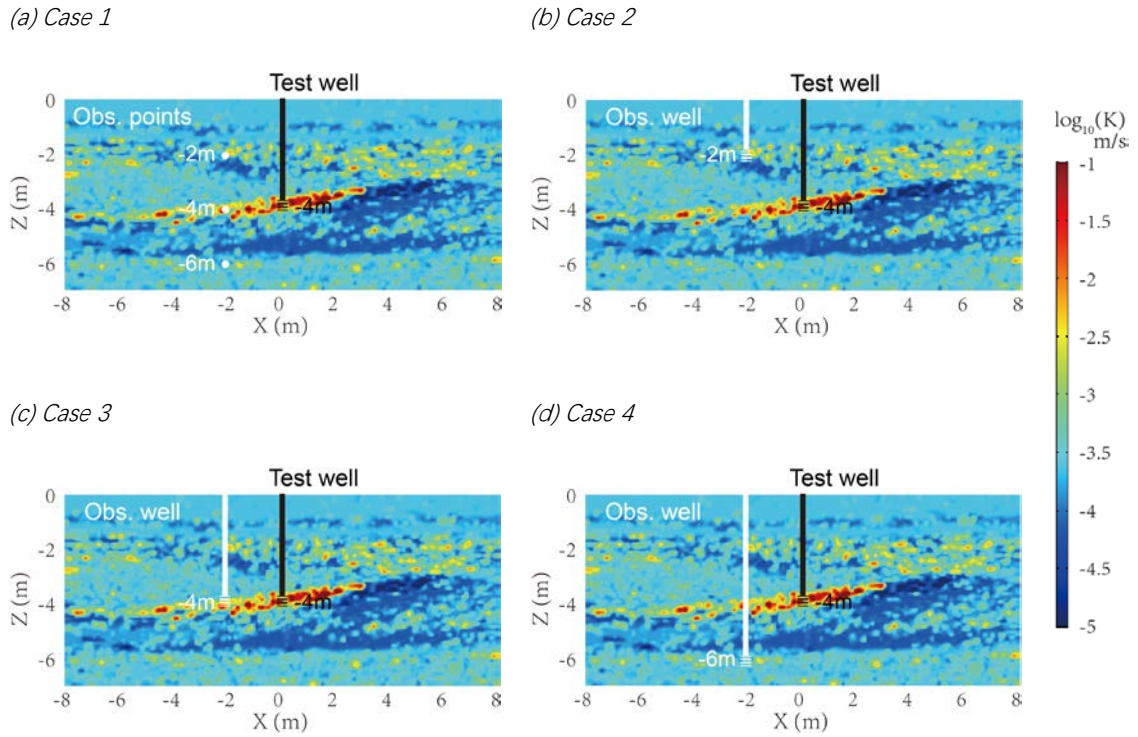

Figure 3.6: The settings of the four cases of cross-well slug tests in the view of the XZ-plane at Y=0.

The impact of inertial effects to the water level in the wells without skin effects are firstly assessed. After the simulations, four test-well normalized head curves are initially obtained (Figure 3.7a). As shown, the phases of these oscillatory curves are virtually identical, while the amplitudes are slightly different. Considering the curve of Case 1 as a reference, the curve amplitudes from Case 2 and Case 3 are increased especially at the first peak. In comparison, the head amplitude from Case 4 is always smaller. This result shows that the embedded observation wells have slightly interfered with the water level fluctuations in the test well. According to the superposition principle, the perturbation at the observation well can in turn influence the water level at the test well, especially when two wells are positioned at a short distance. This amplifies or damps the water level oscillations in the test well, depending on the embedded well depth and the hydraulic connectivity contrast between the test and observation wells. The head curve at the midpoint of the screen is utilized to replace the pressure change in the aquifer close by the test interval. The head curves at the midpoints of the screen in the four test wells are depicted in Figure 3.7b. All head curves have

a large attenuation and phase shift compared to the water levels, and the differences between these curves are reduced.

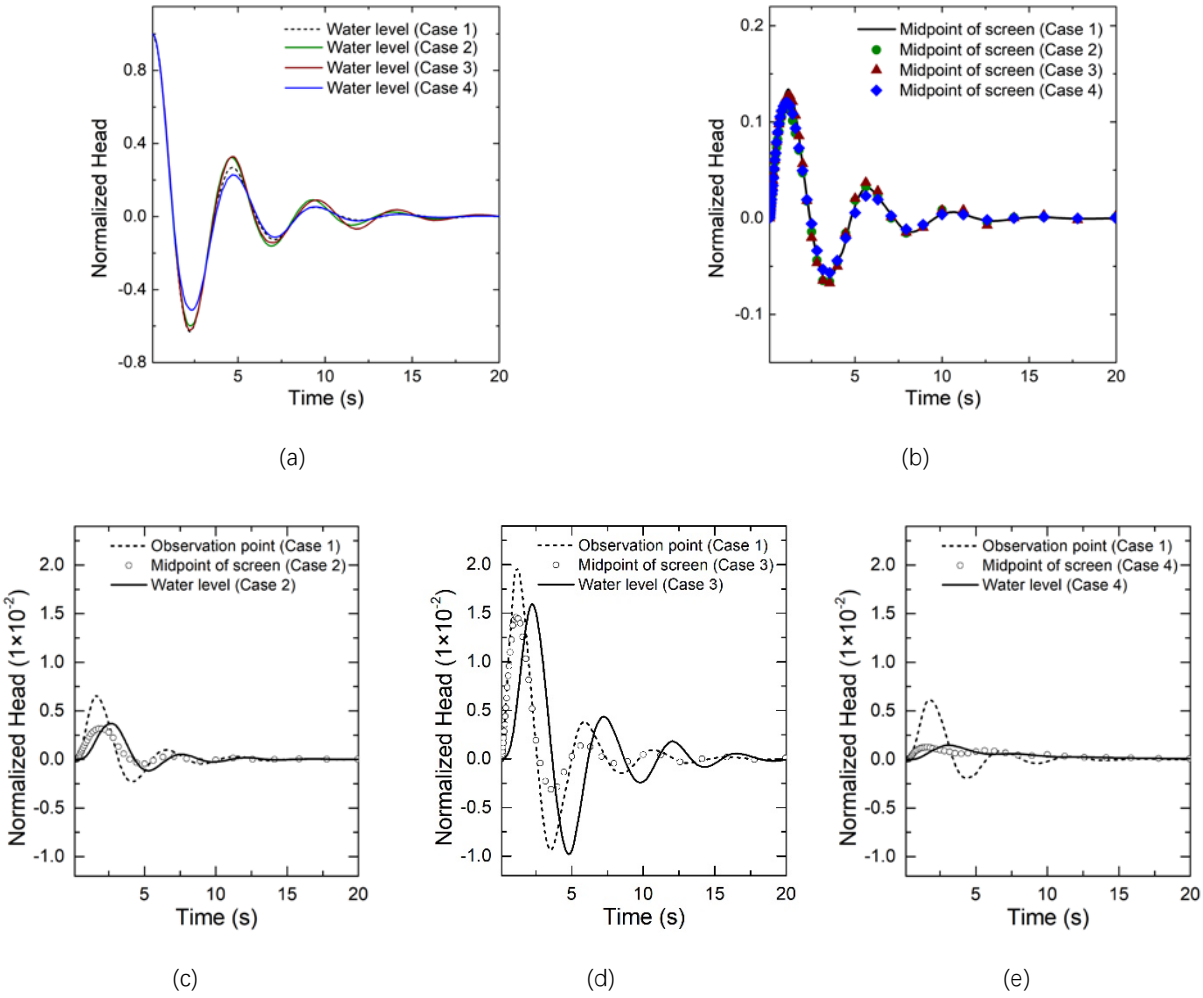

Figure 3.7: Normalized curves of (a) water level and (b) head at the midpoint of the screen in the test well, and the normalized head responses from the observation point, midpoint of the screen and the water level at the various observation wells/point depths of (a) 2 m, (b) 4 m, and (c) 6 m.

The head change curves from observation points or wells are plotted in Figure 3.7c - e, which includes three head curves of the observation points from Case 1, three water level curves and three head curves at the midpoint of each screen in the observation wells from Case 2, Case 3 and Case 4, respectively. Firstly, we compare the heads from the observation points (dashed lines) and the midpoint of the screen (circles) at the same depth to reveal the pressure changes in the aquifer before and after the installation of the observation well. It can be found, especially in Figure 3.7e, that the head of the midpoints of screen is significantly reduced. This reveals that the installation of the observation well reduced the normalized head amplitude near the observation interval.

Secondly, comparing the water level curves (solid lines) with the head curves at the midpoints of screen (circles), the influence of inertial effects in the well on water level fluctuations can be evaluated. The results show that the water level curves present obvious phase delay and amplitude change. Especially in Figure 3.7d, the amplitude of the oscillatory water level is significantly enhanced after the first peak. It implies that the inertial effect in the well can enhance the amplitude of the water level. However, in Figure 3.7c and e, the enhancement of the amplitude is not obvious, which indicates that this amplification may depend on the depth of the well and the aquifer heterogeneity.

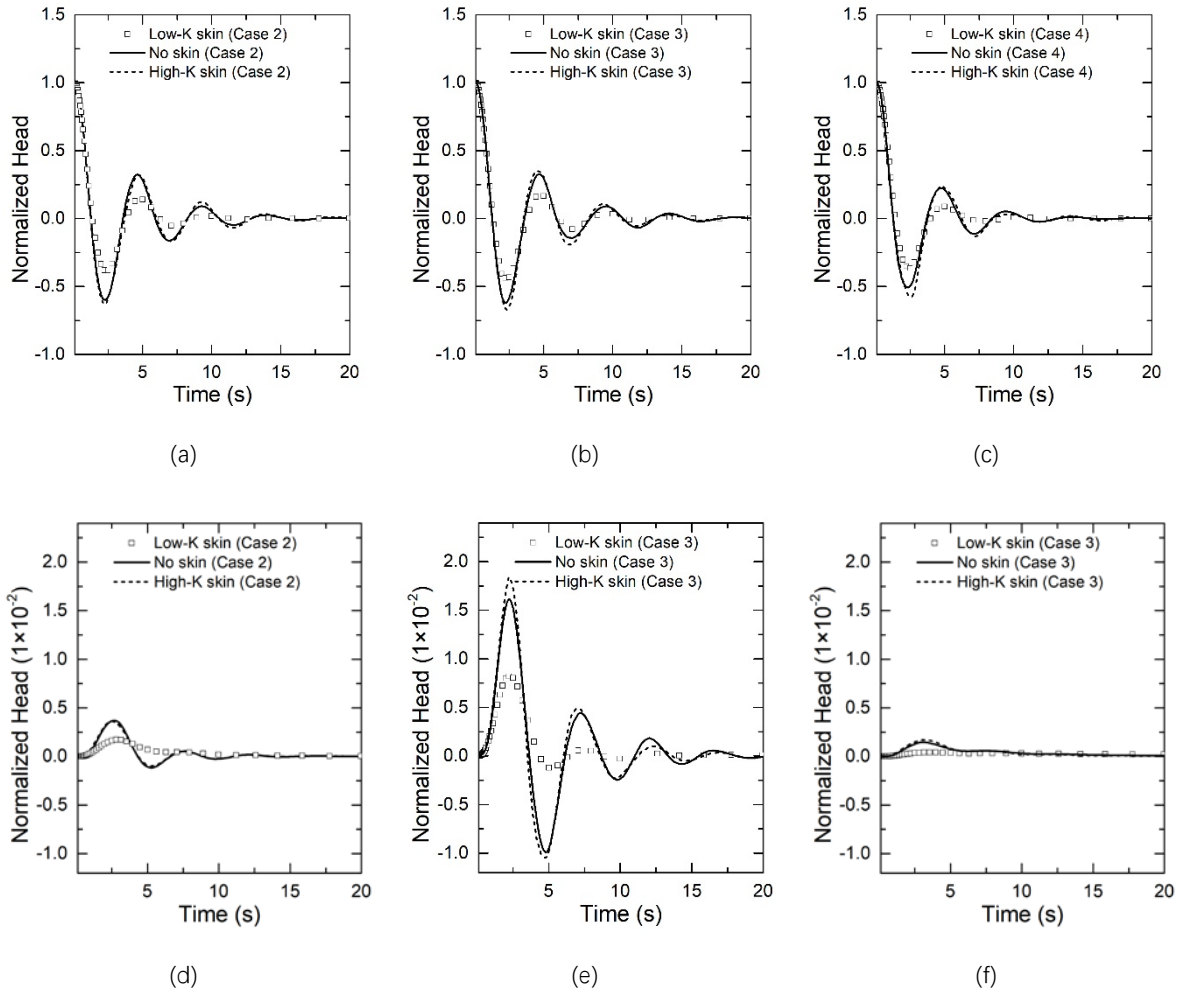

Figure 3.8: Normalized curves of water level in cross-well slug tests with low-k skin, no skin and high-K skin. The curves in (a) - (c) and (d) - (f) show the head responses at the test well and at the observation well in Cases 2, 3 and 4, respectively.

Considering the important role of skin effects in multi-well slug testing, their impact on the water level responses in test and observation wells is evaluated. Generally, the hydraulic conductivity of the skin can either be higher or lower than that of the ambient formation. Based on the outcrop analogue, a low-k and a high-k value, which are 0.1 times and 5 times of the original k, are therefore assigned to the simulated skin

around the wells. To eliminate the effect of the skin thickness on the simulated results, the infinitely thin skin model which has been used in well hydraulics field for decades (Dougherty & Babu, 1984; Faust & Mercer, 1984; Ramey et al., 1975) is adopted. The groundwater flow in the skin region is accounted for by the steady-state representation of the groundwater flow equation, which neglects elastic storage properties. Therefore, head changes caused by the different types of skin are only related to the ratio of the k value of the skin to that of the original formation. The impact of the skin effects can be demonstrated directly by comparing the head responses under various skin k-values. Based on the Cases 2, 3 and 4 shown in Figure 3.6, two additional series of cross-well slug tests with low-k skin and high-k skin are simulated. The results including the water level responses with no skin effect (shown in Figure 3.7) are both plotted in the Figure 3.8. The result reveals that the low-k skin has a much larger effect on the water level responses in the wells than high-k skin. The effect of the high-k skin is quite small, while the low-k skin significantly dampens the oscillatory behavior of the water level, especially in the observation well. These results are consistent with the findings in many previous studies (Butler et al., 1994; Hyder et al., 1994; Malama et al., 2011).

3.4 Discussion

3.4.1 Wellbore storage effects of observation wells

As shown in Figure 3.7c - e, after observation wells are installed, the pressure around the observation interval represented by the head at the midpoint of the screen is obviously attenuated. In fact, groundwater wells are often considered to be conduits for fast groundwater flow and contaminant migration (Chesnaux et al., 2006; Koh et al., 2016; Lacombe et al., 1995). This means, observation wells have the capacity to release the pressure rapidly from the aquifer, i.e. they may show wellbore storage effects. However, due to aquifer heterogeneity, the wellbore storage effects of the observation wells embedded at different depths are variable. For the observation depth of 4 m, the head amplitude in the aquifer is reduced only slightly before and after the observation well is installed, due to the highly permeable layer at about 4 m depth. In contrast, being embedded in a low conductivity zone, the head amplitude at the bottom of the 6 m observation well is strongly attenuated. If the observation well is considered as a fast flow conduit, the head amplitude at the midpoint of the screen directly reflects the conductivity near the observation interval. Accordingly, the wellbore storage effects of the observation well depends heavily on the conductivity distribution close to the observation interval. The higher the conductivity is, the stronger the wellbore storage effects could be.

To more clearly illustrate the relationship between the wellbore storage effects and aquifer heterogeneity, the XZ-plane profiles of the four cases at Y = 0 are chosen. Their normalized head contour maps at 2.3 s are shown in Figure 3.9. At this moment, the water levels in all test wells almost reach the minimum value and the heads at the bottom of these wells are around zero (see Figure 3.7a and b). Here the minimum value of the normalized head in the legend is adjusted to -0.01 to have the aquifer pressure gradient more clearly

displayed. Figure 3.9 illustrates that the contour line at the bottom of each observation well has shrunk inward. Especially in Figure 3.9d, due to the low conductivity, the contour line is concave at the bottom of the observation well. Moreover, comparing to Figure 3.9a, the influence range of the test wells in the other three maps is reduced, particularly in Figure 3.9b and 9d. In Figure 3.9c, this impact of reduction is relatively weak, because there is a good hydraulic connection between the observation and the test well. All these results indicate that the wellbore storage mechanism of the observation well will introduce a pressure redistribution according to the hydraulic conductivity in the vicinity of the observation interval.

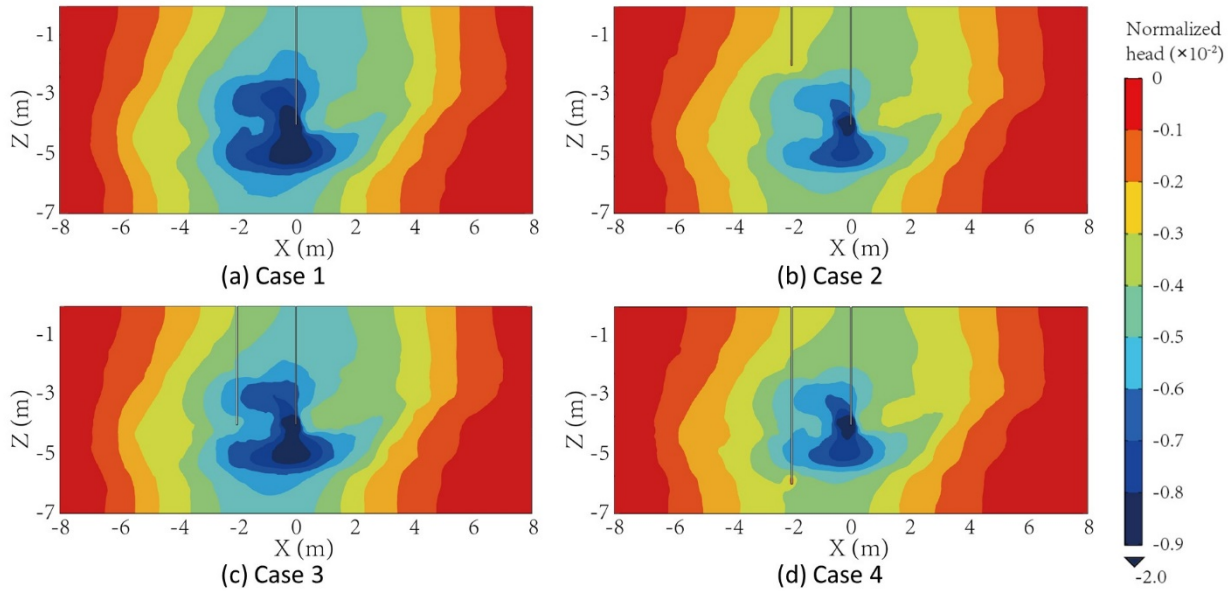

Figure 3.9: Normalized head contour map on the XZ-plane profiles (at Y=0m) of the four cases at 2.3s after slug test initiated.

For the test well, the difference of the hydraulic dissipation process in the four cases can also be attributed to wellbore storage effects. It has been discussed in numerous single-well slug test studies (Bredehoeft et al., 1966; Hyder et al., 1994; McElwee & Zenner, 1998) that the wellbore storage capacity recorded by the water level fluctuation is dominated by the aquifer hydraulic conductivity. However, in cross-well slug tests, the impact of wellbore storage effects will be more complicated, due to a pressure redistribution within the heterogeneous test volume and in turn an impact on the water level recovery in the test well (Figure 3.7a).

3.4.2 Inertial effect of the water column in cross-well slug tests

Another important factor influencing the cross-well slug test results is inertia of the water column moving inside the well. The inertial effect manifests as oscillatory well water level response. Butler and Zhan (2004) considered inertial effects by using the simplified momentum balance equation in their homogeneous slug test model and pointed out that inertial mechanisms can have a dramatic impact on the early-time drawdown.

However, so far these inertial effects are rarely considered in heterogeneous models.

In the presented analog outcrop study, the water level oscillations induced by inertial effects are obvious. When compared with the head curves at the midpoint of the screen in each observation well in Figure 3.7c - e, it is revealed that the water level curves not only show a phase shift but also an amplitude enhancement. To quantify the differences between these two types of curves, the maximum amplitude and its corresponding peak time are calculated and plotted in Figure 3.10. In Figure 3.10a, the peak times of these two types of curves are significantly different. The peak time of the water level is always larger. Aside from this, the difference line (dashed line) reveals a near-linear correlation between the peak time difference and the observation depth, i.e. the water column height. From the perspective of maximum amplitude, we can see that the values of the water level are slightly higher, especially for the 4 m observation depth.

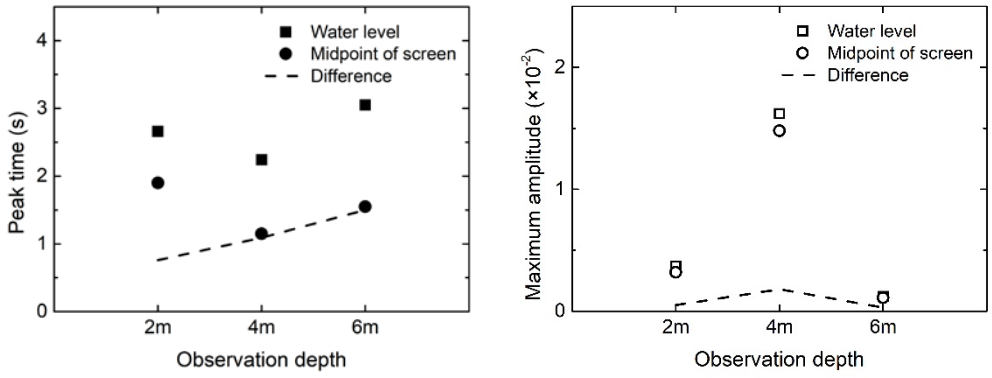

Figure 3.10: The peak time (a) and maximum amplitude (b) of the water level and head curves at midpoint of the screen at different depths of observation wells. The corresponding differences between water level and head at the midpoint of the screen are given by the dashed line.

Consideration of the hydrodynamic process in the well will inevitably lead to a peak-time delay of the water level compared to the head curve at the well bottom, and this delay should be proportional to the water column height in this well. In addition, the inertial effects can also enhance the water-level amplitude. Cooper et al. (1965) discussed this amplification effect of the well, which is used to describe the water level response to harmonic seismic waves. If the head excited in the test well is viewed as an attenuating wave source, the amplification theory can be equally applied to interpret water level response of the observation well in the cross-well slug tests. When the test is initiated, the observation well will show a response according to its “natural frequency”, which is determined by the well geometry and aquifer transmissivity. When the observation well and test well have a good hydraulic connection and follow a similar natural frequency, a water-level resonance may even occur. For example, in Case 3, the water-level amplitudes are significantly amplified, especially after the first peak (Figure 3.10d). Together with the water level curve in the test well,

a resonance behavior can be inferred in this case. However, the impact of the amplification effect will generally be diminished in space, because the hydraulic disturbance in the slug test is weak and will be further attenuated by the heterogeneous aquifer. In short, considering the well effects, such as inertial and wellbore storage effects, will result in a phase and amplitude change in the water level curves. Indeed, despite the amplification of the water level amplitude exists, it can take place only under special conditions, such as a very good hydraulic connection but a small distance between the test interval and the observation interval.

3.4.3 Potential error analysis without well effects

One of the main purposes of slug test modeling is to estimate aquifer parameters. Based on the corresponding relations established by the mathematical model, the heterogeneous parameters could be inverted through the water level response by using some inversion algorithms (Brauchler et al., 2007; Brauchler et al., 2011; Brauchler et al., 2010; Yang et al., 2015; Zhu & Yeh, 2005). However, the water level response not only represents the hydraulic signal propagation process within the aquifer but also the well effects. If these effects are not considered, the hydraulic parameters estimated directly from the water level will therefore include potential errors.

In early studies using heterogeneous models (Butler et al., 1994; Melville et al., 1991; Widdowson et al., 1990), groundwater flow in the well is neglected. Without well effects, these models cannot handle the oscillatory water level response, and the simulated head will not attenuate following the wellbore storage mechanism. This resulting estimation error can only be diminished in low conductivity aquifers with a large well spacing. Subsequently, although the groundwater flow in the well has been considered in some models, it is replaced by the Darcian flow with a high conductivity value (Brauchler et al., 2007; Yang et al., 2015). This means that it is still difficult to handle the oscillatory water level by these improved models, because the inertial term is ignored. However, the wellbore storage effects of the well are somewhat included. To date, the suitability of these models in highly permeable aquifers remains to be examined. Although the inertia-induced oscillation of the water level in observation well could be neglected when the distance from the test well is sufficiently large, McElwee et al. (1995b) pointed out that only an observation well fairly close to the test well, at a distance of about 10 m or less, can vastly improve parameter estimates, and it is suggested to use one or more observation wells. In order to improve the parameter estimation, a closer well spacing would be required. Moreover, previous work (Quinn et al., 2018; Zurbuchen et al., 2002) has shown that frictional losses within the well casing and screen play an important role in testing highly conductive media. Ignoring friction losses will lead to an underestimated hydraulic conductivity. This means that a more rigorous slug test model is needed, which can consider well effects, aquifer heterogeneity and head losses within the casing and at the screen.

3.5 Conclusions

In this work, 3DHIM, a 3D slug test model considering inertial effects both in test and observation wells in a heterogeneous aquifer is introduced. After inspecting various existing models of slug test analysis, two analytical solutions (Butler & Zhan, 2004; McElwee & Zenner, 1998) and a numerical solution of Butler et al. (1994) are chosen to compare the slug test results obtained using the new 3DHIM model. Based on a successful validation, this model is finally used to simulate a series of synthetic slug tests in a highly heterogeneous three-dimensional (3D) aquifer outcrop analogue, which has been developed during the excavation of unconsolidated glacio-fluvial sediments near the town of Herten in southwest Germany.

Single-well slug tests with varying well radius, water column height and screen length are firstly simulated within the synthetic heterogeneous aquifer. Unlike in a homogeneous aquifer, the results show that the water level oscillations in the test well are no longer sensitive to the screen length and water column height, but are heavily affected by inertial effects of the water column and by heterogeneity of hydraulic conductivity at the well test interval.

Based on the established single-well slug test model, three observation wells with different depths (i.e. 2m, 4m and 6m) are installed 2m away from the test well. Together with the single-well slug test (without observation well), the water levels and pressure changes in the aquifer in these four cases are compared to study the impact of inertial effects. Results show that the water level fluctuations do not only reflect the hydraulic signal propagation process within the aquifer but also wellbore storage and water column inertial effects. Specifically, wellbore storage effects at the observation well yield a pressure redistribution within the aquifer and a large water level amplitude change, which is related to the heterogeneity of hydraulic conductivity near the observation interval. The water column inertia in both test and observation wells will result in a phase shift of the water level fluctuation, which is proportional to the water column height. When the observation well and the test well have a good hydraulic connection and similar well geometry, the water level amplitude could be amplified. Therefore, if these effects are not considered, the hydraulic parameter estimation based on water level will potentially be incorrect.

Although the new 3DHIM model allows to consider water column inertial effects in heterogeneous aquifers, it still has some challenges. It assumes a linear friction force within the riser pipe and screen, and it ignores non-Darcian flow within the skin or aquifer. The influence of water column inertia on the parameter estimation in heterogeneous aquifer remains to be studied. In any case, the proposed model provides a reliable tool to explain the oscillatory water level response in a 3D heterogeneous aquifer.

4

Hydraulic tomography using slug test responses

Contents

This chapter is under preparation for:

Liu, Q., Hu, R., Hu, L., Xing, Y., Ptak, T.. (Submission to Water Resources Research in progress). Characterization of aquifer heterogeneity by tomographic slug tests considering wellbore effects.

Abstract

Slug tests provide an efficient way to obtain the spatial heterogeneity information of an investigated site. Combining with the imaging method of hydraulic tomography, they can present a broad application prospects in aquifer reconstruction. However, unlike pumping tests, the water level responses of slug test may be significantly affected by wellbore effects, especially for underdamped cases. This study proposes a new characterization framework for aquifer heterogeneity based on the water level responses recorded during cross well slug tests with tomographic arrangement. The peak head of each water level response and its corresponding time, i.e. the hydraulic travel time, are utilized in the inversion process, rather than the whole water level curves. To eliminate the influence of wellbore effects, two correction methods with respect to the hydraulic travel time and peak head amplitude are developed. Based on corrected data, the distributions of hydraulic diffusivity (D) and specific storage (S_s) are obtained through travel time-based and attenuation-based inversions, respectively. The new framework is verified by a series of simulated tomographic slug tests through a synthetic example based on an aquifer outcrop analog, where the hydraulic parameter distribution is known. The verification results indicate that the distributions of k and S_s are well estimated. With the same method, a field application is performed at a fractured rock experimental site located at Göttingen, Germany. Three potential transmissive fractures are revealed with the hydraulic conductivities varying from 6.9×10^{-5} to 3.4×10^{-4} m/s. The uncertainty of the inversion results is discussed for future studies and related applications.

4.1 Introduction

Slug test is a method for obtaining local hydraulic parameters of an aquifer, and is particularly suitable for the investigation of contaminated sites as it requires no additional water injection or extraction. Over the past few decades, slug test has been developed intensively in model and field testing techniques due to its simplicity of execution, low cost, and relatively short duration. Some slug test models have been improved to accommodate various scenarios, considering wellbore effects (Malama et al., 2011; McElwee & Zenner, 1998), partially penetrating wells (Butler Jr & Zhan, 2004; Hyder et al., 1994), and heterogeneous aquifers (Beckie & Harvey, 2002; Liu et al., 2020). To estimate the heterogeneity of aquifers, some novel testing techniques based on slug tests have also been proposed. For instance, multilevel and multi-well slug tests incorporating direct-push techniques have been implemented in field tests (Butler Jr et al., 2002; Lessoff et al., 2010). Hydraulic tomography is a well-established method for characterizing aquifer heterogeneity (Brauchler et al., 2013; Cardiff et al., 2020; Fischer et al., 2017; Paradis et al., 2016; Schöniger et al., 2012; Zha et al., 2018), whereby the spatial distribution of hydraulic parameters can be effectively estimated from head data collected in conventional hydraulic tests. In view of the above advantages of slug tests, hydraulic tomography based on slug tests presents a broad application prospect.

Compared with pumping tests, slug tests are quite competitive in terms of test time and economics. However, slug test responses are inevitably affected by wellbore effects, such as wellbore storage, water column inertia and well wall friction losses. Many studies pointed out that more pronounced water level oscillations can be observed when testing in highly permeable aquifers with smaller well radii, longer screen lengths, or larger water column heights (Butler, 2019; Butler Jr, 2002; Liu et al., 2020). This implies that the influence of wellbore effects needs to be considered in the hydraulic tomography inversion when using the slug test response. To account for wellbore effects, several forward slug test models have been developed by introducing the nonlinear momentum equations to describe the motion of water column in the well (Butler Jr & Zhan, 2004; Liu et al., 2020; Malama et al., 2011; McElwee & Zenner, 1998). However, this also poses a significant challenge to the inversion framework. That is, the forward slug test model is highly nonlinear, consisting of coupled in-well momentum equations and groundwater flow equations in the aquifer, making it difficult to incorporate into a partial differential equation-based hydraulic tomography inversion, such as the inversion strategy by Zhu and Yeh (2005). This could be one major reason why hydraulic tomography is rarely based on the slug test response.

To characterize aquifer heterogeneity through tomographic slug tests, excluding the wellbore effects from the observed slug test response can be an alternative. Zlotnik and McGuire (1998) derived a momentum equation to describe wellbore effects throughout a double-packer system in a test well. A similar equation is applied in the work of Zurbuchen et al. (2002), which transforms model-generated water level into transducer

readings in the water column. Quinn et al. (2018) further refined this equation in a field situation to predict aquifer pressure variations based on measured slug test responses from test wells. These studies imply that wellbore effects on slug test responses measured from test wells can be eliminated, but not for observation wells to date. Nevertheless, the influence of wellbore effects in observation wells is also evident during the tomographic slug test. For instance, a significant phase delay may occur between the water level response and the aquifer pressure at the observation location when observed in deep wells. Liu et al. (2020) revealed a quasi-linear correlation between this phase delay and the water column height in the observation well.

Brauchler et al. (2011) provides an alternative approach to remove the wellbore effects on the slug test response and successfully applies it to address aquifer heterogeneity at a field site. In their approach, the hydraulic travel time corresponding to the peak head of slug test response is utilized to invert the hydraulic diffusivity distribution of the aquifer. They assume that the wellbore effect is almost independent of aquifer heterogeneity and thus can be eliminated in an equivalent homogeneous aquifer at the target site characterized by preliminary hydraulic tests. A conversion factor is introduced, which is defined as the ratio of the ideal travel time propagating in the aquifer solely to the theoretical travel time calculated by an appropriate analytical solution including wellbore effects. This approach allows dealing with the impact of wellbore effects on travel time delays in both test and observation wells, but does not involve the hydraulic head attenuation, which may be important for specific storage estimates (Brauchler et al., 2013). Moreover, the conversion factor assumes a proportional relationship between the two travel times, which can lead to unreasonable estimates when the in-well travel time delay is considerable.

In this study, a new framework is presented for characterizing aquifer heterogeneity using tomographic slug tests that can be performed more quickly and economically than pumping tests. To exclude wellbore effects on hydraulic travel time of slug test responses, a linear correlation between the hydraulic travel time propagating in the aquifer and in both wells and the total travel time is established, which replaces the conversion factor introduced in Brauchler et al. (2011). The method of Quinn et al. (2018) is also used to correct the wellbore effects on the hydraulic head attenuation. Based on the corrected travel time and attenuation, the spatial distribution of hydraulic diffusivity and specific storage are reconstructed. This new characterization framework is then validated in a synthetic example based on an aquifer analog and further applied to a fractured rock experimental site located in Göttingen, Germany. Finally, the uncertainty of the inversion results is discussed, considering future research and related applications.

4.2 Methodology

4.2.1 Influence mechanism of wellbore effects on slug test responses

Cross-well slug test is one of the common field testing techniques for estimating the hydraulic properties of

aquifers. Figure 4.1 illustrates the setup of a pneumatic cross-well slug test in a heterogeneous aquifer and the head responses observed at different locations in the test and observation wells. The pneumatic cross-well slug test is initiated by instantaneous release of the injected gas in the riser pipe of the test well and is implemented by observing the water level responses in the riser pipes, which are recorded by the pressure transducers placed at a shallow depth below the static water level, e.g. the locations of the pressure transducers 1 and 4 shown in Figure 4.1. In practice, to obtain the spatial information on heterogeneity, a combination of multilevel slug tests with a straddle packer system, i.e., spaced target testing or observation intervals, is commonly used.

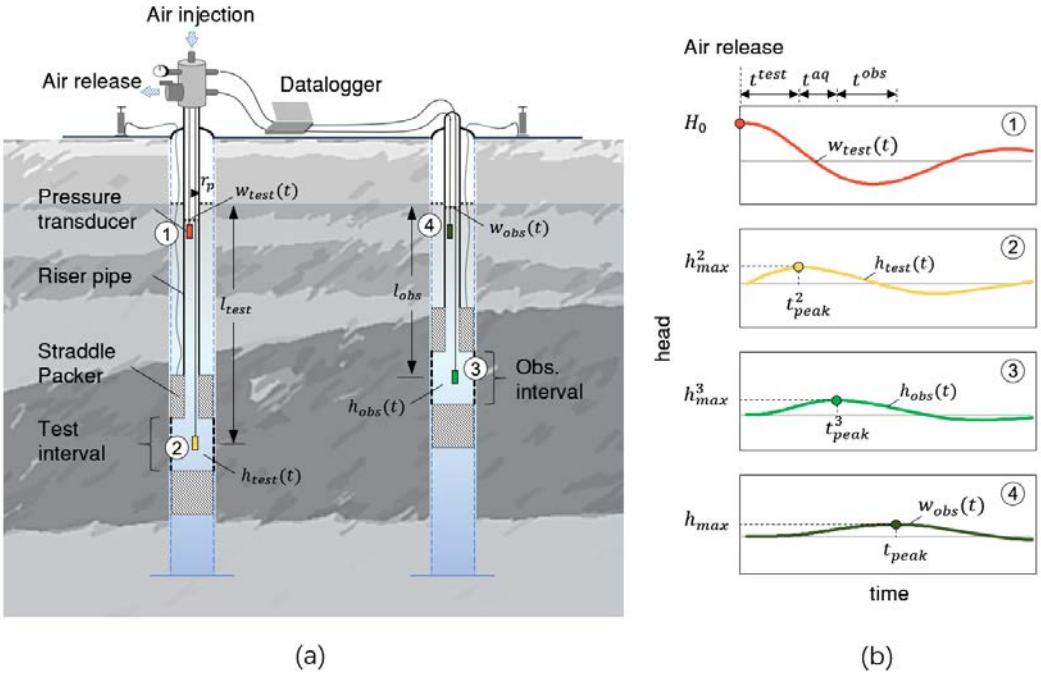

Figure 4.1: Sketch of a pneumatic cross-well slug test in a heterogeneous aquifer. (a) setup of pneumatic cross-well slug test, and (b) slug test responses at different locations in the test and observation wells

Tomographic slug test consists of a series of multilevel slug tests between several wells. Combined with a number of imaging methods, namely hydraulic tomography, the results of the tomographic slug tests can be used to reconstruct the aquifer heterogeneity. In a cross-well slug test, the test well can be considered as a Dirac source, and the water level response measured in the observation well is in the form of damped oscillations. Some studies declared that the first peak of the water-level response (h_{max}) and its corresponding hydraulic travel time (t_{peak}) are the two important features, which are related to the specific storage and hydraulic diffusivity, respectively. Therefore, only t_{peak} and h_{max} data need to be analyzed to obtain the heterogeneity, rather than the entire water level profile, which greatly reduces the computational cost in the inversion framework.

However, the measured t_{peak} and h_{max} are affected by many factors, not only by the hydraulic properties of the aquifer, but also by the radius of the riser pipe and the water column length. For instance, a larger water column length indicates a stronger water column inertia, which can lead to a significant delay in t_{peak} and changes in h_{max}. Figure 4.1b shows the hydraulic head observed by pressure transducer placed at the shallow depth of the riser pipes and at the test and observation intervals. A gradual time delay and head attenuation can be observed in the hydraulic signals measured from transducer 1 to 4. The aquifer-induced attenuation of hydraulic signal is only part of the water level attenuation measured in observation well. Therefore, if the observed t_{peak} and h_{max} are used directly, significant errors can be introduced in the parameter estimation process.

4.2.2 Characterization framework

Travel time-based inversion

In cross-well slug tests, test well can be considered as a pressure-pulse source. Based on the work of Vasco et al. (2000), the 3D propagation of a pressure pulse in the subsurface can be described by a line integral which relates the hydraulic travel time propagating in the aquifer (t^{aq}) to the hydraulic diffusivity (D),

$$\sqrt{t^{aq}(\boldsymbol{x}_r)} = \frac{1}{\sqrt{6}} \int_{\boldsymbol{x}_s}^{\boldsymbol{x}_r} \frac{1}{\sqrt{D(s)}} ds, \tag{4.1}$$

where $\boldsymbol{x}_s$ and $\boldsymbol{x}_r$ are the spatial locations of the source and the receiver. $D(s)$ is the distribution of hydraulic diffusivity along the propagation path (s), whereby the hydraulic diffusivity is defined as the ratio of hydraulic conductivity k over the specific storage S_s.

Correction method for hydraulic travel time

The observed hydraulic travel time (t_{peak} in Figure 4.1b) is a cumulative travel time consisting of the hydraulic travel time propagating in the aquifer (t^{aq}) and the hydraulic travel time propagating in the wells. Thus, the t^{aq} can be extracted by,

$$t^{aq} = t_{peak} - t^{test} - t^{obs}, \tag{4.2}$$

where t^{test} and t^{obs} are the hydraulic travel time propagating in the test well and observation well, respectively. Compared to t^{aq}, t^{test} and t^{obs} are less affected by the aquifer heterogeneity. Therefore, the hydraulic travel time propagating in the wells can be approximated in the case of a homogeneous aquifer that is hydraulically equivalent to the heterogeneous aquifer, for instance, the homogenized hydraulic parameters estimated by depth-integrated pumping test.

Specifically, the total hydraulic travel time observed in the observation well in the equivalent homogeneous

aquifer can be calculated by some analytical slug test models, such as the one proposed by Butler Jr and Zhan (2004), which is based on the estimated effective hydraulic parameters ($\bar{k}$ and $\bar{S}_s$) and the slug test configuration. Also, with the estimated $\bar{k}$ and $\bar{S}_s$, theoretical hydraulic time propagating in the aquifer ($\bar{t}^{aq}$) can be estimated by (Brauchler et al., 2007),

$$\bar{t}^{aq} = \bar{S}_s r^2 / 6\bar{k}, \tag{4.3}$$

in which r is the distance between the test and observation intervals. In addition, as the hydraulic travel time in the wells is highly dependent on the depth of the test or observation intervals, we assume that the t^{test} and t^{obs} are linearly related to the water column length (l) in the riser pipe. Therefore, in the equivalent homogeneous aquifer, Eq. (4.2) becomes,

$$\bar{t}^{aq} = c_1 \bar{t}_{peak} - c_2 l_{test} - c_3 l_{obs}, \tag{4.4}$$

where $\bar{t}_{peak}$ represents the hydraulic travel time observed in an observation well that calculated by Butler Jr and Zhan (2004) model. This model is perfectly suitable for our case because it incorporates the wellbore effects and can consider various well constructions. c_1, c_2, and c_3 are the correlation coefficients, which can be determined by using the regression analysis method through randomly adjusting the l_{test} and l_{obs} varying within the survey depth of the target site. It is worth noting that the c_1 will be reduced to the conversion factors defined in the paper of Brauchler et al. (2007), when the travel time delay caused by wellbore effects is also proportional to $\bar{t}_{peak}$.

In practice, the observed hydraulic travel time t_{peak} can be smaller than its theoretical value, for instance, when testing in a layer with the hydraulic conductivity much greater than its estimated homogeneous value. This would lead to a negative t^{aq} estimate by Eq. (4.4). To this end, a logarithmic transformation (base 10) is applied to the t^{aq} data. The multiple regression relationship between the hydraulic travel times and water column lengths can be then described as following,

$$log_{10}(\bar{t}^{aq}) = a_1 \bar{t}_{peak} - a_2 l_{test} - a_3 l_{obs}, \tag{4.5}$$

where a_1, a_2, and a_3 are the regression coefficients after the logarithmic transformation. Since the hydraulic travel time propagating in the wells are less sensitive to the aquifer heterogeneity, the three regression coefficients are assumed to be constant, and the actual hydraulic travel time propagating in the heterogeneous aquifer can be thus corrected by,

$$t^{aq} = 10^{a_1 t_{peak} - a_2 l_{test} - a_3 l_{obs}}. \tag{4.6}$$

Attenuation-based inversion

For slug tests, attenuation of the hydraulic head in the subsurface can be expressed by another line integral which links the attenuation of the head to the inverse of S_s. The line integral reads (Brauchler et al., 2011),

$$\left(\frac{h_{max}(\boldsymbol{x}_r)}{h_{max}(\boldsymbol{x}_s)}\right)^{-\frac{1}{3}} = B^{-\frac{1}{3}} \int_{\boldsymbol{x}_s}^{\boldsymbol{x}_r} \left(\frac{1}{S_s(s)}\right)^{-\frac{1}{3}} ds, \tag{4.7}$$

where $h_{max}(\boldsymbol{x})$ represents the peak of the head response at the location $\boldsymbol{x}$. $S_s(s)$ is the distribution of the specific storage along the propagation path (s). B is a constant during the inversion, which is defined as

$$B = \frac{\pi {r_p}^2}{\left(\frac{2\pi}{3}\right)^{3/2}} e^{-3/2}, \tag{4.8}$$

where r_p is the radius of the riser pipe. According to Eq. (4.7), it is crucial to obtain the h_{max} attenuated in the aquifer. As shown in Figure 4.1b, the h_{max} attenuation in the aquifer, equals the difference between h_{max} observed by transducer 2 and 3, is much smaller than that observed by the transducer 1 and 4. This means that the h_{max} attenuation in wellbore cannot be neglected.

Correction method for head attenuation

The h_{max} attenuation in the wellbore is mainly affected by the wellbore effects, such as the water column inertia and the friction loss, which are proportional to the movement speed of the groundwater in the well (Liu et al., 2020). Since the water movement in the test well is generally much faster than that in the observation well, we assume that the h_{max} attenuation in the observation well is neglected. To exclude the influence of wellbore effects in the test well, it is necessary to derive the hydraulic head changes at the test interval from the measured water level.

Treating the groundwater movement in the test well as a linear damped oscillator, the water level oscillation in the test well can be described by a complex exponential with four real constants (Quinn et al., 2018),

$$w_{test} = e^{\alpha - \gamma t + i(\varphi + \omega t)}, \tag{4.9}$$

where t is time, α and φ represent the amplitude and phase of the water level oscillation at $t = 0$, respectively. γ is the damping constant and the ω is the angular velocity of the water level oscillation. The four real constants can be determined by curve fitting, and the water level of test well can be delineated by Eq. (4.9). Note that this equation is based on an assumption of laminar flow.

To describe the relationship between the water level and the head measured by the deep pressure transducer, several models has been developed (Quinn et al., 2018; Zlotnik & McGuire, 1998; Zurbuchen et al., 2002). Considering the effects of water column inertia and friction loss in the wellbore, the head changes in the test interval (h_{test}) can be derived by (Quinn et al., 2018),

$$h_{test} = \left(c_a {w_{test}}'' + \frac{8\nu}{{r_p}^2} c_f {w_{test}}'\right)(l_{test} + w_{test})/g + w_{test}, \tag{4.10}$$

where ν is the kinematic viscosity of water, and g is the gravitational acceleration. c_a and c_f are the correction factors with respect to water column acceleration and friction loss, respectively. Details on the calculation of these two factors can be found in the study of Quinn et al. (2018). Therefore, the head changes in the test interval h_{test} can be corrected from the measured water level by Eq. (4.10) and the peak head at the test interval (h^{test}) can be accordingly obtained. Since the head attenuation in the observation well is neglected, the peak head at the observation interval (h^{obs}) approximately equals to the peak value of the water level measured in the observation well.

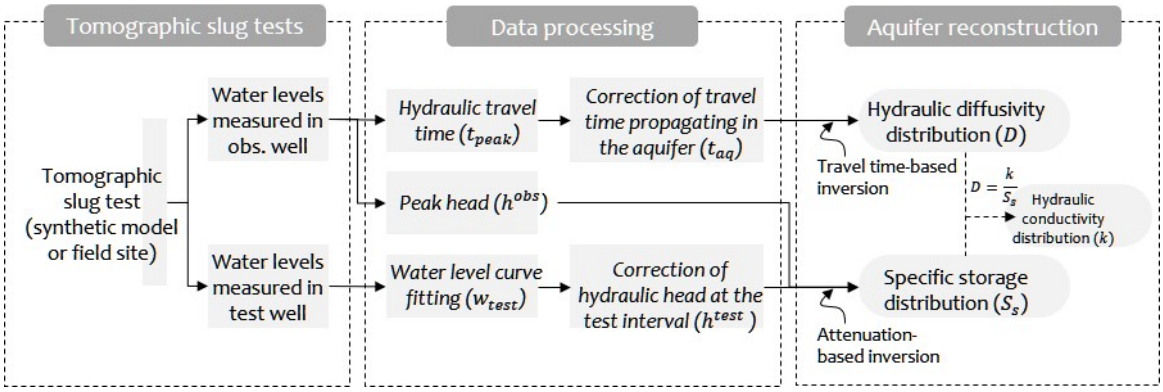

Figure 4.2: Characterization framework of aquifer heterogeneity using tomographic slug tests

In summary, to characterize the aquifer heterogeneity by the tomographic slug test, the first step is to extract the hydraulic travel time (t_{peak}) and peak head (h_{max}) from the measured water levels. Afterwards, the t_{peak} and the peak head at the test interval (h^{test}) are corrected according to the method introduced in Section 4.2 to exclude time delay and wellbore effects in the wells. Finally, corrected hydraulic travel time data (t^{aq}) and the peak head data (h^{test} and h^{obs}) are used to invert the hydraulic diffusivity and specific storage, respectively. Figure 4.2 shows the main steps of how aquifer heterogeneity is characterized in this study by using tomographic slug tests.

4.3 Synthetic case

4.3.1 Aquifer outcrop analog

In order to validate the proposed method, a synthetic case is first performed on an aquifer outcrop analog (Bayer, 2000). This aquifer analog was created by digitizing unconsolidated fluvial sediments located near the town of Herten in southwestern Germany during their ongoing excavation. Figure 4.3 illustrates the distribution of hydraulic conductivity and specific storage in the Herten analog. The size of this analog is 16 m × 10 m × 7 m, and the resolution of the parameter distribution is 0.1 m × 0.1 m × 0.1 m. Hydraulic conductivity (k) varies from 6×10^{-7} m/s to 1 m/s. Relatively high k zones with k values above 0.0025 m/s can be observed in the middle of the aquifer (Figure 4.3b). The specific storage (S_s) in the Herten analog

varies from 3.6 × 10^{-5} 1/m to 2 × 10^{-4} 1/m. In Figure 4.3d, a relatively high S_s layer (>1 × 10^{-4} 1/m) can be seen at depths between -27 m and -26 m. The major advantage of using an outcrop analog in this study is that the distribution of hydraulic parameters is known and can be readily compared with the aquifer reconstructed from tomographic slug tests without the need for physical efforts.

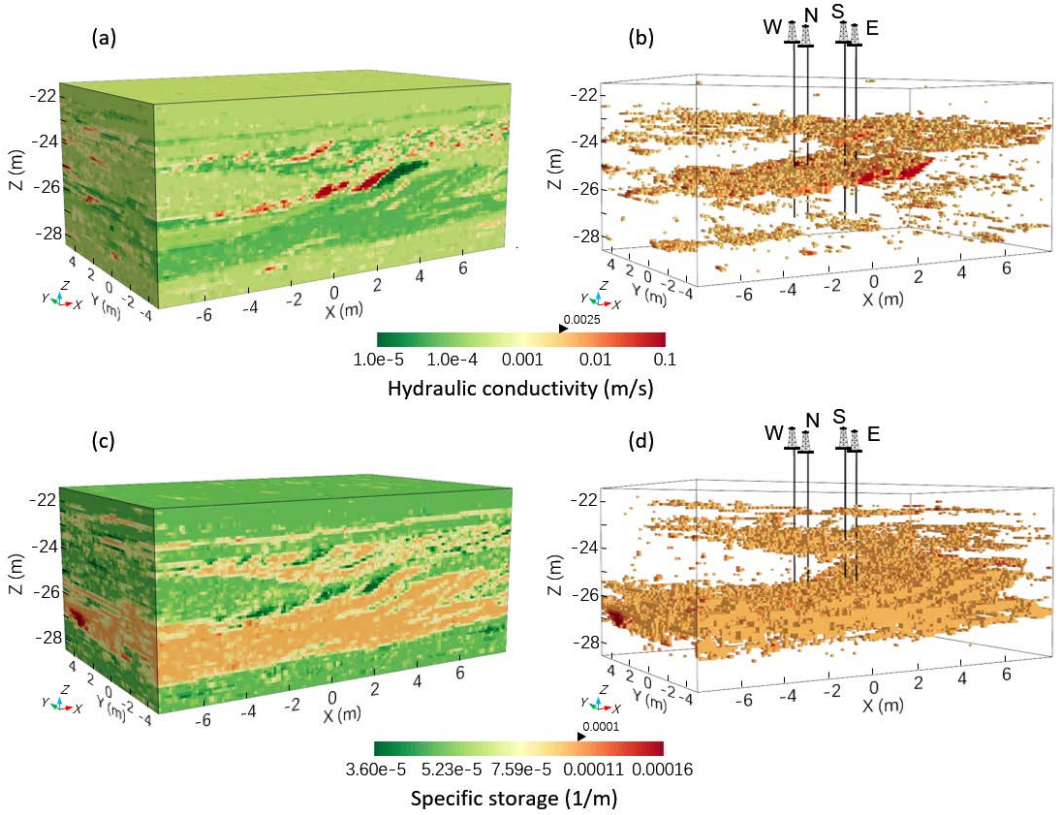

Figure 4.3: Aquifer heterogeneity of the Herten analog: hydraulic conductivity distribution (a) in 3D-view and (b) greater than 0.0025 m/s, and the specific storage distribution (c) in 3D-view and (b) greater than 0.0001 1/m. Note that the colors indicate log scale.

4.3.2 Tomographic slug tests

In order to perform tomographic slug tests on the Herten analog, a slug test model that considers both heterogeneous aquifers and wellbore effects is required. Liu et al. (2020) developed a three-dimensional numerical slug test model (3DHIM) that fulfills this requirement. In the 3DHIM model, groundwater flow in the aquifer follows Darcy's law, while in the wellbore it is governed by the Navier-Stokes equation. These two governing equations are coupled by the velocity and pressure continuity conditions on the well screen. To track the oscillating water level in the riser pipe, a free-moving boundary is assigned on the water surface by using an arbitrary Lagrangian-Eulerian method. For more details on the 3DHIM model, please refer to the paper by Liu et al. (2020).

As shown in Figure 4.3b, four groundwater wells (W, E, S, and N) are installed in the center of the Herten analog. Wells W and E are aligned along the X-axis at Y = 0 m, and the distance between these two wells is 3 m. Wells S and N are aligned along the Y-axis at X = 0 m, also at a distance of 3 m. The Herten analog is set as a confined aquifer located between Z = -28.5 m and -21.5 m, where Z = 0 represents the depth of the static water level.

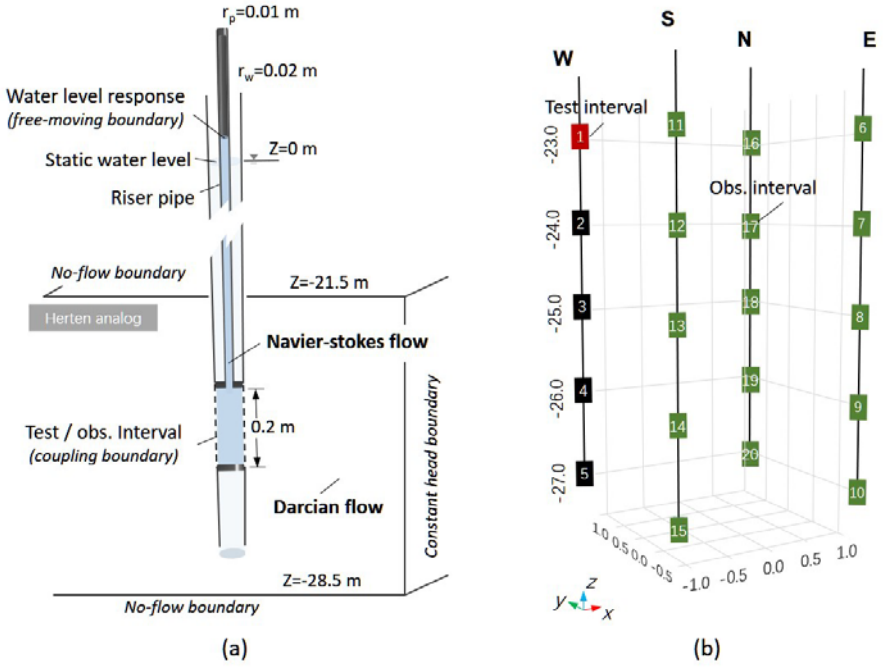

Figure 4.4: Design of the tomographic slug test in the Herten analog. (a) The settings in the 3DHIM slug test model and (b) arrangement of the test and observation interval locations.

Figure 4.4 shows the detailed settings in the 3DHIM slug test model and the arrangement of test and observation intervals in the tomographic slug tests. The model settings in these four wells are similar, except that the initial displacement of the test well is 0.1 m. As shown in Figure 4.4a, the well radius is 0.02 m, the radius of the riser pipe is 0.01 m, and the screen length is 0.2 m. The top and bottom boundaries are no-flow boundary, and the side boundaries are constant head boundary. Skin area is not considered in the slug test model as it will obscure the focus of this study. To form a tomographic slug test, five screen intervals are settled in each well at the depths from -27 m to -23 m. The distance between adjacent screen intervals is 1 m. The specific arrangement of test and observation intervals is illustrated in Figure 4.4b. Taking the first screen interval of well W as an example, when an initial displacement of 0.1 m is slugged in well W, this pressure pulse will be received by the 15 observation intervals (Figure 4.4b). After switching through the 20 test interval locations, a total of 300 cross-well slug tests are simulated, and 300 water level curves are obtained in the test well and observation well, respectively.

4.3.3 Correction for hydraulic travel times and head attenuations

According to the simulation results, the 300 t_{peak} and h^{obs} values are extracted from the water level responses of the observation well, and the h^{test} data are also obtained from the water levels of the test well. Following the method introduced in Section 4.2, the following step is to correct the t_{peak} and h^{test} data to exclude the wellbore effects. Firstly, in order to obtain the hydraulic travel time t^{aq} propagating through the aquifer only, a single-well slug test is performed in the 3DHIM model to preliminary estimate the effective hydraulic parameters of the Herten analog. The test well is fully penetrating and installed at the center of the analog. According to the water level response, the effective $\bar{k}$ and $\bar{S}_s$ are estimated to be 4.72 × 10^{-4} m/s and 8.45 × 10^{-5} 1/m, respectively. With the same well configuration as presented in Figure 4.4a, a cross-well slug test model with a well distance of 3 m is then established by using the Butler Jr and Zhan (2004) model. After randomly specifying 8 intervals in the test and observation wells, 64 cross-well multilevel slug tests are analyzed. Based on the calculated $\bar{t}_{peak}$, the depth of test interval l_{test} and depth of observation interval l_{obs}, and the theoretical $\bar{t}^{aq}$ calculated by Eq. (4.3), a multiple regression model in the form of Eq. (4.5) is built up. The three regression coefficients a_1, a_2, and a_3 are 0.58, 0.085, and 0.072, respectively. According to Eq. (4.6), the t^{aq} propagating in the Herten aquifer can thus be extracted. As the larger t_{peak} data simulated in the Herten analog will be severely magnified through the logarithmic transformation, the extracted t^{aq} data greater than 1 s are discarded. Afterwards, to correct the peak head at the test interval (h^{test}), each simulated water level of the test well is fitted by Eq. (4.9) to determine the four coefficients. Hydraulic head changes at the test interval are then derived by Eq. (4.10), and the h^{test} can be thus obtained.

To illustrate the impact of wellbore effects, the corrected data are compared with the corresponding simulated values and plotted in Figure 4.5. Hydraulic travel times are summarized according to the different test interval locations marked in Figure 4.4b and depicted in Figure 4.5a~d according to the well to which the test interval belongs. The results indicate that the t_{peak} delay due to wellbore effects can be greater than 4.5 s. Most of the corrected t^{aq} data are less than 0.5 s, and the distribution of corrected t^{aq} data corresponding to different test interval locations pose a significant difference. For instance, when the test interval locations are at depths around 25 m, i.e. locations 3, 8, 13, and 18, all their corrected t^{aq} gathers to the smaller values less than 0.3 s. According to Eq. (4.1), this implies that a high hydraulic diffusivity (D) layer could exist around the depth of 25 m. Additionally, head attenuation ratios (h^{obs}/h^{test}) sorted by the test interval location are plotted in Figure 4.5e~h. It can be seen that the corrected head attenuation ratio is always greater than or equal to the simulated data, because the attenuation of h^{test} caused by wellbore effect is considered in corrected ratios. For each test interval location, a quasi-linear relationship is presented between the corrected and simulated ratios. This is because the attenuation of h^{test} for the same test interval is hardly affected by the observation interval locations and the h^{obs} attenuation is ignored. However, the slope of the linear relationship between the corrected and simulated ratios reflects the effects of wellbore on the head attenuation in the test well. The higher the slope is, the greater wellbore effects could be. As shown

in Figure 4.5e~h, significant wellbore effects happen at the test interval locations nearby 25 m that is inferred by the hydraulic travel times to be a high D layer. It implies that the high D layer estimated by travel times is also significant for the specific storage estimates.

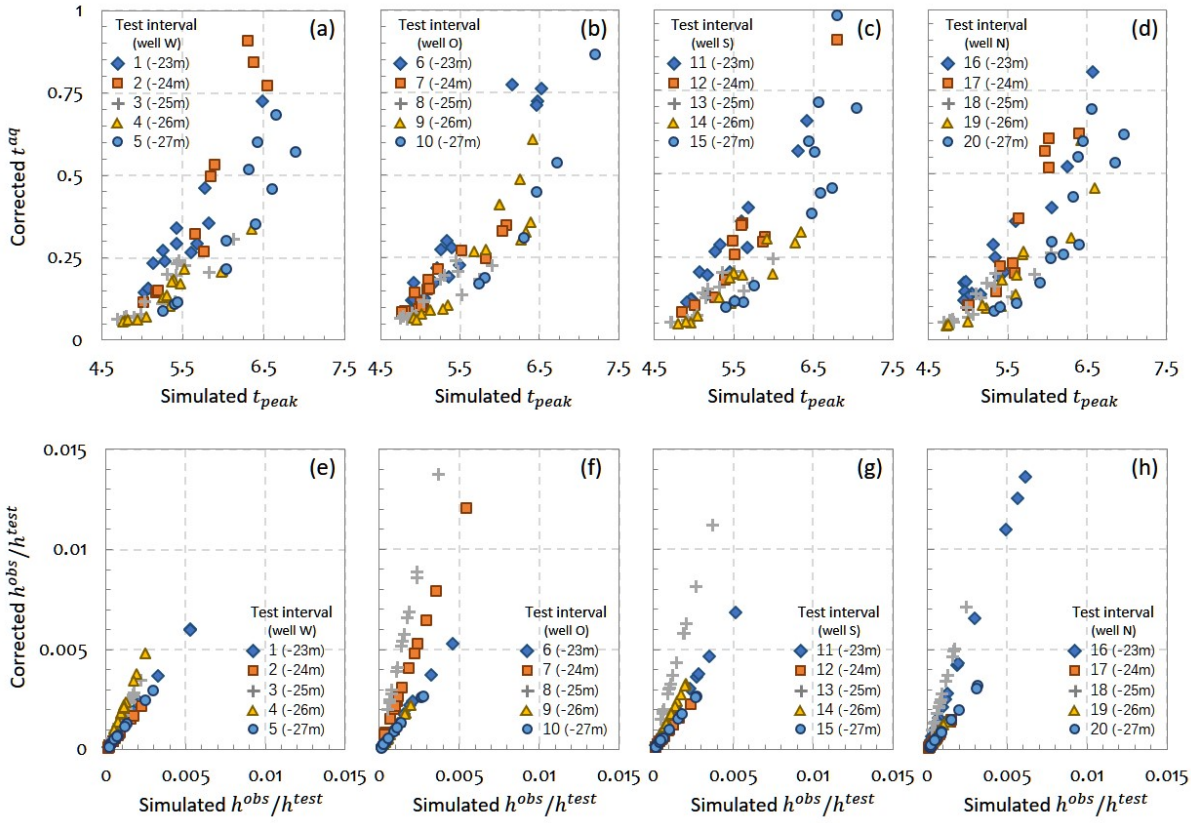

Figure 4.5: Influence of wellbore effects on the hydraulic travel time (t_{peak}) and head attenuation ratios (h^{obs}/h^{test}) by comparing the corrected data with the corresponding simulated data. All data are summarized according to the different test interval locations.

4.3.4 Aquifer reconstruction of the Herten analog

Characterizing the aquifer heterogeneity in this study is to solve the two inverse problems described by Eqs. (4.1) and (4.7). Both of these two equations belong to the eikonal equation, which has been intensively discussed in solving the shortest-path problem, computed tomography, and seismic travel time inversion. To solve Eqs. (4.1) and (4.7), the TravelTime module in the geophysical library pyGIMLi (Rücker et al., 2017) is adopted, although it is originally developed for seismic travel time inversion. Liu et al. (2022) successfully applied this module to reconstruct the hydraulic conductivity profile using the thermal travel time data. Therefore, based on the corrected t^{aq} and h^{test} data, the spatial distribution of hydraulic diffusivity and specific storage in the Herten analog can be reconstructed.

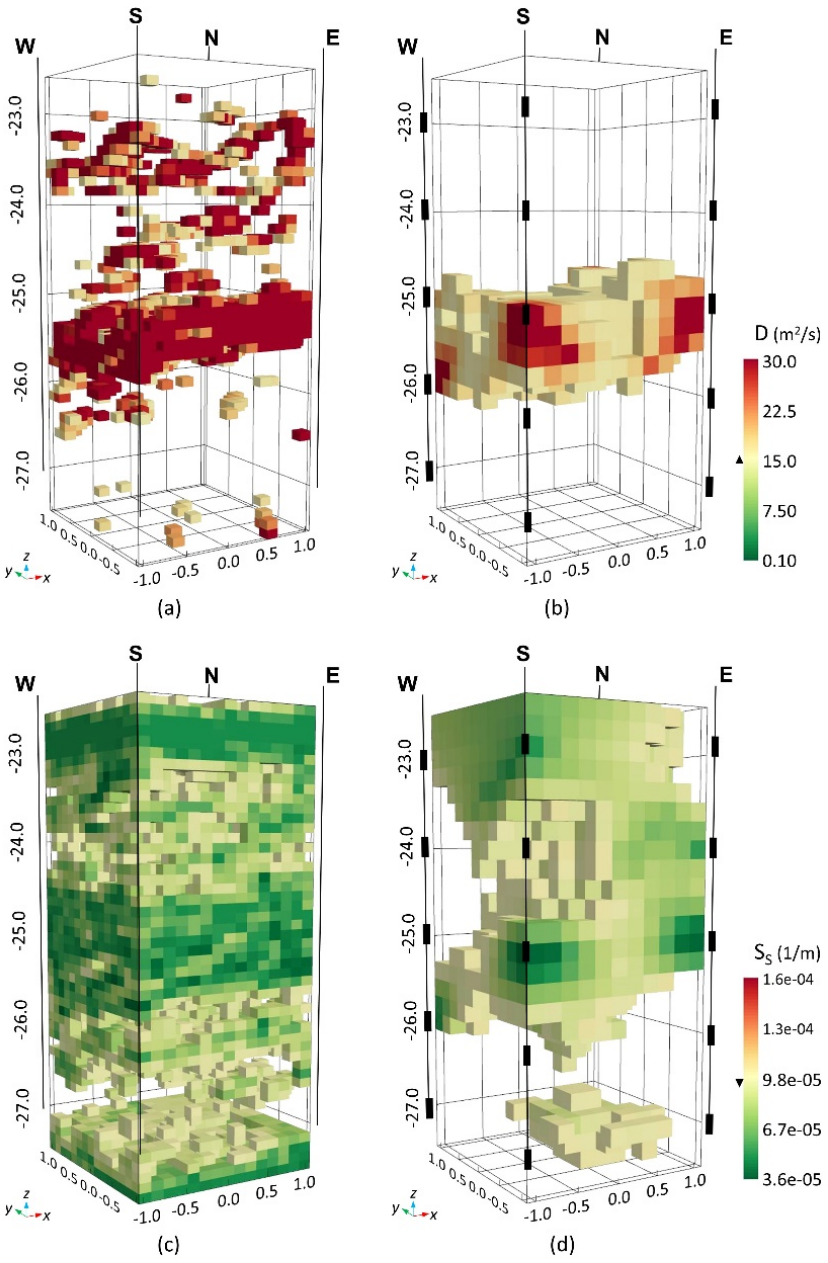

Figure 4.6: Aquifer reconstruction of the Herten analog. The upper plots represent (a) the "true" D distribution and (b) the reconstructed D distribution, and the bottom plots represent the (c) the "true" S_s distribution and (d) the reconstructed S_s distribution.

In the inversion framework, the model size sets to 2.12 m × 2.12 m × 5 m, i.e. the space between the four wells within depths from -27.5 m to -22.5 m. A structured 3D mesh with the equal cell side of 0.2 m is employed. A total of 253 t^{aq} values is utilized for the travel time-based inversion, except for the discarded outliers caused by logarithmic transformation. Also, all 300 h^{test} and h^{obs} values are used in the attenuation-based inversion. The inversion results are depicted in Figure 4.6, whereby the plots on the left side represent the "true" distribution of the Herten analog. The inverted hydraulic diffusivity (D) by the travel times can be validated by comparing the results shown in Figure 4.6a and b. It shows that the high D

layer (greater than 15 m^2/s) at the depth from -26 m to -25 m is well reconstructed. Some thin high-D layers above 25 m are not identified, possibly due to the insufficient test and observation intervals. The magnitude of the inverted D within the high D layer is smaller than the "true" value, which can be related to the correction method for t^{aq} data. Since the regression coefficients determined by the equivalent homogeneous slug test model are assumed to be constant, they may not perfectly match the high D layer and thus introduce errors in the inverted D values.

Additionally, the inverted S_s is plotted in Figure 4.6d. The S_s zone lower than 9.8×10^{-5} 1/m is illustrated because the attenuation-based inversion is solved by calculating the trajectories, which tend to bend towards the lower S_s zone due to the negative exponent in Eq. (4.7). Compared the inverted S_s with the "true" distribution (Figure 4.6c), it can be found that two low S_s layer at the depths about 23 m and 25 m are well reconstructed. The low S_s layer at the bottom (about 27.5 m) is not identified because it covers fewer test or observation intervals. The inverted S_s values are overall slightly higher than the corresponding "true" values, especially near some test interval locations, such as locations at 25 m of well W and at 23 m of well E. The overestimation of S_s values could be due to the correction method for h^{test} data, for instance the error caused by curve fitting and by the possible non-laminar flow at the early time. Still, the aquifer heterogeneity of Herten analog is well characterized by using the proposed method.

4.4 Field application

4.4.1 Field tomographic slug test

The field application was carried out in 2020 at the fractured rock experimental site located at the north campus of the University of Göttingen, Germany. At this site, five groundwater wells with a depth of 80 m are arranged in a cross shape. In order to independently investigate the hydraulic properties of the different strata, each well was divided into nine filter sections. The screen filters are 5 m long and were installed alternately with 3 m impermeable casing. According to the hydrogeological background investigated in some previous studies (Baetzel, 2017b; Qiu, 2020; Werner, 2013; Yang, H et al., 2020), highly permeable fractures are mainly developed within the shallow 40 m, particularly between wells M and O. Therefore, the focus of this study is on the upper 40 m zone between wells M, O, and S.

The configuration of the slug test is shown in Figure 4.7. The distances from well M to wells O and S are 1.9 m and 3 m, respectively. Four screen filters were installed in the upper 40 m of each well (Figure 4.7a). According to the tomographically experimental design, when the slug test was initiated at a screen filter of the test well, 8 water-level response curves can be measured at the observation intervals in the two other observation wells. Therefore, a total of 96 cross-well slug tests were performed at this site. For the fieldwork, a pneumatic slug test setup similar to the one shown in Figure 4.1 was used. Details of the well structure and

straddle-packer system are depicted in Figure 4.7b. The radius of the wellbore and riser pipe are 0.04 m and 0.01 m, respectively. A straddle-packer system was employed to separate the 5 m screen filter. Pressure transducers were placed approximately 1 m below the static water level in the riser pipes. The initial displacement for each slug test was maintained at 1 m. During the tomographic slug test, 96 water level curves were measured in the test well and observation well, respectively.

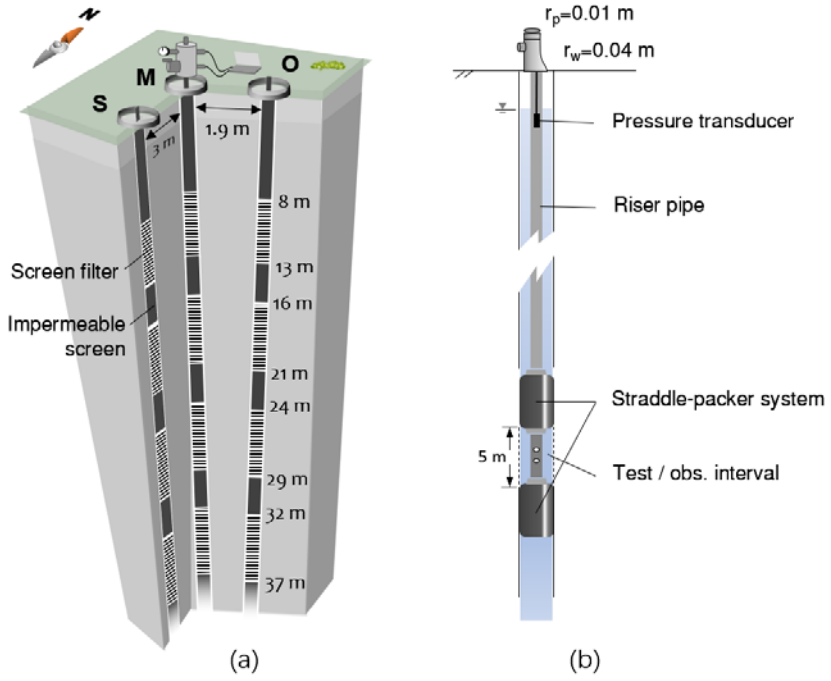

Figure 4.7: The configuration of tomographic slug tests in the field application: (a) the well arrangement and the screen filter locations, and (b) the well construction and the straddle-packer system

4.4.2 Characterization of aquifer heterogeneity at the experimental site

Following the steps introduced in Figure 4.2, an inference depth-integrated pumping test between wells M and O was conducted. The integrated $\bar{k}$ and $\bar{S}_s$ are 7.5 × 10^{-5} m/s and 1 × 10^{-6} 1/m. Based on the configuration of the slug test, a homogeneous cross-well slug test model of the experimental site was built up using the Butler Jr and Zhan (2004) model. After that, through randomly specifying 8 test and observation intervals in the homogeneous slug test model, a multiple regression model defined as Eq. (4.5) was established based on the calculated hydraulic travel times. The regressions coefficients a_1, a_2, and a_3 are estimated to be 0.368, 0.054, and 0.052, respectively. t^{aq} data were then extracted by Eq. (4.6), and h^{test} data were also corrected by using the method described in Section 4.2.

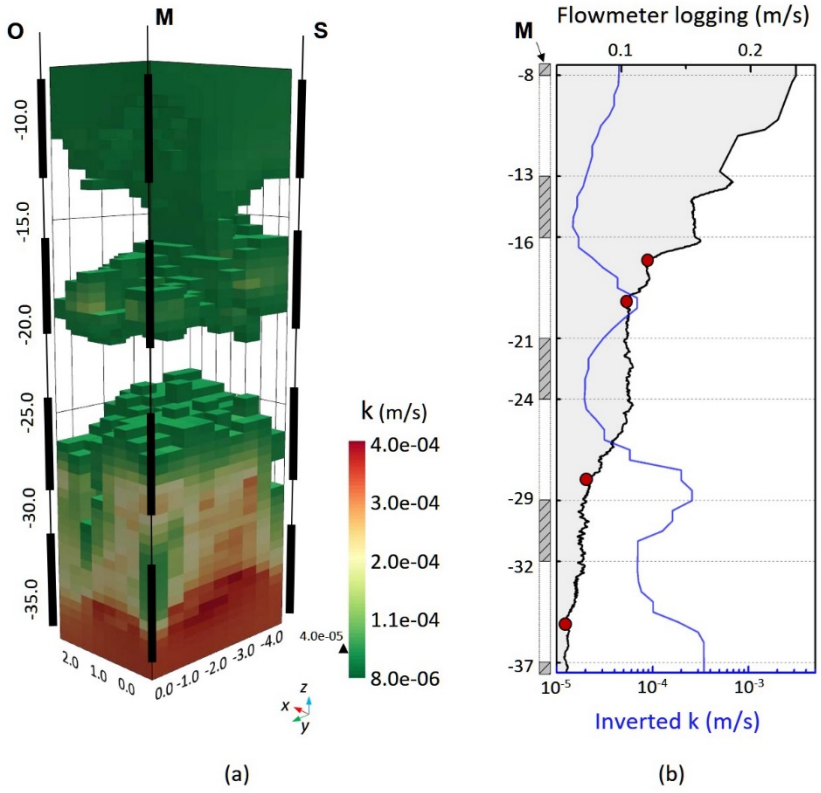

Figure 4.8: (a) Inversion result of k distribution of the fractured rock experimental site located at Göttingen, Germany, and (b) comparison of the inverted k and flowmeter logging in well M, in which the red dots represent the identified locations of the transmissive fracture.

The corrected 82 hydraulic travel times were utilized in travel time based inversion, except for the t^{aq} (greater than 8 s) distorted by the log-transformation. And all 96 peak heads are utilized in the head attenuation-based inversion. The inversion model is a rectangular area between wells M, O, and S, with a size of 3.2 m × 4.5 m × 30 m considering the drilling deviation of the boreholes. A structured mesh is adopted and the side length of each cell is 0.4 m× 0.5 m × 0.5 m. In order to reveal the hydraulic properties of the transmissive fractures at this site, hydraulic conductivity (k) distribution can provide a more intuitive result than the distributions of D and S_s. Based on their relationship ($D = k/S_s$), the k distribution can be obtained by multiplying the inverted D and S_s. After inversion iterations, the distributions of D and S_s for this site were derived and plotted in Appendix A3. The calculated k distribution is depicted in Figure 4.8a. The calculated k values vary from 6.7×10^{-6} to 4.4×10^{-4} m/s, and three high-k zones are revealed in Figure 4.8a at the depths above 12 m and around 19 m, and below 27 m. In particular, at the depths of about 19 m and 35 m, the inverted k distribution shows a good connectivity between these three wells. To validate the inversion results regarding the transmissive fracture locations, the inverted k profile of well M is compared to its vertical flowmeter logging result. The comparison is shown in Figure 4.8b. The four red dots on the flowmeter logging curve represent the locations of the identified transmissive fractures in well

M. The sudden increase in the first screen interval (from 8 m to 13 m) is not considered as fracture locations because of the geological context of this site, i.e. the Quaternary sediments with a thickness of about 13 m (Werner, 2013). By comparison, it indicates that the depths of the inverted high-k depths are in good agreement with the fracture locations determined by flowmeter logging. These three inferred fractures have k values ranging from 6.9×10^{-5} to 3.4×10^{-4} m/s.

4.5 Discussion

4.5.1 Uncertainty in hydraulic diffusivity estimates

Although the distributions of the hydraulic parameters (D and S_s) have been well estimated in the synthetic example, it is still necessary to discuss the uncertainty of the inversion results considering further studies and related applications. For the estimation of D, small differences between the inverted D and the "true" values can be observed in Figure 4.6. According to the inversion method introduced in Section 4.2, the quality of the correction of the t^{aq} data is crucial, and is mainly influenced by two factors, namely the effective hydraulic parameter estimated from conventional hydraulic tests and the logarithmic transformation processing.

To test for uncertainty in the corrected t^{aq} data due to poor estimation of the effective hydraulic parameters, it is assumed that the value of estimated hydraulic conductivity $\bar{k}$ in the synthetic example is 1×10^{-4} or 1×10^{-3} m/s, instead of the appropriate value of 4.72×10^{-4} m/s. And the value of $\bar{S}_s$ remains 8.45×10^{-5} 1/m because it is less sensitive to the slug test. Following the method introduced in Section 4.2, the corrected t^{aq} data with respect to the two assumed $\bar{k}$ can be obtained. Additionally, to assess these corrected t^{aq} data, a tomographic slug test without setting wellbores in the Herten analog is supplemented. That is, the slug test is performed using a Gaussian pulse at the points arranged as the configuration shown in Figure 4.4b. This supplementary test provides the "true" t^{aq} data without the influence of wellbore effects.

The validation results regarding the corrected data are depicted in Figure 4.9**.** All corrected t^{aq} data for the three $\bar{k}$ values are compared to the "true" t^{aq}, and the results are depicted in Figure 4.9a. It can be observed that most t^{aq} data varies within 0.5 s. These early t^{aq} data are corrected better than the late travel times, which are mostly overestimated. Since the early t^{aq} data are crucial for high D zone estimates, the t^{aq} data for the three $\bar{k}$ values within 0.2 s are compared in the zoom-in view. It illustrates that if the $\bar{k}$ is of 1×10^{-4} m/s, the early t^{aq} data are overestimated, and can be slightly underestimated for the $\bar{k}$ of 1×10^{-3} m/s. This means that when the $\bar{k}$ is underestimated by conventional hydraulic tests, the early t^{aq} data will be overestimated, resulting in an underestimation of the inverted values in high D zones, and vice versa.

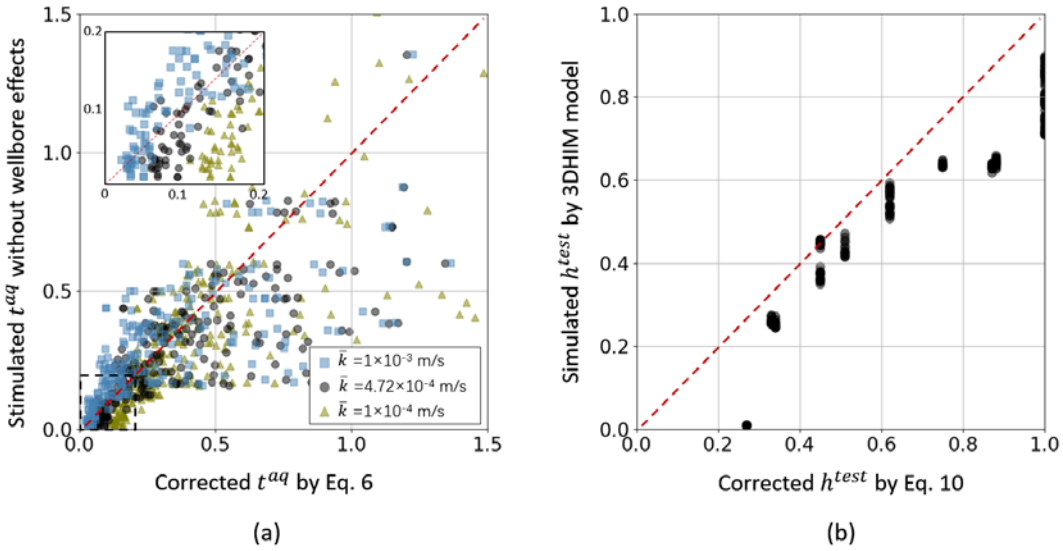

Figure 4.9: Validation results of (a) the corrected t^{aq} data and (b) the corrected h^{test} data.

The log-transformation process defined by Eq. (4.6) is another main factor that can introduce uncertainty into the corrected t^{aq} data. When there is an evident difference between the observed t_{peak} in the field and the theoretical $\bar{t}_{peak}$ calculated by the analytical slug test model, for instance in highly heterogeneous aquifers, this difference will be magnified by the log-transformation process. In Figure 4.9a, a slightly overestimation can be found for the earlier t^{aq} in the zoom-in view, and a significant overestimation can be observed for the later t^{aq} data. This implies that the inverted D values may be underestimated in extremely high D zones, which explains why an underestimation of the inverted D is observed in Figure 4.6b. Since later t^{aq} data are discarded during the inversion due to significant overestimation, estimates in low D zone have higher uncertainty and will be overestimated by deductions from nearby high D values. Therefore, in the field application, it can be inferred that the inverted D of the rock matrix is overestimated while the inverted D could be underestimated. This underestimated D can be remedied by slight overestimation in $\bar{k}$ if the extremely high D zone is of more concern, such as for the identification of fractures. For instance, in the zoom-in view of Figure 4.9a, the corrected t^{aq} data for $\bar{k}$ of 1×10^{-3} m/s are best matched to the "true" values within 0.05 s.

4.5.2 Uncertainty in the specific storage estimates

The specific storage estimation relies on the ratio of the peak head at the test interval h^{test} to that at the observation interval h^{obs}. In the synthetic example, the "true" h^{test} can be in fact simulated by the 3DHIM model during the tomographic slug test. Therefore, a comparison of the "true" h^{test} and the corrected h^{test} by Eq. (4.10) is carried out and plotted in Figure 4.9b. It indicates that the corrected h^{test} data are mostly higher than the "true" h^{test}, especially for the significantly attenuated h^{test} that is caused by the possible high D zone nearby, such as location 8 in Figure 4.5c. The reason is that the higher D of the aquifer, the

faster head release within test interval could be, resulting in a more severe attenuation in h^{test}. But for the correction method in Section 4.2, a high D zone will develop a non-laminar flow in the riser pipe at the early time. Under non-laminar flow, the water level curve of test well cannot be correctly estimated by the four real coefficients in Eq. (4.9) (Quinn et al., 2018), which will lead to a significant overestimation in the corrected h^{test}. Therefore, the S_s could be overestimated nearby the high D zone. This explains why the S_s in Figure 4.6d is slightly overestimated, especially nearby the high D zone illustrated in Figure 4.6a. Moreover, it can be accordingly inferred that the inverted S_s in the field application (Appendix A3) may also be overestimated.

The insufficient arrangement density of the test and observation intervals in the synthetic example could be also a reason that causes uncertainty in the parameter estimation. For instance, in Figure 4.6a, a thin high D layer between 23 m and 24 m did not revealed in the inversion result. We recommend performing the tomographic slug test at higher resolution, if the hydraulic property of thin layers is important. Combining the uncertainty discussion of the inversion results, we do not recommend applying the proposed method in formations with very high heterogeneity.

4.6 Summary and conclusions

This study provides a new framework for characterizing aquifer heterogeneity by using the tomographic slug test. In a tomographic slug test, the slug well is considered as a pressure-pulse source. The 3D propagation of a pressure pulse in subsurface is described by two eikonal equations, which relate the peak head of the water level response and its corresponding arrival time to the distributions of specific storage and hydraulic diffusivity of the aquifer, respectively. Since the observed water levels are inevitably affected by the wellbore effects, such as the water column inertia and friction loss on the well wall, two correction methods are proposed to remove the influence of wellbore effects on hydraulic travel time and peak head data. Firstly, assuming that hydraulic travel time in the wells is independent of aquifer heterogeneity, the influence of wellbore effects on hydraulic travel times can be approximately estimated on an equivalent homogeneous aquifer of the target site, such as characterized by preliminary hydraulic tests. Secondly, to correct the peak head attenuation in the wells, the peak head attenuation of the test well is derived from the observed water level response. And the peak head attenuation in the observation well is ignored because the groundwater movement is much slower than that in the test well. Based on the corrected slug test data, the distribution of hydraulic diffusivity and specific storage can be inverted by using the travel time-based and attenuation-based inversion methods, respectively.

The new framework is verified by a synthetic example, in which the tomographic slug test is simulated on a aquifer outcrop analog. A total of 300 cross-well slug test is simulated between four virtual groundwater

wells. Following the characterization framework, the hydraulic travel time and peak head of each simulated water level response are corrected and then utilized for aquifer reconstruction. Inversion results show that the distributions of hydraulic diffusivity and specific storage are well estimated. And the inverted values for the hydraulic diffusivity are slightly underestimated, and slightly overestimated for the specific storage. A field application of this method is performed at a fractured rock experimental site located at Göttingen, Germany. A total of 96 cross-well slug test are conducted at the upper 40 m between three groundwater wells. The hydraulic conductivity distribution at the target area is obtained, which is calculated by multiplying the inverted hydraulic diffusivity and specific storage. Results indicate that three transmissive fractures are revealed at depths of about 19 m, 28 m, and 35 m with hydraulic conductivities varying from 6.9×10^{-5} to 3.4×10^{-4} m/s.

According to the uncertainty analysis on the inversion results, the higher hydraulic diffusivity zone will be slightly underestimated when the homogenized hydraulic conductivity of the target site is underestimated by the preliminary hydraulic tests, and by the log-transformation process. Conversely, the specific storage could be overestimated nearby the highly hydraulic diffusivity zone due to the possible non-laminar flow in the riser pipe, which will lead to an overestimation in the peak head at the test interval. We recommend applying the proposed method in heterogeneous aquifers with smooth variation, and suggest increasing the arrangement density of the test and observation intervals if the hydraulic property of thin layers is important.

5

Thermal tracer tomography

Contents

This Chapter has been published as:

Liu, Q., Hu, R., Hu, L., Xing, Y., Qiu, P., Yang, H., ... & Ptak, T. (2022). Investigation of hydraulic properties in fractured aquifers using cross-well travel-time based thermal tracer tomography: numerical and field experiments. Journal of Hydrology, 127751, DOI: 10.1016/j.jhydrol.2022.127751

Abstract

Hydraulic properties are well known to be essential in controlling fluid flow, solute migration, and heat transport in fractured subsurface. However, accurate characterization of hydraulic properties including the locations of conductive fracture and their hydraulic conductivities as well as their cross-well connectivity is still challenging. In this work, we modified the inversion framework of travel-time based thermal tracer tomography (TT) firstly based on a numerical study. Considering the features of heat transfer in fractured media, a regularization term and an irregular triangular mesh are introduced. A distortion of thermal travel times caused by annular wall flow at an observation well is eliminated by assigning a specific well zone in the inversion model. The performance of this modified inversion framework in characterizing hydraulic properties of fractured aquifers is firstly analyzed through nine numerical tests. Results indicate that the modified TT method can efficiently identify directly connected or interconnected fractures, even with the presence of an ambient hydraulic gradient, observation well annular wall flow, or measurements based on conventional thermal sensors with less precision. Accordingly, a tomographic thermal tracer test is performed and analyzed at a fractured rock experimental site located at the University of Göttingen, Germany. It can be inferred that there is a directly connected fracture, two interconnected fractures, and an overburden zone, with hydraulic conductivities between 5×10^{-4} m/s and 1×10^{-5} m/s. The outcomes demonstrate that the proposed inversion framework is efficient and robust in characterizing hydraulic properties of fractured aquifers.

5.1 Introduction

In fractured bedrock, the fracture system may form preferential flow paths, it is therefore of great importance for fluid and contaminant migration. For example, in the fields of energy supply (oil and gas industry, geothermal energy production) and of environmental safety (contamination remediation, nuclear waste disposal, CO2 sequestration), it is essential to characterize the hydraulic properties of a fractured system, such as the locations of conductive fracture, their hydraulic conductivities and the cross-well connectivity. However, due to the mostly complex fracture geometry and pronounced hydraulic heterogeneity, this characterization has been long one of the major challenges in hydrogeology.

Within the past decades, numerous studies have been devoted to this field, especially those using cross-well tomographical imaging methods, such as geophysical tomography (Day-Lewis, 2001; Karasaki et al., 2000; Robinson, J et al., 2016), hydraulic tomography (Dong et al., 2019; Illman, WA, 2014; Illman et al., 2009; Klepikova et al., 2020), and tracer tomography(Kittilä et al., 2019; Klepikova et al., 2014). Compared to geophysical methods, hydraulic and tracer tests can directly provide hydraulic information without additional correlation analysis (Hu et al., 2017). Tracer testing provides not only the most intuitive evidence of cross-well hydraulic connectivity, but also implies information on transport connectivity of fractures (Knudby & Carrera, 2005). Recently, with the technological advances in temperature monitoring, such as fiber-optic distributed temperature sensing (DTS) and flexible borehole liners, measuring temperature evolution along a borehole becomes more efficient, accurate and economical (Bakker et al., 2015; Coleman et al., 2015; Maldaner et al., 2019; Pehme et al., 2010; Read et al., 2013). This makes heat as an ideal choice compared to conventional tracers, and using heat as a tracer to investigate hydraulic properties of fractured zone is attracting more and more attention.

Cross-well thermal tracer tomography that combines thermal tracer techniques with imaging methods has been promoted in the past several years to reconstruct aquifer heterogeneity (Doro et al., 2015; Schwede et al., 2014; Somogyvári & Bayer, 2017; Somogyvári et al., 2016; Wagner et al., 2014). This novel technique was intensively studied in porous media so far, including a comparative analysis with hydraulic tomography and joint inversion using head and temperature measurements, etc. (Lee et al., 2018; Ringel et al., 2019; Schwede et al., 2014; Somogyvári et al., 2016; Somogyvári et al., 2019). In order to investigate aquifer heterogeneity in the field, Doro et al. (2015) improved the field-scale experimental design for thermal tracer tomography. Using travel-time based thermal tracer tomography (TT), Somogyvári and Bayer (2017) successfully estimated hydraulic conductivity profiles in alluvial sediments. However, up to now this method was rarely studied for the characterization of fractured media.

Applying cross-well thermal tracer tomography in fractured media still encounters some obstacles. Firstly,

in fractured bedrock, conductive fractures are the preferential channels for groundwater flow and heat transfer. Their hydraulic conductivity can be generally much higher than that of the matrix. When performing a cross-well thermal tracer test, due to different time scales of the experiment and of heat conduction, temperature changes may only be observed at depths where connected fractures are exposed to the observation well. This spatially sparse temperature response can result in a strong ill-posed inversion problem. Secondly, fracture systems usually have a complex geometry, that is, the fractures can be disconnected, connected by a dominant single fracture, or interconnected in a network. And hydraulic conductivities of fractures, controlled by fracture distribution, aperture and filling material, can vary significantly at a small scale (National Research Council, 1996). The connectivity between fractures and their different hydraulic conductivities will increase the non-uniqueness of the inversion result. Also, a classical regular inversion grid may cause difficulties in tracing the irregular fracture geometry, thus introducing calculation errors. In addition, some practical issues, such as ambient groundwater flow or vertical flow within the well, if any, will affect the heat transport processes during tomographic testing, and thus distort the parameter estimation results. Nevertheless, due to the high conductivity contrast between fractures and rock matrix, the injected water and heat will preferentially flow through the fractures. Compared to porous media, the distortion of the flow field induced by a high injection rate can be much lower. Temperature response can be received much faster at the same injection rate, and heat transport will be less affected by heat diffusion.

Facing the foregoing ill-posed and non-uniqueness problem, travel-time based inversion is considered an efficient method (Brauchler et al., 2013; Hu, R et al., 2011; Somogyvári et al., 2016). Thermal travel time is defined as the propagation time of a thermal tracer front in the source-receiver dipole. Since only the thermal travel times need to be matched instead of all temperature data, this approach is robust and can significantly reduce computational cost. Because the inversion problem for travel times is quasi-linear, its solution can be much less sensitive to the initial model, compared to non-linear inversion problems, such as the full-wave inversion (Vasco, 2018). In addition, introducing a regularization constraint in the inversion framework is also an effective method to solve the ill-posed problems (Illman et al., 2015; Wang et al., 2017). Apart from this, using a DTS system to monitor temperature changes is another approach to reduce the uncertainty of inversion results by providing high-resolution temperature data in space and time (Maldaner et al., 2019; Pehme et al., 2010).

Combining these techniques, the intention of this study is to modify and improve the inversion framework and to evaluate the feasibility of thermal tracer tomography to characterize hydraulic properties of fractured media. According to the features of heat transfer in fractured media, we firstly modify the inversion framework of the TT method in Section 5.2. In Section 5.3, the performance of this modified inversion framework in characterizing the hydraulic properties of fractured aquifers is evaluated and validated through

nine numerical tests. Finally, a field-scale thermal tracer tomography experiment is implemented at a fractured rock experimental site, located at the north campus of the University of Göttingen, Germany, and the fracture connectivity as well as the cross-well hydraulic conductivity profile are finally delineated. Through the numerical and field experiments, the advantages and disadvantages of the TT method in obtaining hydraulic characteristics of fractured media are discussed, considering future studies and related applications.

5.2 Inverse modeling of thermal tracer tomography in fractured aquifers

5.2.1 Travel time based thermal tracer tomography

Vasco and Datta-Gupta (1999) first derived a trajectory-based integral formula that directly links the solute travel time to hydraulic conductivity k. Based on the similarity of the solute transport and the heat transfer equations, Somogyvári et al. (2016) further extended this trajectory-based integral formula for thermal tracer tomography. They considered thermal retardation and proposed an early-time diagnostics method to improve the accuracy of the inversion result. The thermal travel time t_{tt} is defined as the propagation time of a thermal tracer front along the path l from the injection source $\boldsymbol{x}_s$ to a receiver $\boldsymbol{x}_r$, which is given in Somogyvári et al. (2016),

$$t_{tt}(\boldsymbol{x}_r) = \int_{\boldsymbol{x}_s}^{\boldsymbol{x}_r} \frac{\phi(l)}{Rk(l)\nabla h(l)} dl, \tag{5.1}$$

in which ϕ is the porosity distribution, ∇h is the hydraulic gradient, and R is the thermal retardation factor, defined as,

$$R = \frac{\rho_b C_b}{\rho_w C_w}, \tag{5.2}$$

where ρ is the density and C represents the specific heat capacity, and the subscript b and w denote the rock material and water respectively.

To invert the hydraulic conductivity distribution using thermal travel times, some other assumptions need to be made. In Eq. (5.1), the thermal travel time is not only affected by the hydraulic conductivity field, but also by the porosity, the hydraulic gradient and by the thermal retardation factor. Nevertheless, comparing to k, the variance of the other three parameters is usually much smaller for a fractured medium. Thus they can be approximated by a constant value in the entire model (Somogyvári et al., 2016).

Assuming that a site of interest contains m source-receiver pairs and the site domain is discretized into n cells in the inversion model, the path integral, Eq. (5.1), can be discretized into a matrix form,

$$\boldsymbol{t} = \mathbb{M}\boldsymbol{a} \tag{5.3}$$

where $\boldsymbol{t}$ is an m-vector of observed thermal travel time. $\mathbb{M}$ is an $m \times n$ matrix and its elements $\mathbb{M}_{ij}$ represent the trajectory lengths of the ith ray through the jth element. $\boldsymbol{a}$ is a n-vector containing a homogeneous and isotropic material property a_j in each cell, which is defined as $a_j = \phi_j / Rk_j \nabla h_j$. According to Fermat's principle, Eq. (5.3) is subject to the so-called shortest path problem which is widespread in network optimization and seismic tomography. In a highly heterogeneous fractured medium, the shortest path propagates toward the high-k fracture zone, which makes the matrix $\mathbb{M}$ very sparse. In this study, Dijkstra's algorithm is applied to trace the shortest paths for the sparse matrix. More details about Dijkstra's algorithm can be found in Dijkstra (1959), Xu et al. (2007) and Zhao et al. (2004).

5.2.2 Numerical techniques

Regularization constraint

When inverting the thermal tracer test data from fractured aquifers, one of the main challenges is a spatially sparse temperature response. This is because temperature changes in observation wells can only be observed at those depths where the connected fractures are exposed to the well screen, considering the time scales of the experiment and of heat conduction. As a result, the inversion framework will be ill-posed since the number of measurements is much less than the discretized cells in the inversion model. To solve this problem, a regularization term is commonly introduced into the objective function Φ, which is given by (Rücker et al., 2017),

$$\Phi = \left\| \boldsymbol{W}_{fit}(\boldsymbol{t} - \boldsymbol{D}(\boldsymbol{a})) \right\|_2^2 + lam \left\| \boldsymbol{W}_{reg}(\boldsymbol{a} - \boldsymbol{a}_0) \right\|_2^2, \tag{5.4}$$

where $\boldsymbol{W}_{fit}$ is the weighting matrix containing the observation errors, and $\boldsymbol{W}_{reg}$ is the model constraint matrix to restrict the parameters to be varying in reasonable ranges. $\boldsymbol{D}$ represents the forward operator using the Dijkstra's algorithm, and $\boldsymbol{a}_0$ is a reference parameter model. lam is a parameter weighting the importance of the parameter model constraints, which can be regarded as a smoothness operator. To minimize this objective function, the Gauss-Newton iteration method is adopted.

In field applications, such as predicting the spread of a contaminant plume, the main target is on obtaining the hydraulic properties of highly conductive fractures, which form preferential pathways. It is therefore necessary to retain more information on the short thermal travel times in the inversion framework. This can be achieved in the numerical iteration process by reducing the weight of the regularization term lam or by adjusting the weighting matrix of the observation error $\boldsymbol{W}_{fit}$. In order to avoid introduction of new uncertainties, only lam will be adjusted during the iteration in this study.

Irregular inversion mesh

Another main feature of heat transfer in fractured aquifers is a sharp thermal front and the complex pathway of the front which is controlled by the hydraulic conductivities of fractures and their geometry. Since the travel-time tomography is trajectory-based, it is suitable for detecting the preferential pathways. The trajectories are typically restricted to iterate along the mesh in the inversion domain. In a regular grid, the calculated trajectory could thus be longer than the actual fracture, leading to overestimated k values. Using an irregular triangular mesh to discretize the model could be more conducive, because at a fixed mesh density, the irregular mesh will provide more reasonable channels for trajectory tracing. Additionally, a secondary node is also added to each mesh edge to make the trajectory calculation more accurate.

Specific well zone

Vertical flow may occur in an observation well when there is a head difference between the fractures covered by the well, which can deflect the flow field significantly and affect the heat transfer process (Pehme et al., 2010). To hinder the thermal signal from being distorted by vertical flow, a flexible borehole liner is employed in some studies (Coleman et al., 2015; Munn et al., 2020). However, unsealed or fully screened observation wells are still common in field testing.

To investigate and to consider the distortion of thermal travel times caused by vertical flow, an open observation well is represented in the inversion model. A well zone is cut out from the inversion domain. By adjusting the constraint weights to zero at the interface between t5he well zone and the aquifer domain, the hydraulic conductivity of the well can be inverted independently of the surrounding aquifer. The shortened travel time observed at a sensor placed along the open observation well can be thus corrected. Based on the generalized form of Darcy's law, the hydraulic conductivity $k(\boldsymbol{x})$ within the well zone is assumed to be uniform and approximated by (Bear, 2013; Hu, LT et al., 2011),

$$k(\boldsymbol{x})|_{\boldsymbol{x}\in\Omega_{wel}} = \frac{{r_w}^2}{8}\frac{\rho_w g}{\mu}, \tag{5.5}$$

where r_w is the well radius, ρ_w is the water density, g is the acceleration due to gravity, and μ is the dynamic viscosity of water. The $k(\boldsymbol{x})$ will be assigned for the observation well in the following forward modeling to consider the vertical flow, and will also be set as the initial value for the well zone in the inversion framework to correct the measured travel time data.

5.2.3 Numerical implementation

The inverse modeling of the thermal tracer tomography is implemented in an open-source Python code using a framework built based on the geophysical library pyGIMLi (Rücker et al., 2017). The TravelTimeManager module is originally developed for seismic travel time inversion. It can be extended to solve the travel-time

based thermal tracer tomography problem due to the similarity of the inversion formula. In the inversion framework, the initial k of the well zone is calculated by Eq. (5.5) depending on the well radius. For the aquifer zone, the initial model is estimated by the measured thermal travel time. The range of the inverted k values of the aquifer zone will be limited between 1×10^{-8} m/s and 0.1 m/s. This is reasonable because the observed thermal signal mainly contains the hydraulic information of the conductive fractures. In addition, an optimized smoothness operator lam_{op} will be determined by the numerical tests in the next section.

5.3 Synthetic examples for model performance evaluation

5.3.1 Numerical setup

In order to evaluate the performance of the thermal tracer tomography in a fractured medium, a series of numerical tests were carried out in a two-dimensional (2D) model. Although flow in fractured rocks is usually three-dimensional, the 2D approximation is still reasonable in certain local zones, such as in a zone with obvious principal stress directions (Lang et al., 2018), or near geological structures that control the local seepage field. In the forward modeling, the discrete fracture matrix (DFM) model is utilized, which preserves the dominant fractures, and upscales and replaces the secondary fractures by averaged quantities of the porous matrix. This is due to the fact that during a thermal tracer test, the heat transport process is dominated by heat advection in the connected fractures and by heat diffusion in the porous rock matrix, which consists of discrete disconnected fractures. The forward hydrothermal processes are simulated using the finite volume method. Details on derivation of the equations and on the modeling method are provided in the Appendix A4.

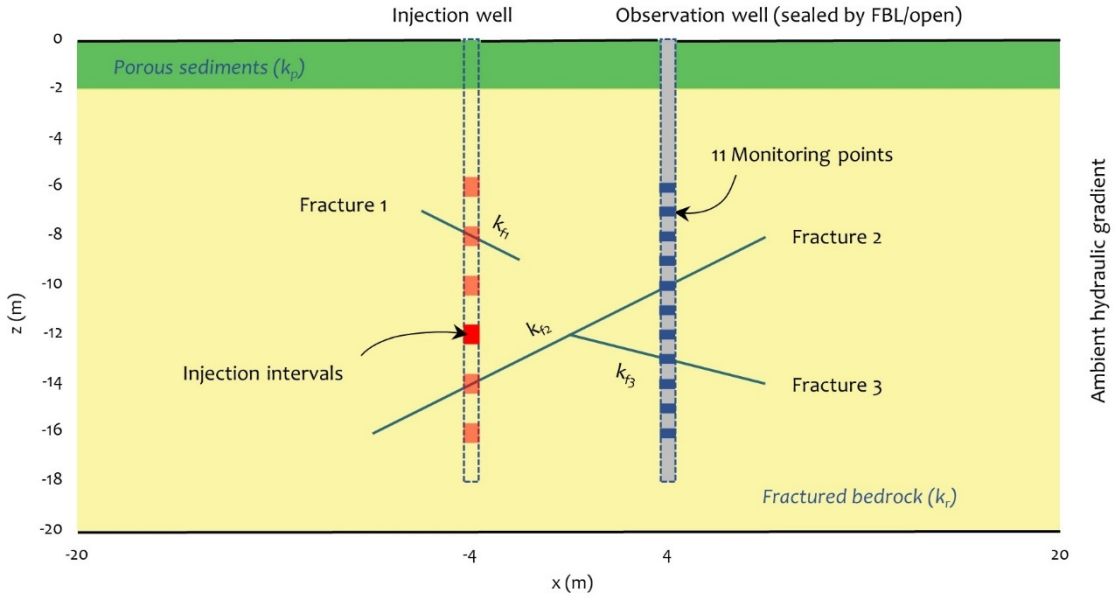

Figure 5.1: Geometry of the forward model for the tomographic thermal tracer test simulations (observation well is open just for Case 9).

As shown in Figure 5.1, a 2D geometric model (40 m × 20 m) consisting of an upper porous layer and a fractured bedrock is set up. Hydraulic conductivities k in each domain are isotropic and homogeneous. The k values of the upper layer and the bedrock are 10^{-6} and 10^{-8} m/s, respectively. Fractures are inserted as line elements and assumed to be straight with various lengths, angles and k values, which will be adjusted for different scenarios. For simulating the tomographic thermal tracer tests, six injection intervals and eleven monitoring points are placed. Considering that the straddle packer system is often employed during heat injection, heat and water flow in the injection well is neglected. The effects of the unsealed observation well on heat and water flow will be evaluated in the following case study.

Table 5.1: Main parameters of nine different test scenarios.

	Case 1	*Case 2*	*Case 3*	*Case 4*	*Case 5*	*Case 6*	*Case 7*	*Case 8*	*Case 9*
k_{f1} (m/s)	**10^{-4}**	10^{-4}	10^{-4}	**10^{-6}**	10^{-4}	10^{-4}	10^{-4}	10^{-4}	10^{-4}
k_{f2} (m/s)	/	**10^{-4}**	10^{-4}	10^{-4}	**10^{-6}**	10^{-4}	10^{-4}	10^{-4}	10^{-4}
k_{f3} (m/s)	/	/	**10^{-4}**	10^{-4}	10^{-4}	**10^{-6}**	10^{-4}	10^{-4}	10^{-4}
∇h_1 (-)	0	0	0	0	0	0	**-0.2***	0	0
δT_0 (K)	0.001	0.001	0.001	0.001	0.001	0.001	0.001	**0.1**	0.001
k_{well} (m/s)	/	/	/	/	/	/	/	/	**3125**

The negative sign means the gradient is from right to left.

Based on this geometric model, nine different scenarios were designed aiming at different fracture connectivity, k distributions, and some practical issues. Table 5.1 lists the main parameters for these cases. Three fractures (in Figure 5.1) represent three modes of cross-well hydraulic connectivity, i.e., disconnected (Fracture 1), directly connected (Fracture 2) and interconnected (Fractures 2 and 3). From Case 1 to Case 3, a fracture is added each time, and the hydraulic conductivity of the added fracture k_f is set to 1×10^{-4} m/s. From Case 4 to Case 6, k_f of these three fractures is reduced individually to 1×10^{-6} m/s. From Case 7 to Case 9, three practical issues are considered, including ambient hydraulic gradient ∇h_1, temperature sensor accuracy δT_0 and vertical flow in the observation well. In Case 9, an observation well is implemented with a radius of 0.05 m and a length of 18 m. The vertical flow inside the observation well is achieved by assigning a high hydraulic conductivity k_{well} (3125 m/s) to the well, which is defined as Eq. (5.5) in Section 5.2.

According to these scenarios, nine forward and inverse model simulations are carried out. Table A5 shows all the simulation parameters of the hydrothermal processes. In the forward modeling, continuous thermal injection tests are simulated at the six injection intervals sequentially. The injected water temperature is 10 °C above the background temperature, and the injection rate is 0.5 l/s. All the injections are simulated for ten days. By comparing the inverted k with the true values, the optimized smoothness operator lam_{op} is set to 10. The thermal travel times at the eleven monitoring points (Figure 5.1) are recorded and then used to invert the hydraulic conductivity profiles. Only the total temperature changes at a monitoring point greater than 0.001 °C will be included in the inversion procedure considering thermal sensor accuracy. To consider

the heat diffusion effects on the thermal travel time, the early-time diagnostics method proposed by Somogyvári et al. (2016) is employed. Additionally, accounting for the observation error, a Gaussian noise with a standard deviation of 1% is added to the travel time datasets.

5.3.2 Inversion model performance

Figure 5.2 shows the nine inverted hydraulic conductivity profiles corresponding to the designed cases. The orange lines denote the "true" fracture geometry, and the grey curves are the calculated trajectories between the sources and receivers. All nine k tomograms can be divided into three categories. The tomograms in the top row (Figure 5.2a-c) corresponding to Case 1-3 reflect the capability of the inversion to detect the cross-well hydraulic connectivity. The results indicate that fracture connectivity can be clearly identified if the "true" fracture geometry is cross-well connected, as shown in Figure 5.2b and c. Once a fracture is disconnected, such as shown in Figure 5.2a, the inversion result cannot retrieve it because the travel times observed at each monitoring point have minor differences which are hardly to form a preferential channel. In Figure 5.2c, although the connected fracture is bifurcated on the right side, the position of the bottom fracture (Fracture 3) is deflected. The reason could be the impact of the top disconnected Fracture 1 on the seepage field, thus disturbing the thermal travel times.

The second aim is to test the inversion procedure in identifying the hydraulic properties of fractures under different k contrasts. The inversion results based on Case 4-6 are shown in Figure 5.2d-f. It illustrates that different k contrasts between fractures have a significant impact on the inverted hydraulic profile. In Figure 5.2e, when the k of Fracture 2 decreases to 1×10^{-6} m/s and the k of Fracture 1 and 3 keep at 1×10^{-4} m/s, only one potential fracture is revealed. Its trajectory is close to the high k path, i.e., the left part of Fracture 2 plus Fracture 3. However, the inverted k value along this trajectory is averaged, which is close to 5×10^{-5} m/s. This indicates that it is hard to distinguish the changes of the k value in a connected fracture using the trajectory-based inversion method. Additionally, as shown in Figure 5.2f, when a low k fracture (Fracture 3) inserts in a high k fracture (Fracture 2), the low k fracture is covered. From the calculated trajectories, Fracture 3 is ignored, and instead more is passing through Fracture 2 to make up the misfit in thermal travel times. This implies that the inverted profile tends to reveal the preferential flow path, if there is no additional fracture geometry information. When the k of interconnected fractures is equivalent, as illustrated in Figure 5.2d, the k value is accurately estimated and the fracture geometry is very similar to the truth. Comparing to Figure 5.2c, it is further confirmed that the k magnitude of the top disconnected fracture can affect the thermal travel times, although this fracture is not recognized. In future applications, prior information such as fracture geometry and matrix data (Zhao et al., 2021) can improve the inversion results through correcting the thermal travel time.

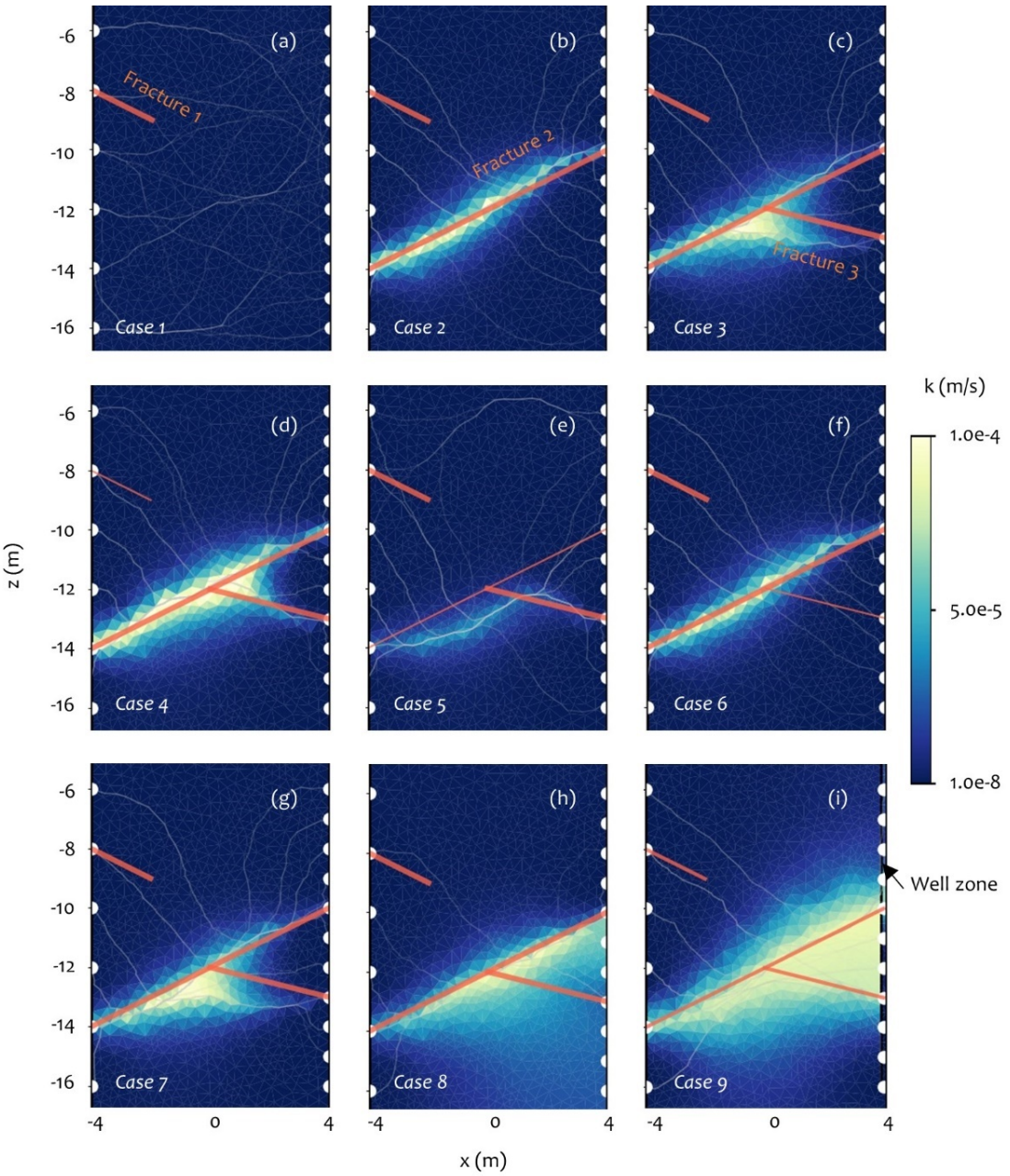

Figure 5.2: Inversion results of hydraulic conductivity for the nine different scenarios. The line width represents the magnitude of the k value.

To examine the uncertainty of the inversion results considering some practical issues, three scenarios are considered in the last category. Firstly, Figure 5.2g shows the inversion result of thermal tracer tomography under an extremely high natural hydraulic gradient of 0.2 m/m from the right to the left side. The result shows that the interconnected fractures (Fracture 2 and 3) can be clearly recognized, and the k distribution is very close to the case without ambient gradient (Figure 5.2c). This indicates that the ambient hydraulic gradient has less influence on the inversion results when the injection rate is around 0.5 l/s. Secondly, Figure 5.2h is the inversion result of the case in which the accuracy of the temperature sensor is assumed to be 0.1 °C. That is, only the travel times in which the observed temperature responses vary more than 0.1 °C are

used for inversion, which means that only several sensors near the fractures can receive temperature responses. This makes the inverted data matrix more sparse and the inversion gets more ill-posed. However, the inversion result in Figure 5.2h can still identify a connected fracture (Fracture 2). From the calculated trajectories, the other one (Fracture 3) can also be recognized. Thirdly, to correct the distorted thermal travel times caused by vertical flow in the open observation well, a well zone is added at the right side of the inversion model with the width of 0.1 m, i.e. the diameter of the observation well represented in the forward model. The k in the well zone is iterated separately from the aquifer, thus it can be much higher than that of the aquifer. The inverted k distribution shown in Figure 5.2i indicates that the high k distribution in the aquifer not only covers the connected fractures but also an area between the fractures and the well. This is because the thermal travel times observed at the sensors between the identified fractures become very similar due to the rapid flow inside the well. The calculated trajectories thus short-circuit in this area. Overall, these nine numerical tests show that the travel time-based inversion procedure is efficient and robust in identifying the connected fractures and in estimating the k distribution.

5.4 Field application

5.4.1 Site description

The fractured rock experimental site is located at the north campus of the University of Göttingen, Germany. This test site consists of six groundwater wells with a depth of 80 m. Well BHE and W were built in 2007 for the study of shallow geothermal energy problems. In order to investigate the hydraulic properties of fractures and apply hydraulic and thermal tracer tomography, another four groundwater wells (well N, O, M and S) were installed at this site in 2013. The well arrangement, lithology, and well design are illustrated in Figure 5.3.

Geologically, this test site is located at the eastern shoulder of the Leinetalgraben, which is a distinctive zone of subsidence in the southern part of Lower Saxony, Germany. Its geological structure is very complicated due to polyphase tectonic development under various tension forces (Leiss, 2011). Following Werner (2013), especially in the eastern shoulder including this site, it is dominated by NNE-striking faults with high offsets and a number of folds. Fractures have also well-developed. Lithologically, this area is located in the Lower and Middle Keuper which mainly consists of clay sequences and silt-sandstone layers. The main lithology exposed by the drill cores is shown in Figure 5.3b. Moreover, the geophysical loggings show that the bedding planes dip constantly with approximately 75° towards SE. The acoustic and optic televiewer data delivers three trends of the dip angle and azimuth of inserted fractures: 351/06, 221/37 and 045/59 (Werner, 2013).

The well design is depicted in Figure 5.3c. To achieve tomographic testing at this site, each well has been provided with separated nine filter sections that are hydraulically connected to different geological strata.

The diameters of the boreholes and the well pipes are 0.2 m and 0.08 m, respectively. The well pipe, except the top 8 m casing, is composed of alternating 5m screened and 3m non-screened sections. The corresponding filling materials outside the well pipe are filter gravel and clay pellets. Additionally, fiber-optical cables for DTS based groundwater temperature monitoring are installed along the well pipes. In this study, the spatial resolution of the DTS system is 0.5 m, and the standard deviation of a temperature value is 0.1°C.

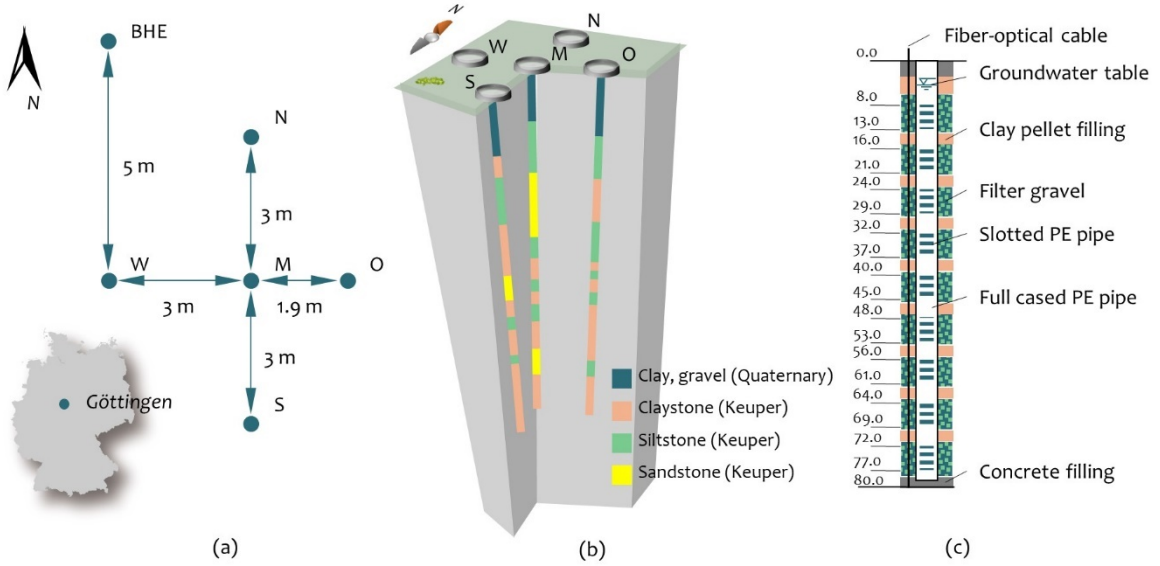

Figure 5.3: Sketch of (a) well arrangement at the fractured rock test site in Göttingen, Germany, (b) lithology profiles from drill cores based on Werner (2013), and (c) the well design.

5.4.2 Preliminary testing

Several other studies have been carried out at this site, including geophysical loggings, hydraulic tomography and groundwater temperature monitoring (Baetzel, 2017a; Jahr et al., 2020; Oberdorfer et al., 2013; Schuster, 2015; Werner, 2013; Yang, HC et al., 2020). Their findings demonstrate that highly conductive fractures are mainly distributed at the top 40 m, particularly between well M and O. Still, it is hard to figure out the accurate locations of the connected fractures between the wells, and their hydraulic conductivities.

5.4.3 Tomographic thermal tracer test

With the experience from the numerical tests and the preliminary testing results, a tomographic thermal tracer test was designed and implemented at the top four screen intervals (ca. 40 m length) between well M and O. Experimental design of this test is depicted in Figure 5.4. Warm water heated to about 20 °C was first injected sequentially at each of the top four 5 m screen intervals in well M. A double packer system was employed to isolate the 5 m sections in the injection well. Each injection lasted for at least 5 hours at a rate of 0.4 l/s, then waiting for heat dissipation for about two days. Afterwards, this multilevel thermal injection

test was repeated in well O in the same way. Only well M and well O are selected because the evident thermal signal is only observed in these two wells during the 5 hours of each test, which corroborates the finding of the preliminary tests showing that the hydraulic connection between well M and O is better than between the others (Baetzel, 2017a). The temperature evolutions along all the wells were recorded by the DTS with a spatial resolution of 0.5 m and a temporal resolution of 1 min. Note that, since the observation well was open during the tests, the temperature evolutions in this well may be affected by vertical well flow.

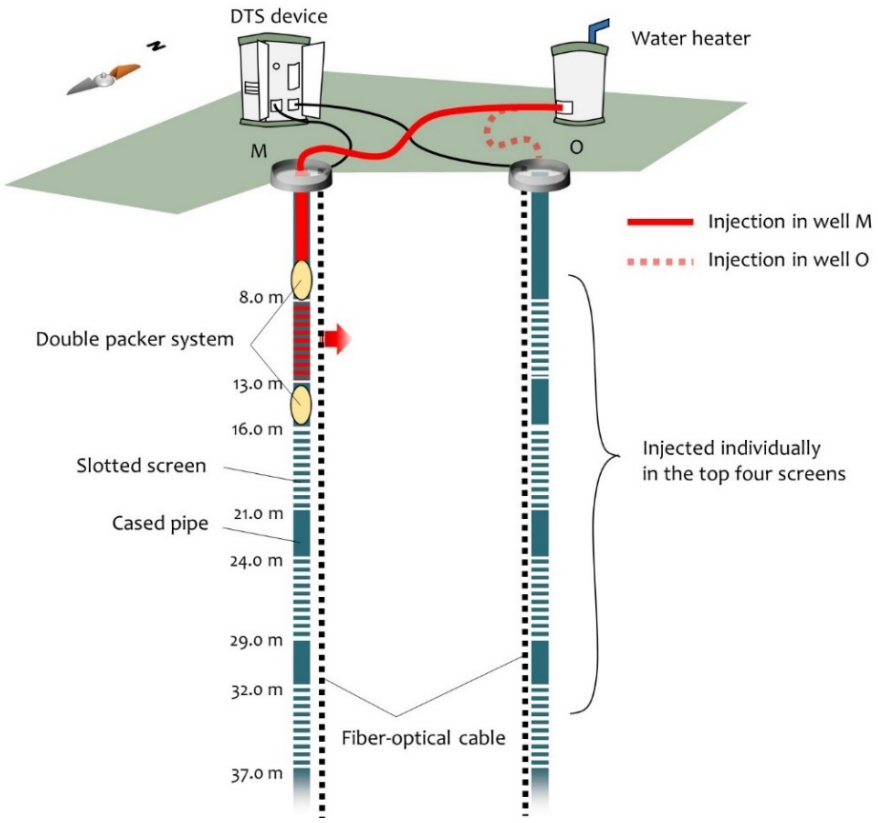

Figure 5.4: Experimental configuration of the tomographic thermal tracer tests.

Figure 5.5 shows the temperature evolutions along the observation wells above 40 m. The heatmaps in the first row represent the temperature evolution in well O when the warm water was injected sequentially at the top four screen sections of well M. In turn, heatmaps in the second row represent the temperature responses in well M when injecting in well O. It is obvious that a clear temperature response can be observed in all cases, except in Figure 5.5e. When injecting at screen sections other than the first, a rapid and multiple-depth temperature response can be observed. In Figure 5.5b-c and f-h, the temperature observed at similar depth compared to the injection section varies more sharply than the others. And the temperature changes along the well seems to be impacted by the well construction, such as the temperature depression at the depth of 13-16 m in Figure 5.5b-d. Overall, the observed temperature evolutions reflect that some well-connected fractures exist between these two wells. The observed multiple-depth temperature response may be due to the vertical flow in the open observation well.

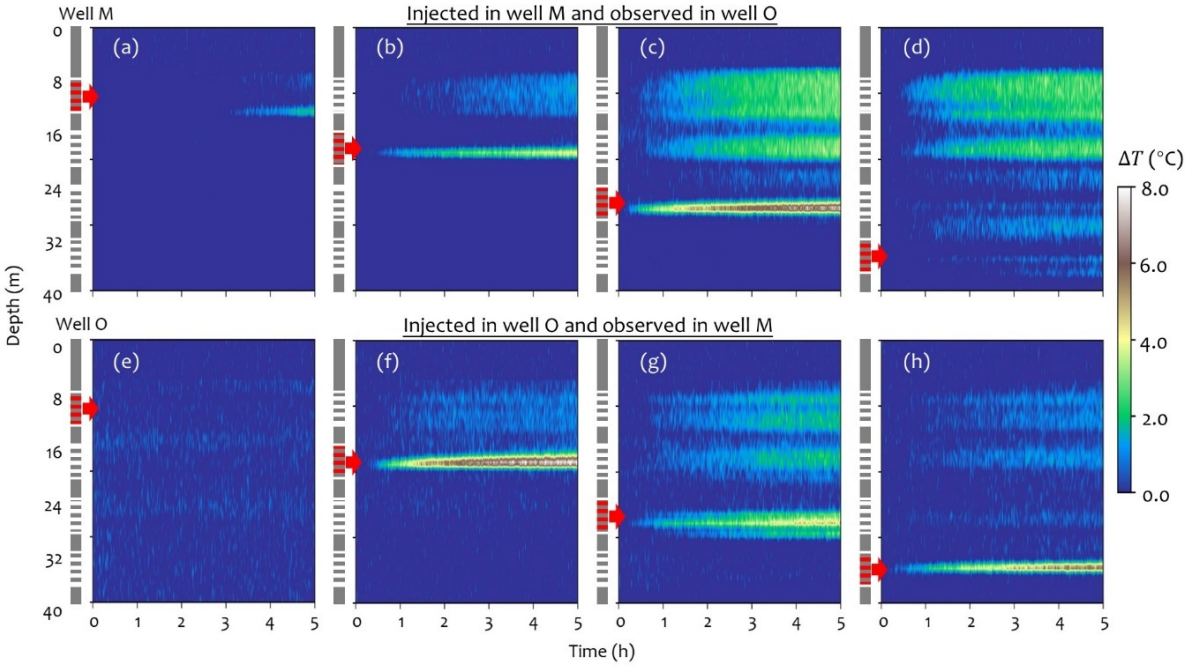

Figure 5.5: Observed temperature evolutions along observation wells at the top 40 m. The column sketch on the left of each heatmap denotes the well construction, and the red screen section represents the injection depth interval.

5.5 Inversion results and discussion

After denoising the observed temperature datasets using the method proposed by Yang, HC et al. (2020), a total of 264 thermal travel times were extracted based on the early-time diagnostic method. After identifying the peak value of each thermal response curve, the early travel time corresponding to 10% of the peak value can be found. The early travel time is then extrapolated to the ideal travel time that takes heat diffusion into account (Somogyvári et al., 2016). In the inversion procedure, the inversion domain is 40 m deep and 2.8 m wide, consisting of well M and O and the aquifer between them. The borehole radius is 0.1m, and the horizontal distance between these two wells is set to 2.4 m, which is the average distance considering the borehole drilling deviation. According to geophysical loggings, such as the ultrasonic pulse velocity test (Baetzel, 2017a; Schuster, 2015), some inversion parameters are determined. The density of the rock ρ_b is about 2500 kg/m^3, the porosity ϕ is averaged to 0.2, and the specific heat capacity c_b of the bedrock is estimated to 1300 J/kg/K. An average hydraulic gradient of ∇h=0.08 in the east-west direction is calculated by head measurements during the test. In addition, the vertical flow in the observation well is considered.

After the numerical calculations, the inversion result of the reconstructed $log_{10}(k)$ field and the calculated trajectories are presented in Figure 5.6. The tomogram in Figure 5.6a reveals four high-k connected zones between well M and O, at a depth of ca. 10 m, 20 m, 28 m, and 36 m. The inverted k values of these zones are in a range from 5×10^{-4} m/s to 1×10^{-5} m/s. They can be considered as potentially connected fractures,

except for the top zone (at about 10 m). This is because the k values nearby the top zone are obviously lower than the others, and the high-k zone is relatively larger. Combining with the lithological background (Figure 5.6b), this zone can be determined as the overburden. Additionally, several sub-high k zones, in which the values are around 1×10^{-5} m/s, are present near the inferred fractures, such as the zones nearby well M at a depth of around 17 m and 31 m close to well O. According to the calculated trajectories shown in Figure 5.6b, their appearance seems to be caused by the high hydraulic conductivity between the well and the corresponding DTS sensing points. Note that, the inverted minimum k value of 1×10^{-6} m/s in this tomogram does not represent the hydraulic conductivity of the rock matrix. This is because the travel times used for the inversion only include the temperature response that can be detected within 5 hours, but not the travel time through rock matrix which would be much longer.

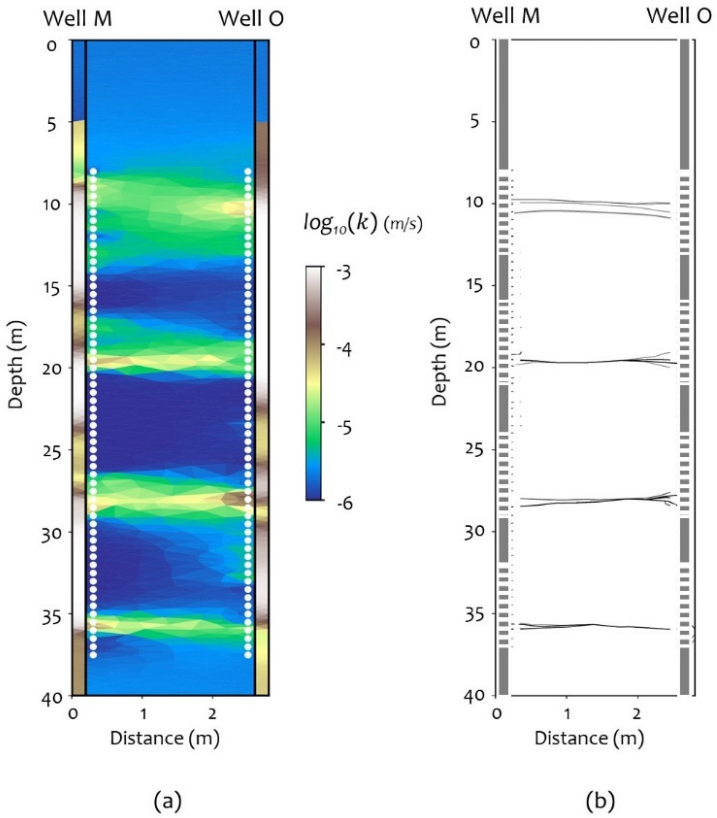

Figure 5.6: Inversion result: (a) the reconstructed $log_{10}(k)$ field and (b) the calculated trajectories. In the left tomogram, k values within the two well zones of well M and O are also estimated. The white circles represent the sensing points of the DTS. Note the scale distortion.

Moreover, the k values within the well zones are also estimated in the inversion procedure. The inverted k values in these zones shown in Figure 5.6a are much higher than those within the aquifer, except for the top 5 m. Their distribution, however, is not the direct reflection of the flow velocity in the well but a common manifestation of the conductivity including the part within the well and the part from the well to the DTS

sensing points. Due to the well construction, the hydraulic connectivity between the well and the different sensing points is distinct, thus the k distribution in the well zone is not very smooth. In summary, the inverted tomogram has clearly identified an overburden above 14 m and three connected fractures at ca. 20 m, 28 m, and 35 m between well M and O with k values between 5×10^{-4} m/s and 1×10^{-5} m/s.

The validation of the inversion results includes two aspects, i.e. the fracture locations and the magnitude of k. Validation results for the two wells M and O are shown in Figure 5.7. Firstly, to verify the fracture locations, the inverted k profiles are compared with the vertical well flow rate profiles measured by flowmeter logging under pumping. In the flow rate curves, the location of the conductive fractures can be figured out through a sudden increase of the vertical flow rate. Accordingly, the inferred locations of fracture are marked by the red points in Figure 5.7. By comparison, it can be found that the fracture locations identified by these two results in each well are quite consistent.

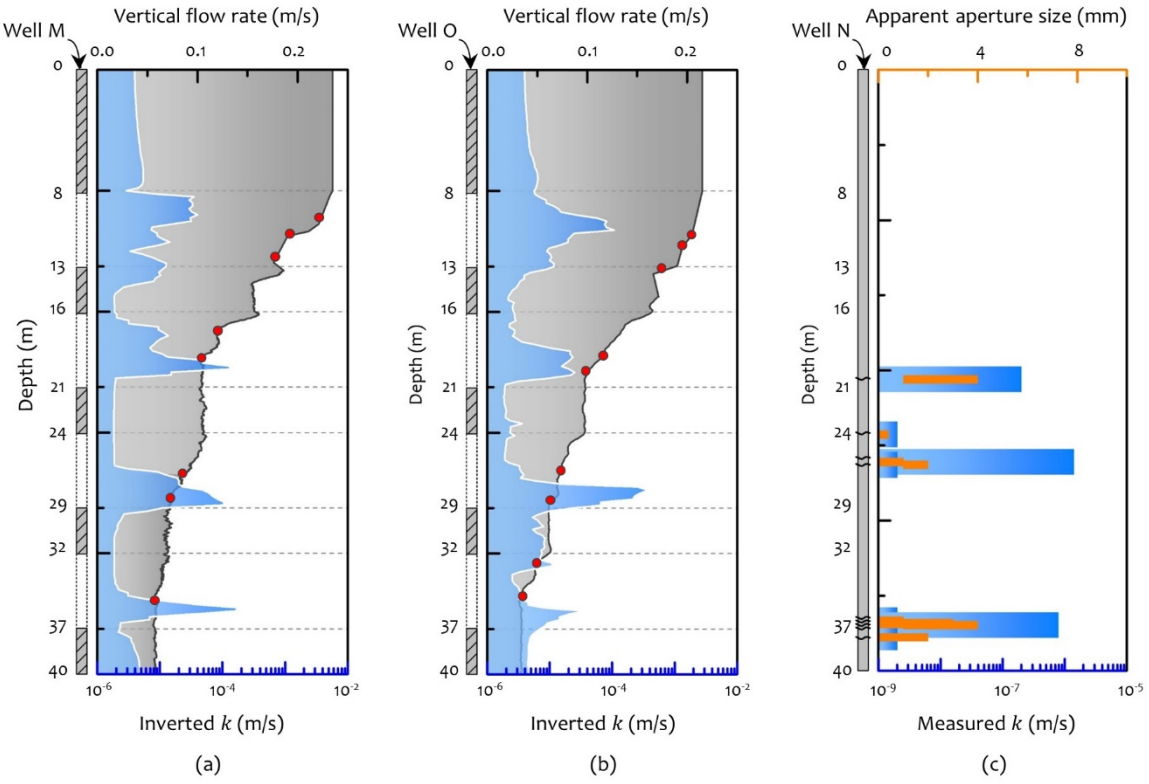

Figure 5.7: The validation of inversion results by comparing the inverted k (blue) with the vertical well flow rate curves measured during the flowmeter tests under pumping in (a) well M and (b) well O. The red points represent the inferred fracture locations from the flowmeter logging. And (c) the measured k from laboratory permeability tests and the apparent aperture size of fractures exposed on rock cores from well N.

Secondly, to verify the k magnitude, the inverted k values are compared with results from permeability tests on rock drill cores from well N and with results from conventional pumping tests in well M and O. In

the drill cores from well N, nine fractures were found at the top 40 m and tested in laboratory for permeability by Schuster (2015). The bar chart shown in Figure 5.7c depicts the measured k and the apparent aperture size. Three high-k fractures are revealed. Although the locations are similar to the inversion results, the magnitude of measured k from the laboratory is approximately two orders lower compared to the inverted values. However, according to pumping tests conducted in well M and O, the estimated k values are 6.68×10^{-5} m/s and 6.78×10^{-4} m/s, respectively. These results demonstrate that the magnitude of the inverted k is much larger than the measured k from rock cores at laboratory scale, but slightly smaller than the estimated k from the pumping tests. Considering spatial variability and lab-field scale effects of k measurements, this difference is reasonable.

Based on experiences gained from numerical tests, several uncertainties of travel-time based inversion results from field tests can be recognized. The first is that cross-well disconnected fractures may not be revealed by the inversion procedure, including high-k fractures. According to the numerical results shown in Figure 5.2a, although there is a local preferential flow path, it cannot shorten thermal travel times because of the extremely low k in the rock matrix. The second point is that there is an uncertainty in the k magnitude of the revealed fractures. As shown in Figure 5.2e, when the k magnitude changes along the connected fracture, this change will be averaged along the entire trajectory by the inversion procedure. Therefore, in Figure 5.6a, the k values in each revealed fracture are also averaged. Thirdly, the vertical flow in the observation well may mask some interconnected fractures. The travel time difference among the DTS sensing locations placed at depths between the inserted fracture locations is hard to recognize due to the rapid vertical flow. This results in a short-circuit area of inverted k, as shown in Figure 5.2i. In Figure 5.6a, some similar areas nearby well M at a depth of around 17 m and approx. 31 m deep close to well O can therefore be interpreted as interconnected fractures. It is worth noting that this inference may be impacted by the structures beyond the inversion domain, which is not considered in the travel time approach.

The modified thermal tracer tomography shows a good applicability for characterization of hydraulic properties of fractured media. With the high spatial and temporal resolution of DTS, thermal tracer tomography can efficiently and accurately capture the locations of conductive fractures as well as fracture connectivity and provide the spatial distribution of k values. Furthermore, even if the thermal travel times are disturbed by vertical flow in the observation well, reliable inversion result can still be obtained from field experiments. Although the fracture is assumed to be straight due to the short distance between the wells in this study, we believe that the proposed method can be easily upscaled. For instance, the inversion model can be constrained by supplementing the orientation of fractures (Zhao et al., 2021).

5.6 Conclusions

Through numerical experiments, it is demonstrated that the modified TT method tends to reveal the cross-well connected fractures, especially the highly permeable ones. It is insensitive to the natural hydraulic gradient if applied at an injection rate of around 0.5 l/s at the investigated scale. The influence of vertical flow in the observation well on the inversion result can be significantly reduced by adding well zones to the inversion approach. Given these experiences, the hydraulic properties of a fractured sedimentary rock site located at the north campus of the University of Göttingen, Germany, are investigated. The inversion results show that there is a directly connected fracture, two interconnected fractures, and an overburden zone between well M and O. The inverted k values of the detected fractures are between 5×10^{-4} m/s and 1×10^{-5} m/s. Their locations and k magnitudes are verified by comparing with the results from flowmeter logs, drill core permeability testing, and field scale pumping tests.

From a practical point of view, it is valuable to use thermal tracer tomography to investigate hydraulic properties of fractured media. Thermal tracer tomography not only reduces a lot of experimental efforts but is also easy to operate. For example, it only requires injection of warm water and monitoring of temperature changes along the wells. Somogyvári and Bayer (2017) even completed this testing method by reinjecting pumped water into the well after being heated by the sunlight. However, it is worth noting that the testing period can be much longer compared to hydraulic tomography, especially when the well spacing is large. Also, in order to avoid interference with pervious thermal tests, a relatively long break may be needed between experiments for heat dissipation. In order to reduce the uncertainty of inversion results, it is a good choice to use a flexible borehole liner sealing within the observation wells, or to add more prior information to constrain the inversion procedure, such as the fracture orientations. In addition, since hydraulic diffusion is much more sensitive to low-permeable fractures and rock matrix than thermal diffusion, we also recommend to combine thermal tracer tomography and hydraulic tomography to improve the characterization of hydraulic and structural properties of fractured media.

6

Performance comparison of two tomographic methods

Contents

This chapter is to compare the performance of slug test-based hydraulic tomography (HTs) and thermal tracert tomography (TT) during field testing at the Göttingen site. The aim, on the one hand, is to obtain a more comprehensive evaluation of the hydraulic properties of the experimental site. On the other hand, the advantages of each tomographic method can be clarified to guide further related applications.

6.1 Comparison of theory and testing techniques

According to the test results obtained at the experimental site, the performance of slug test-based hydraulic tomography (HTs) and thermal tracer tomography (TT) can be analyzed and compared. The differences in theory and testing techniques of the HTs and TT methods configured at the Göttingen site are firstly compared, which are listed in Table 6.1.

Theoretically, the HTs method relies on the hydraulic diffusion process that is solely related to hydraulic parameters, such as hydraulic conductivity (k), specific storage (S_s), and hydraulic diffusivity (D). Using the travel time-based inversion and attenuation inversion, the D and S_s distributions can be directly inverted. The TT method is based on the heat transfer process, which is not only controlled by hydraulic parameters but also by thermal properties. To estimate k, an assumption that convection is dominating in the heat transfer process is made in the TT method. This assumption is reasonable for characterizing conductive fractures because conductive fractures are always the main channel for groundwater flow in fractured aquifers. But it limits the application of the TT method to the characterization of the low-k medium of fractured aquifers.

Table 6.1: Comparison of HTs and TT methods used at the Göttingen site

Factors		*HTs method*	*TT method*
Theory	Physical process	hydraulic diffusion	heat transfer
	Inversion methods	travel time & attenuation inversion	travel time inversion
	Inversion parameters	D and S_s	k
Testing technique	Measurement device	pressure sensor	DTS
	Packer system	yes	no
	Spatial resolution	8 m	0.5 m
	Testing time	minutes	> 5 hours
	Logistics	/	electricity, water
Performance	Advantages	short testing time simple and economical test equipment no additional support required both D & S_s estimations	little physical efforts high-resolution measurements
	Disadvantages	cumbersome physical labor spatially low-resolution measurements	long testing time expensive test equipment water & electricity required only k estimation
	Limitations	/	convection-dominated heat transfer

Technical factors, such as testing time, equipment, and logistics, are important for the application and promotion of the methods. In the HTs method, the packer system is necessary to separate the borehole into serval testing or observation intervals. In a well-developed wellbore, the interval length must be adjusted

according to the installed screen length. For instance, during the HTs at the experimental site, the testing or observation interval is 5 m long, and the distance between the neighboring intervals is 3 m according to the well structure shown in Figure 2.3. The spatial resolution of hydraulic measurements is therefore 8 m. In the TT method, using DTS, the minimum distance of thermal sensors can reach 0.5 m, and the temperature measurements can be collected simultaneously along the DTS cable, which greatly reduces the cumbersome labor for adjusting the position of packers in the HTs method. By contrast, the TT method enables higher-resolution measurements with much less physical effort than the HTs method, at the cost of more expensive equipment and logistics. While, due to the relatively slow heat transfer process, the TT method typically requires a much longer testing time (e.g. hours or days).

6.2 Comparison of inverted hydraulic conductivities

Hydraulic parameters of the fractured rock experimental site have been estimated by the HTs in Chapter 4 and by the TT methods introduced in Chapter 5. Since the TT method can only invert k, and the HTs method can also calculate k by multiplying the estimated D by S_s, the performance of the two tomographic methods can be thus analyzed by comparing their inverted k distributions. The comparison results are summarized in Figure 6.1.

In Figure 6.1, the HTs result is a 3D distribution of k between wells M, O, and S, while the k inverted by the TT method is only 2D tomogram between wells M and O. Although the well S is involved during thermal tracer tests, no evident temperature change was observed. In my opinion, there are two reasons related to testing techniques. Firstly, the testing time of each thermal tracer test performed at this field site is only 5 hours, which can be insufficient for heat transfer processes between well S and the others due to the longer distances. Secondly, the observation well is open (without a packer system) during thermal tracer tests. It implies that when warm water is injected into well M or well O, a higher hydraulic gradient occurs between these two wells due to the shorter distance (only 2 m), resulting in less groundwater flow into well S. These possible reasons demonstrate that testing techniques, including testing time and observation well setup, can have a significant impact on measurements of the TT method.

In detail, the high-k zones estimated by both inversion results (Figure 6.1a and b) are almost horizontal, and their locations are also similar, especially at depths of about 10m, 19 m, and 35 m. According to the lithology shown in Figure 2.3, it can be inferred that the thick high-k zone around 10 m is sedimentary overburden. The high-k zones located at depths of approximately 19 m and 35 m can be inferred to be conductive fractures since their k values are much higher than adjacent formations. Due to the much higher resolution measurements, the TT method provides a much clearer fracture identification, particularly, the fracture at the depth of around 35 m. The high-k zones at the depth of about 28 m can be determined as a conductive

fracture by the TT method, but it is not easy to be recognized by the HTs method (Figure 6.1a) because of the overlying medium-k zones. One of the reasons could be related to the low-resolution measurements in HTs tests, which failed to identify the low-k zones between 30 m and 35 m. Conversely, another reason could be that the medium-k zones are covered by the high-k fractures, as *Case 6* illustrated in Section 5.3. Additionally, the fractures inferred by HTs and TT methods can be further confirmed by comparing them with the fractures detected by televiewer logs in borehole M, as shown in Figure 6.1c. Although a total of 7 fractures are detected by televiewer logs in borehole M (Figure 6.1c), comparison results indicate that only three of the fractures located in permeable screen sections are hydraulically conductive and their location can be mutually authenticated.

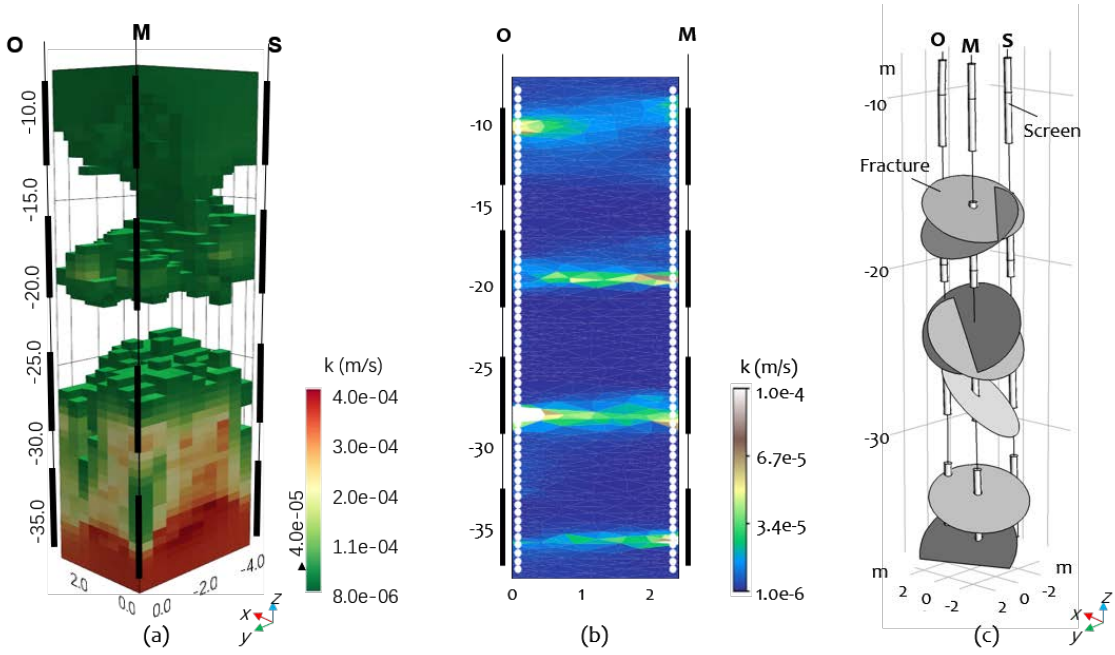

Figure 6.1: Inversion results of k distributions inverted by (a) the HTs method and (b) the TT method, and (c) the disc-shaped fractures inferred based on the measured fracture azimuths and dips by televiewer logs in borehole M (Werner, 2013).

The k values inverted by the HTs method and TT method are slightly different. To quantify the difference, k values inverted by the two methods along wells M and O are depicted in Figure 6.2. For the result from the HTs method, the inferred fracture at the depth of about 35 m has the largest k value around 3×10^{-4} m/s. But for the result of the TT method, the highest k fracture is located at about 28 m depth, especially the part close to the well O, where the k value reaches 3.8×10^{-4} m/s. With respect to the rock matrix, here defined as the formation except for the inferred fractures, its k value inverted by the HTs method is overall slightly higher than that inverted by the TT method. Theoretically, rock matrix k inverted by the HTs method is more reliable, because the low-k rock matrix is more sensitive to hydraulic diffusion than heat transfer. The slow heat transfer process may not reach observation points within the limited testing period in practice or distort the explanation of hydraulic properties due to the thermal conduction in the rock matrix.

In summary, the inversion results of two tomographic methods on revealing the fracture locations and their hydraulic conductivities are similar. Differences occur at the inverted k values of inferred fractures and the remaining rock matrix. With the high-resolution measurements, the TT method can provide a more accurate characterization of the location and hydraulic properties of high-conductive fractures. Given the fast hydraulic diffusion process, the HTs method can theoretically offer a more accurate hydraulic characterization of the medium-k fractures and rock matrix.

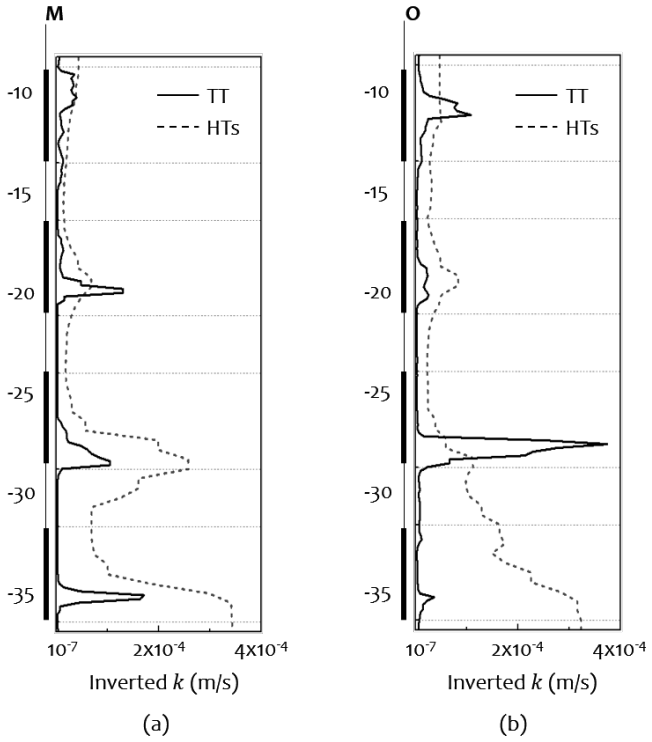

Figure 6.2: Results of k values inverted by HTs and TT methods along (a) well M and (b) well O.

6.3 Comparison of estimated hydraulic connectivity

According to the inverted high-k zones shown in Figure 6.1, good hydraulic connectivity can be preliminarily identified at the inferred fractures with depths of about 19 m, 28 m, and 35 m. However, there are some slight differences between the hydraulic connectivity revealed by the two tomographic methods. Based on the heat transfer process, the TT method majorly provides intuitive information on the transport connectivity of fractures, which is more focused on revealing the dominantly conductive fractures and is much more sensitive to the continuity of high-k paths. Whereas the HTs method is based on the hydraulic diffusion process, it prefers to reveal the flow connectivity which is sensitive to the conductive fractures as well as the medium-k rock matrix including some secondary fractures.

Inversion results from the experimental site also reflect the subtle differences between HTs and TT methods

in characterizing hydraulic connectivity of fractures. The inversion algorithms employed in the HTs and TT methods are both trajectory-based. The trajectory will iterate during inversion processes and bend to the high-k zones. It implies that the zones traversed by more trajectories could be inferred as conductive fractures with better hydraulic connectivity. In the trajectory-based inversion algorithm, the total length traversed by trajectories within one cell is defined as ray coverage (COV). Figure 6.3 illustrates the ray coverage calculated during the HTs and TT inversions. It indicates that the calculated ray coverage by the TT method is more concentrated than that by the HTs method.

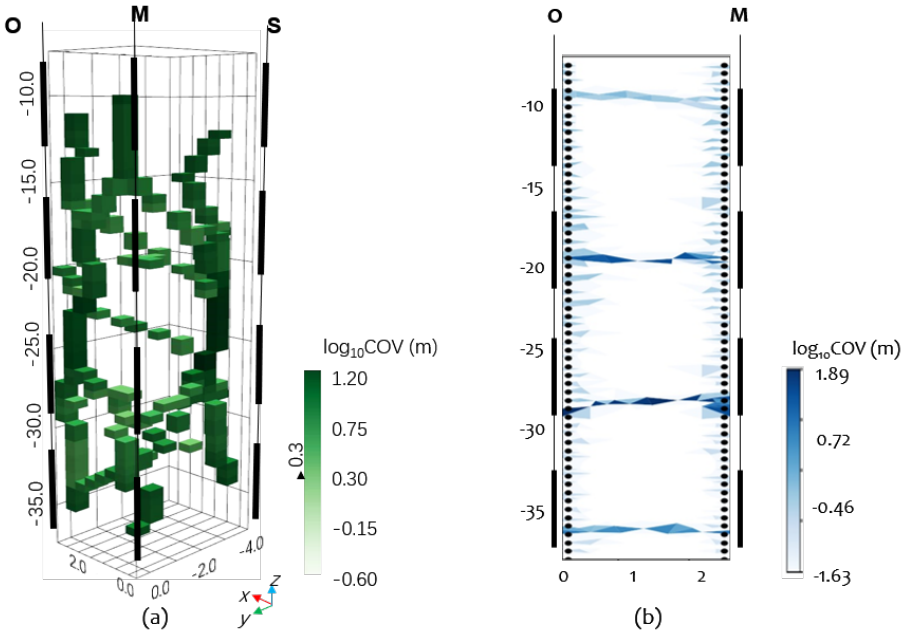

Figure 6.3: Ray coverage calculated by the (a) travel time-based HTs method and (b) the TT method. Note that the ray coverage results are plotted in logarithm, and the result of HTs inversion only shows the high values (greater than 0.3) for a clear view.

7

Conclusions and outlook

7.1 Conclusions

Characterization of the hydraulic properties in fractured aquifers at field scales, including the conductive fracture locations, hydraulic parameters, and hydraulic connectivity, is significant but quite challenging work. In this thesis, two tomographic methods, i.e. slug test-based hydraulic tomography (HTs) and thermal tracer tomography (TT), are employed, which have been well-established for the porous media. Considering the characteristics of fractured aquifers, such as the complex fracture geometry, highly hydraulic heterogeneity, and relatively deep formation, the applicability of these two tomographic methods was firstly verified by the synthetic experiments and then tested at a fractured rock experimental site in Göttingen which is described in Chapter 2.

Chapters 3 and Chapter 4 describe the application of the HTs method in characterizing the hydraulic properties of fractured aquifers. In deep or highly permeable fractured aquifers, wellbore effects including inertial effects and wellbore storage can have a significant impact on slug test responses. In order to investigate the influence of wellbore effects, a forward slug test model (3DHIM) that can consider both wellbore effects and skin effects in a heterogeneous aquifer was first developed. Based on this model, a series of multilevel cross-well slug tests were simulated in a highly heterogeneous aquifer analogue. Simulation results indicate that due to wellbore effects, the hydraulic travel time delay in the wellbore is quasi-linear to the water column height, and the head attenuation in the observation well can be neglected. According to these findings, a new method for removing the influence of wellbore effects from the observed slug test responses was further proposed. The new method was then verified by successfully reconstructing the hydraulic parameters (i.e. hydraulic diffusivity and specific storage) of the aquifer analogue using the travel time inversion and attenuation inversion. The aforementioned HTs method was finally applied at the fractured rock experimental site, and three conductive fractures were revealed at the depths of about 19 m, 28 m, and 35 m.

With advantages of high spatial resolution and efficient monitoring techniques, the TT method is also employed in characterizing the hydraulic properties of fractured aquifers in Chapter 5. Considering the

features of heat transfer in fractured media, such as concentrating on the highly conductive fracture and controlling by the complex fracture geometry, some modifications were first made to the thermal travel time-based inversion framework. Based on a synthetic fracture geometry, the performance of this modified framework in characterizing hydraulic properties of fractured aquifers was then tested through numerical experiments. Inversion results indicate that the modified TT method can efficiently identify directly connected or interconnected fractures, even with the presence of some practical issues, like the ambient hydraulic gradient, observation well annular wall flow, or measurements based on conventional thermal sensors with less precision. Accordingly, the TT method was finally applied at the fractured rock experimental site, and it revealed a directly connected fracture and two interconnected fractures at similar depths identified by the HTs method.

Chapter 6 analyzed the performance of HTs and TT methods on the hydraulic characterization of fractured aquifers. Based on the field tests performed at the fractured rock experimental site, differences in theory and testing techniques and their influences on the inversion results, specifically, on the inverted hydraulic conductivity and connectivity, were analyzed. Due to the relatively fast hydraulic process, the HTs method can be more reliable for the identification of medium-k fractures than the TT method. Due to the pretty high resolution in measurements, the TT method can provide a better characterization of the locations and hydraulic conductivities of high-k fractures. Moreover, inversion results of the HT and TT methods have subtle differences in characterizing the connectivity of conductive fractures. Transport connectivity estimated by the TT method is more concentrated on revealing the dominantly conductive fractures, while the flow connectivity estimated by the HTs method is sensitive to the conductive fractures with medium-k as well. This difference was confirmed by the ray coverage calculated by two tomographic methods.

Overall, the presented thesis validates the feasibility of two tomographic methods for characterizing the hydraulic properties of fractured aquifers and facilitates research on the hydraulic characterization of fractured aquifers at the field scale. TT methods equipped with DTS tend to provide a high-resolution characterization of the dominantly conductive fractures locations and their hydraulic conductivities, while HTs methods provide more hydraulic information in medium-k media but with relatively lower resolution.

7.2 Outlook

In order to further promote the application of these two tomographic methods in practice, it is recommended to conduct further studies on three main aspects, i.e. uncertainty analysis, joint inversion, and experimental improvement.

Uncertainty analysis at larger-scale or deep-aquifer sites

In many subsurface projects, large or deep aquifer sites can be frequently encountered, such as geothermal exploration sites or nuclear waste storage sites with surface sizes up to hundreds of meters. In these sites, the investigation of hydraulic properties is typically one of the crucial tasks. To my best knowledge, the two tomographic methods adopted in this thesis, i.e. HTs and TT methods, can be still applicable just by replacing the conventional slug test with an oscillatory slug test or by prolonging the heat injection time of the HT method to expand the disturbance area. However, some uncertainties in the inversion results caused by the new field conditions need to be assessed. For instance, in a deep well, the influence of wellbore effects can be more significant, and the relationship between the induced hydraulic travel time delay and water column height may not be quasi-linear. And in a large-scale site, the thermal tracer tests may affect by the local geological and hydrogeological conditions which may introduce the ambient disturbance into the observed temperature data during the long-term heat injection period.

Joint inversions

A joint inversion can not only be helpful for upscaling the application of the two tomographic methods to large-scale sites, but also can improve the accuracy of the inversion results by complementing the two methods. As mentioned in Chapter 6, TT methods can provide high-resolution results and HTs methods give more hydraulic information of medium-k media. A joint inversion based on the measured hydraulic and thermal signal collected at the same site will offer a better characterization of the fractured aquifers. Apart from this, a joint inversion combining geological and geophysical information is also recommended. The detected fracture locations and geological tectonics can be used to constrain the HTs and TT inversion models, which will greatly reduce the uncertainty of the inversion results.

Experimental improvements

The improvement in testing techniques is also significant for the field-scale hydraulic characterization in fractured aquifers. For the HTs tests, the measured slug test responses will rely not only on wellbore effects but also on wellbore development, screen installation, and skin effects. To minimize their impacts, it would be necessary to develop a device that can stimulate slug tests within the packer system. A high-resolution observation system similar to DTS is also quite helpful for reducing the current cumbersome efforts. Additionally, some novel techniques regarding the thermal tracer tests are increasingly developed, for instance, the active-DTS device, flexible borehole liner, and passive temperature tomography. How to combine these new techniques to further improve the accuracy and resolution of hydraulic characterization of fractured aquifers will be one of the important directions for further work.

Appendices

A1 Borehole deviation

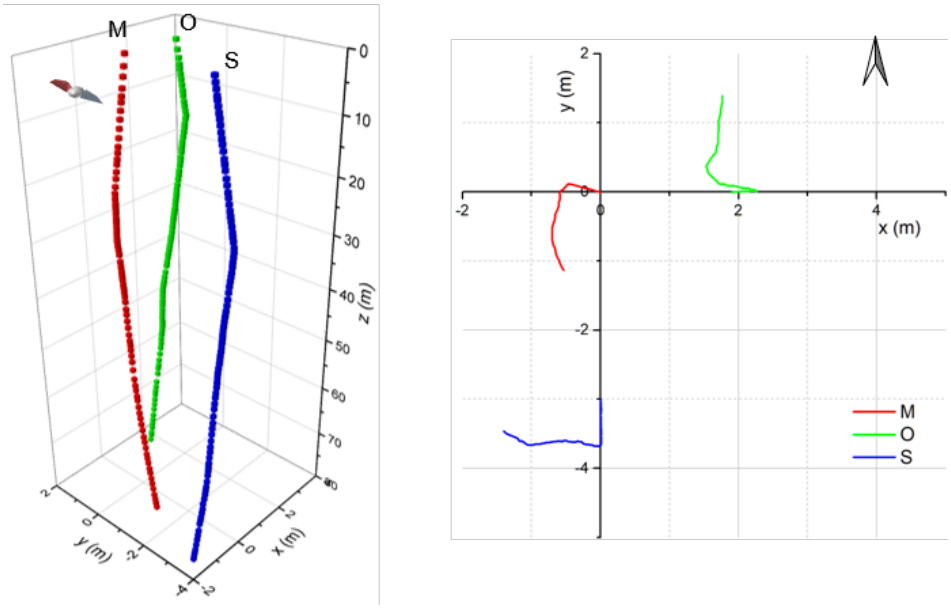

Figure A1: Borehole vertical deviation of well M, O, and S located at the fractured experimental site in Göttingen: 3D view (left) and top view (right). Data is cited from Werner (2013)

A2 Weak form of the Navier-Stokes equation in slug test modeling

Within the wellbore region (Ω_f), we assume that the groundwater motion can be described by the incompressible NS equation as Eq. (A2.1). This particular form is derived from the generic Cauchy momentum equation (Goraj, 2016),

$$\rho \frac{D\boldsymbol{v_f}}{Dt} = \nabla \cdot T + f \tag{A2.1}$$

where $\frac{D}{Dt}$ is the material derivative, defined as $\frac{\partial}{\partial t} + \boldsymbol{v_f} \cdot \nabla$, T is the Cauchy stress tensor, and f represents the body forces. Within the incompressible fluid domain, the Cauchy stress tensor can be set to the sum of a pressure term $-p_f \boldsymbol{I}$ and a viscosity term $\mu(\nabla \boldsymbol{v_f} + (\nabla \boldsymbol{v_f})^T$.

During the slug test, the groundwater flow in the well is dominated by the vector of flow velocity $\boldsymbol{v_f}(\boldsymbol{u}, \boldsymbol{v}, \boldsymbol{w})$ and scalar pressure p. In 3D cartesian coordinates, the symmetric stress tensor can be written as (Malvern, 1969):

$$T = \begin{bmatrix} -p + 2\mu\frac{\partial \boldsymbol{u}}{\partial x} & \mu(\frac{\partial \boldsymbol{u}}{\partial y} + \frac{\partial \boldsymbol{v}}{\partial x}) & \mu(\frac{\partial \boldsymbol{u}}{\partial z} + \frac{\partial \boldsymbol{w}}{\partial x}) \\ & -p + 2\mu\frac{\partial \boldsymbol{v}}{\partial y} & \mu(\frac{\partial \boldsymbol{v}}{\partial z} + \frac{\partial \boldsymbol{w}}{\partial y}) \\ & & -p + 2\mu\frac{\partial \boldsymbol{w}}{\partial z} \end{bmatrix} \tag{A2.2}$$

To improve computational efficiency, the groundwater flow in the well can be simplified to axisymmetric flow. Eq. (A2.1) can be transformed from Cartesian coordinates (x, y, z) to cylindrical coordinates (r, θ, z) by using an operator,

$$\Lambda = \frac{\partial}{\partial r} r + \frac{1}{r}\frac{\partial}{\partial \theta}\theta + \frac{\partial}{\partial z} z \tag{A2.3}$$

For the axisymmetric flow, the tensor can be expressed as (Malvern, 1969):

$$T = \begin{bmatrix} -p + 2\mu\frac{\partial \boldsymbol{u}}{\partial r} & \mu[r\frac{\partial}{\partial r}(\frac{\boldsymbol{v}}{r}) + \frac{1}{r}\frac{\partial \boldsymbol{u}}{\partial \theta}) & \mu(\frac{\partial \boldsymbol{u}}{\partial z} + \frac{\partial \boldsymbol{w}}{\partial r}) \\ & -p + 2\mu(\frac{1}{r}\frac{\partial \boldsymbol{v}}{\partial \theta} + \frac{\boldsymbol{u}}{r}) & \mu(\frac{\partial \boldsymbol{v}}{\partial z} + \frac{1}{r}\frac{\partial \boldsymbol{w}}{\partial \theta}) \\ & & -p + 2\mu\frac{\partial \boldsymbol{w}}{\partial z} \end{bmatrix} \tag{A2.4}$$

In order to find the variational form for numerical analysis, the weak form of Eq. (A2.1) can be expressed as,

$$0 = -\int_{\Omega_f} \rho[\frac{\partial \boldsymbol{v_f}}{\partial t} + (\boldsymbol{v_f} \cdot \nabla)\boldsymbol{v_f}] \cdot \boldsymbol{\tau} - \int_{\Omega_f} T \cdot \nabla\boldsymbol{\tau} + \int_{\Omega_f} f \cdot \boldsymbol{\tau} + \int_{\Gamma_f} T \cdot \boldsymbol{\tau} \tag{A2.5}$$

Accordingly, this weak form can be solved by the finite element method, such as implemented in the COMSOL software, and coupled with Darcy's law for description of groundwater flow (Hanspal et al., 2006).

A3 Supplementary results at the experimental site by the HTs method

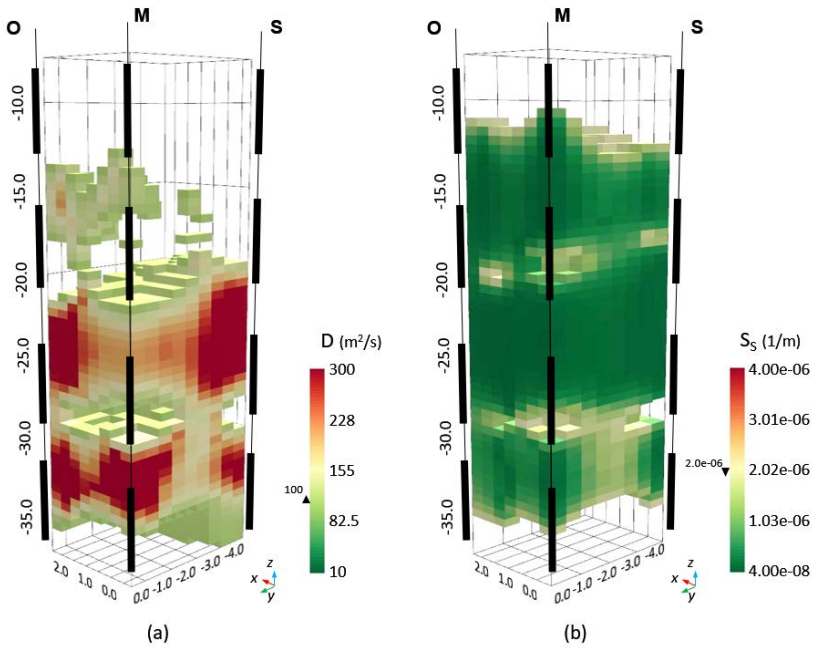

Figure A3: Distribution of (a) D and (b) S_s estimated by the slug test-based hydraulic tomography performed at the fractured experimental site

A4 Forward model of thermal tracer tomography in a fractured aquifer

We assume that the groundwater flow in both fractures and porous matrix follows Darcy's law. The steady-state hydraulic head field $h(\boldsymbol{x})$, where $\boldsymbol{x}$ is the spatial location, can be obtained by solving the groundwater flow equation:

$$-\nabla \cdot \big(k(\boldsymbol{x})\nabla h(\boldsymbol{x})\big) = Q_H, \tag{A4.1}$$

subject to the two boundary conditions:

$$h(\boldsymbol{x})|_{\boldsymbol{x}\in\Gamma_{lat}} = \boldsymbol{h}_0, \tag{A4.2}$$

$$\boldsymbol{n} \cdot \big(k(\boldsymbol{x})\nabla h(\boldsymbol{x})\big)\big|_{\boldsymbol{x}\in\Gamma_{inj}} = q_{inj}, \tag{A4.3}$$

where $k(\boldsymbol{x})$ is the isotropic hydraulic conductivity field, and Q_H is the volumetric source density. Eq. (A4.2) indicates a constant head boundary at the lateral boundary Γ_{lat}. Considering the possible ambient groundwater flow, the constant head $\boldsymbol{h}_0$ can be a vector containing unequal elements assigned on different lateral boundaries to achieve a natural hydraulic gradient. At the injection boundary Γ_{inj}, a Neumann boundary condition is assigned to simulate the water injection on it with a constant volumetric flux q_{inj}. $\boldsymbol{n}$ denotes the unit normal vector pointing inwards.

The groundwater flow velocity $\boldsymbol{u}$ is related to $k(\boldsymbol{x})$, $h(\boldsymbol{x})$, and the porosity distribution $\phi(\boldsymbol{x})$,

$$\boldsymbol{u} = -k(\boldsymbol{x})\nabla h(\boldsymbol{x})/\phi(\boldsymbol{x}). \tag{A4.4}$$

For the transient heat transfer, buoyancy effects can be ignored if the injected groundwater is heated below 15 °C (Ma & Zheng, 2010). Thus the convection-diffusion equation is utilized for heat transfer in both fractures and the porous matrix, which is expressed as (Anderson, 2005; Hu, R. et al., 2018; Sarris et al., 2018; Schwede et al., 2014),

$$\frac{\rho_b C_b}{\rho_w C_w}\frac{\partial T(\boldsymbol{x},t)}{\partial t} = \nabla \cdot \left[\frac{\rho_b C_b}{\rho_w C_w} D(\boldsymbol{x})\nabla T(\boldsymbol{x},t)\right] - \boldsymbol{u} \cdot \nabla T(\boldsymbol{x},t) + Q_T, \tag{A4.5}$$

subject to the boundary conditions:

$$\boldsymbol{n} \cdot \left(\frac{\rho_b C_b}{\rho_w C_w} D(\boldsymbol{x})\nabla T(\boldsymbol{x},t)\right)\Big|_{\boldsymbol{x}\in\Gamma_{lat}} = 0, \tag{A4.6}$$

$$\boldsymbol{n} \cdot \big(\boldsymbol{u}T(\boldsymbol{x},t)\big)\big|_{\boldsymbol{x}\in\Gamma_{inj}} = q_{inj}\Delta T, \tag{A4.7}$$

$$T(\boldsymbol{x},0) = T_{amb}, \tag{A4.8}$$

where $T(\boldsymbol{x},t)$ denotes the evolution of the temperature distribution, t is the time. ρC represents the

volumetric heat capacity, the subscript b and w denote the rock block and water. $D(\boldsymbol{x})$ is the thermal diffusion tensor, defined as the ratio of thermal conductivity $\lambda_b(\boldsymbol{x})$ and $\rho_b C_b$. Q_T is the heat flux source. The conductive or diffusive flux at Γ_{lat} and other unallocated boundaries is assumed to be zero. Eq. (A4.8) represents the heat flux at Γ_{inj} with a constant injected temperature ΔT, i.e., the temperature difference between the heated water T_{inj} and the background temperature T_{amb}.

Based on the volume averaging method, the thermal properties of the rock block can be computed as the weighted arithmetic mean of the rock matrix (r) and water (w):

$$\rho_b C_b = \phi(\boldsymbol{x})\rho_w C_w + \big(1-\phi(\boldsymbol{x})\big)\rho_r C_r, \tag{A4.10}$$

$$\lambda_b(\boldsymbol{x}) = \phi(\boldsymbol{x})\lambda_w(\boldsymbol{x}) + \big(1-\phi(\boldsymbol{x})\big)\lambda_r(\boldsymbol{x}). \tag{A4.11}$$

The above partial differential equations of the hydrothermal processes are solved by the finite volume method, and implemented by using the open-source Python code based on the geophysical library of pyGIMLi (Rücker et al., 2017).

A5 Parameter settings for numerical thermal tracer tests

Table A5 Parameters used in the numerical tests

Variable	Description	Value
Geometry and model discretization		
Ω	Domain size (m)	40×20
Z_1	Thickness of the top sediments (m)	2
Z_2	Thickness of the fractured bedrock (m)	18
$\boldsymbol{L}_1$	Location of Fracture 1 (m)	[(-6,-7), (-2,-9)]
$\boldsymbol{L}_2$	Location of Fracture 2 (m)	[(-12,-18), (12,-6)]
$\boldsymbol{L}_3$	Location of Fracture 3 (m)	[(0,-12), (-12,-15)]
δ	Aperture of all fractures (m)	0.01
α	Maximum of mesh area (m^2)	0.2
Setup of the multi-level thermal tracer tests		
X_{inj}	x location of the injection intervals (m)	-4
$\boldsymbol{Z}_{inj}$	z locations of the injection intervals (m)	[-6,-8,-10,-12,-14,-16]
δz	Length of injection interval (m)	0.2
X_{obs}	x location of the monitoring points (m)	4
$\boldsymbol{Z}_{obs}$	z locations of the monitoring points (m)	[-6,-7,-8,-9,-10,-11,-12,-13,-14,-15,-16]
δT_0	Accuracy of the thermal sensor (K)	0.001
δt	Time sampling interval (min)	1
Transport parameters		
ϕ	Porosity (all domain) (-)	0.3
q_0	Injection rate (l/s)	0.5
T_{inj}	Temperature of the injected water (℃)	20
T_{amb}	Ambient temperature (℃)	10
∇h_0	Ambient hydraulic gradient (-)	0
k_p	Hydraulic conductivity of top layer (m/s)	10^{-6}
k_r	Hydraulic conductivity of bedrock (m/s)	10^{-8}
$\boldsymbol{k}_{f1}$	Hydraulic conductivity of Fracture 1 (m/s)	[10^{-4},10^{-6}]
$\boldsymbol{k}_{f2}$	Hydraulic conductivity of Fracture 2 (m/s)	[10^{-4},10^{-6}]
$\boldsymbol{k}_{f3}$	Hydraulic conductivity of Fracture 3 (m/s)	[10^{-4},10^{-6}]
ρ_w	Density of water (kg/m^3)	1000
c_w	Heat capacity of water ($J/kg/K$)	4200
λ_w	Thermal conductivity of water ($W/m/K$)	0.6
ρ_r	Density of rock matrix (kg/m^3)	2000
c_r	Heat capacity of rock matrix ($J/kg/K$)	2700
λ_w	Thermal conductivity of rock matrix ($W/m/K$)	3.0
lam_{opt}	Optimized regularization factor	10
Special conditions		
∇h_1	Ambient hydraulic gradient in Case 7 (-)	0.2
δT_1	Accuracy of thermal sensor in Case 8 (K)	0.1
d_w	Diameter of observation well in Case 9 (m)	0.1
l_w	Depth of observation well in Case 9 (m)	18
k_{well}	Hydraulic conductivity of the well in Case 9 (m/s)	3125

A6 Slug test results measured in the fractured experimental site

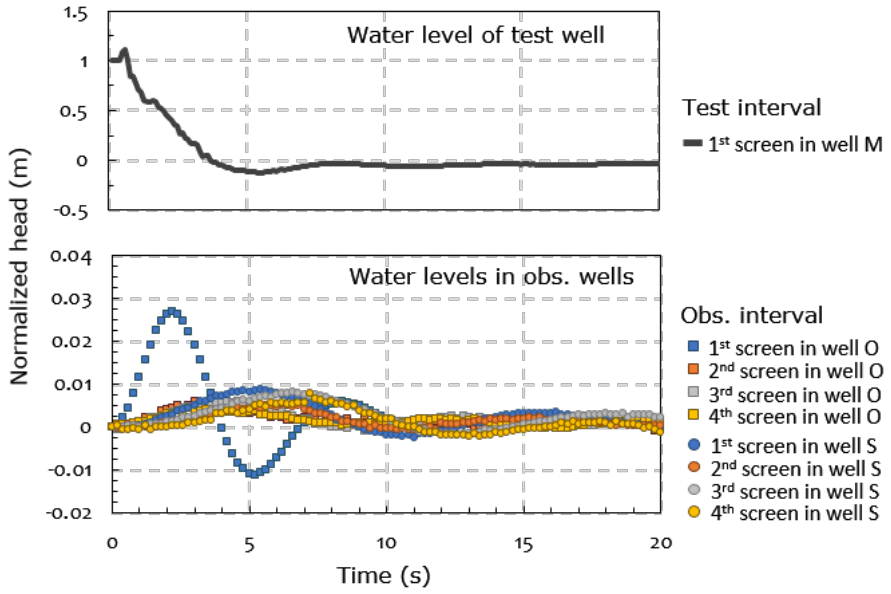

Figure A5.1: Slug test responses when testing at the 1st screen interval in well M (8 m ~ 13 m shown in Figure 4.7).

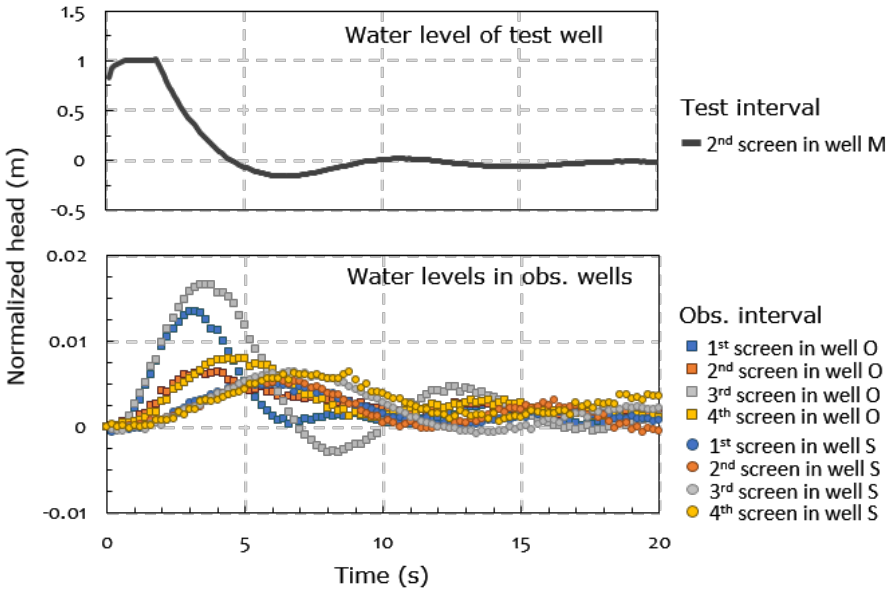

Figure A5.2: Slug test responses when testing at the 2nd screen interval in well M (16 m ~ 21 m shown in Figure 4.7).

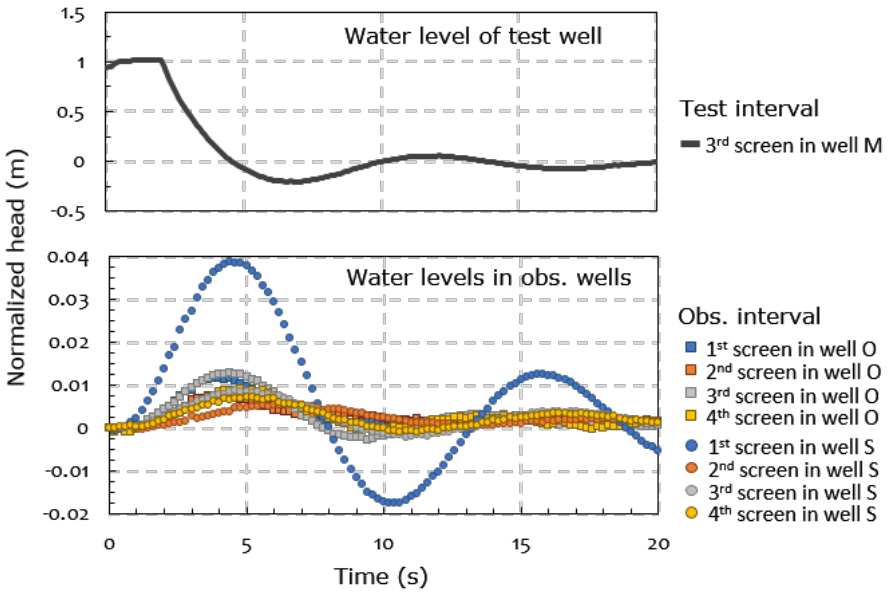

Figure A5.3: Slug test responses when testing at the 3rd screen interval in well M (24 m ~ 29 m shown in Figure 4.7).

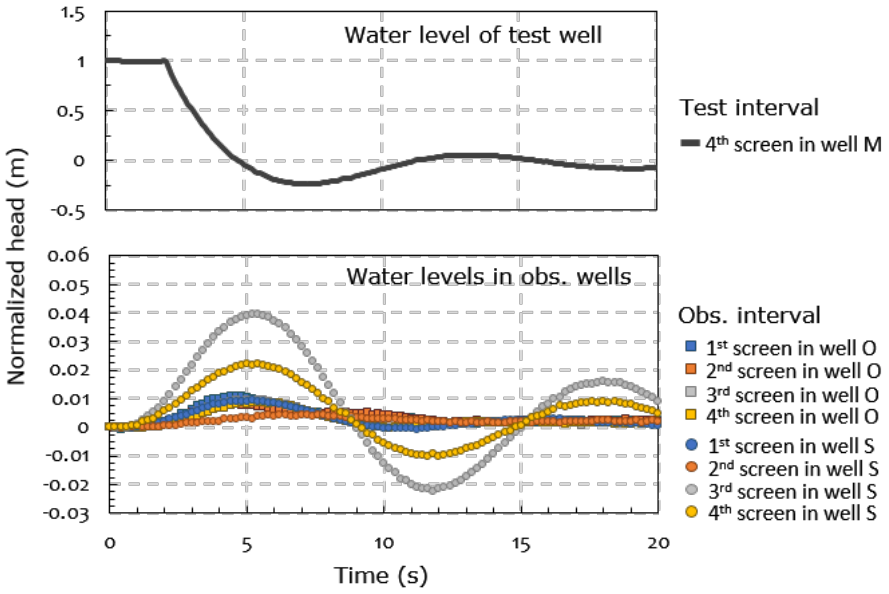

Figure A5.4: Slug test responses when testing at the 4th screen interval in well M (32 m ~ 37 m shown in Figure 4.7).

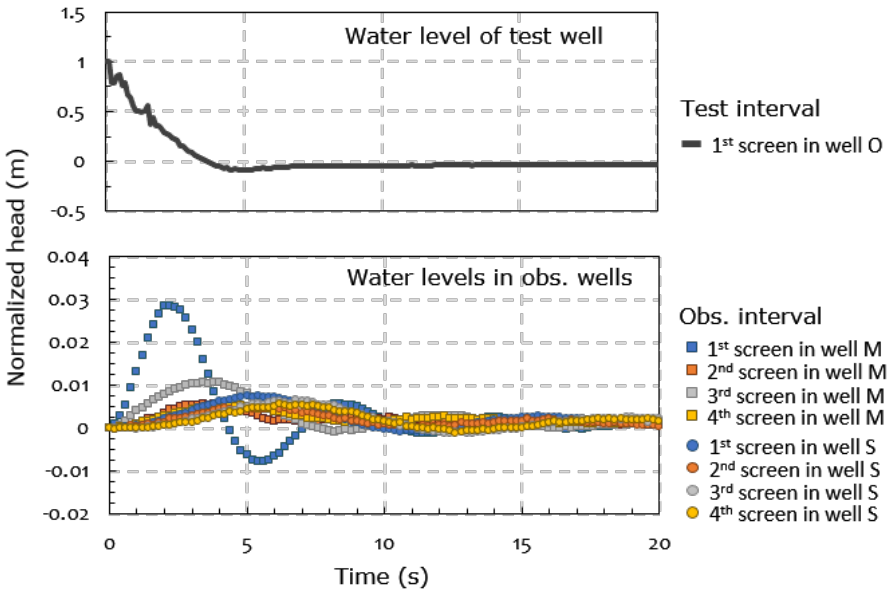

Figure A5.5: Slug test responses when testing at the 1st screen interval in well O (8 m ~ 13 m shown in Figure 4.7).

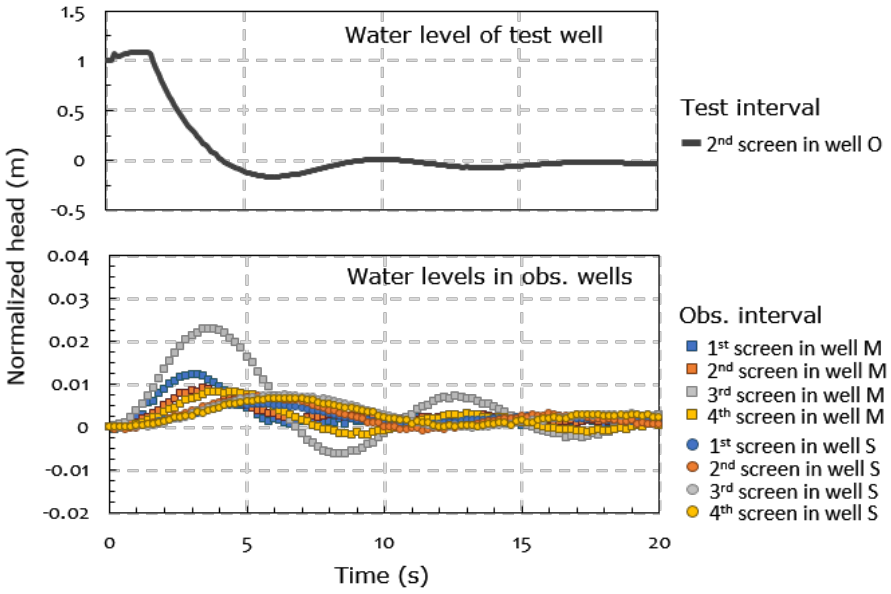

Figure A5.6: Slug test responses when testing at the 2nd screen interval in well O (16 m ~ 21 m shown in Figure 4.7).

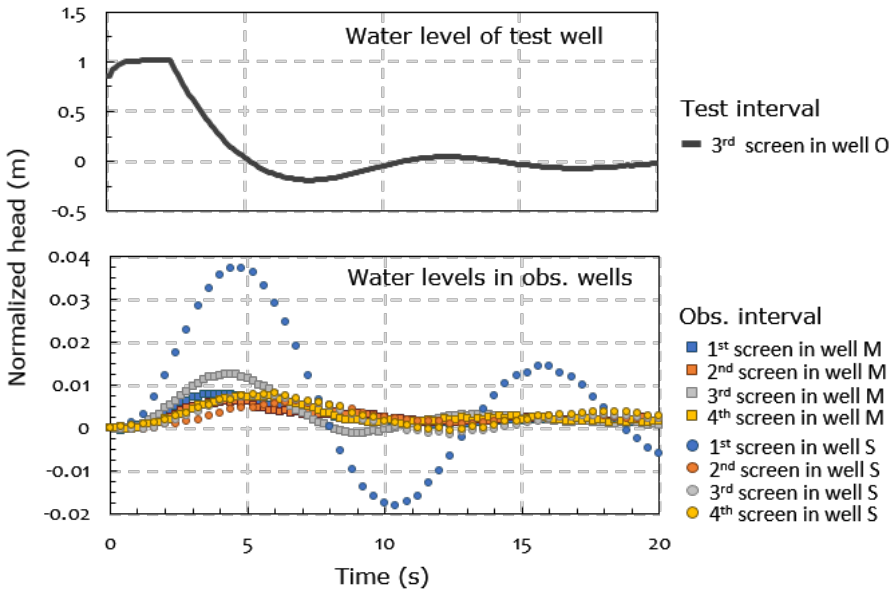

Figure A5.7: Slug test responses when testing at the 3rd screen interval in well O (24 m ~ 29 m shown in Figure 4.7).

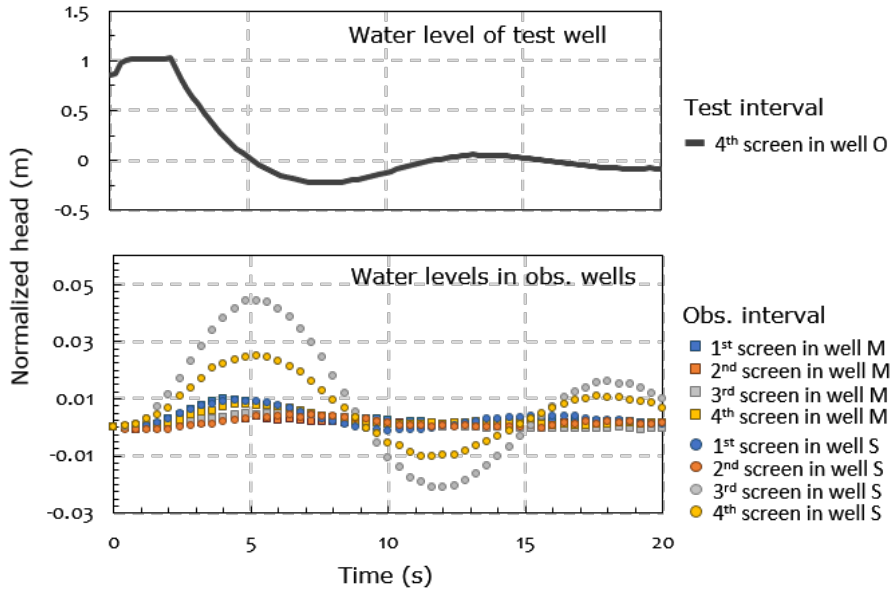

Figure A5.8: Slug test responses when testing at the 4th screen interval in well O (32 m ~ 37 m shown in Figure 4.7).

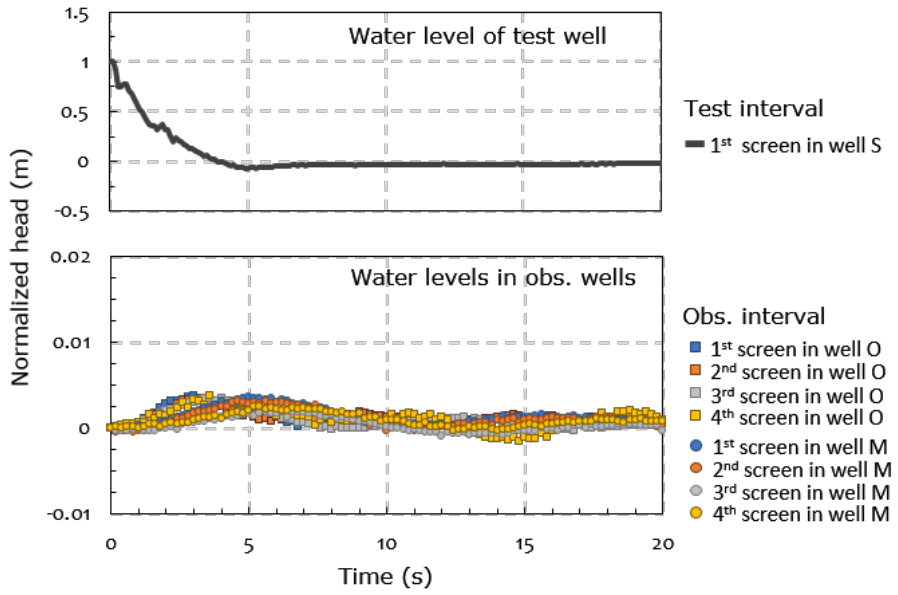

Figure A5.9: Slug test responses when testing at the 1st screen interval in well S (8 m ~ 13 m shown in Figure 4.7).

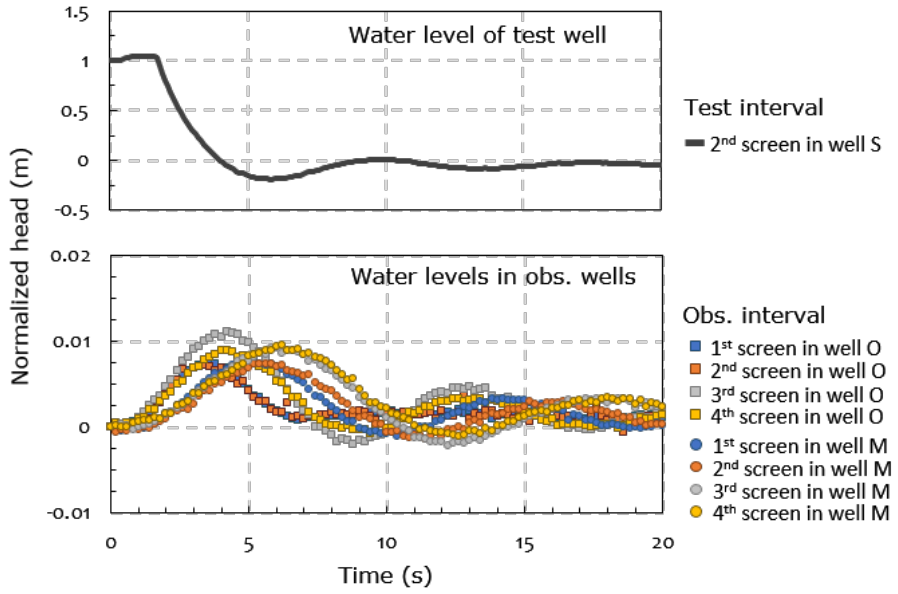

Figure A5.10: Slug test responses when testing at the 2nd screen interval in well S (16 m ~ 21 m shown in Figure 4.7).

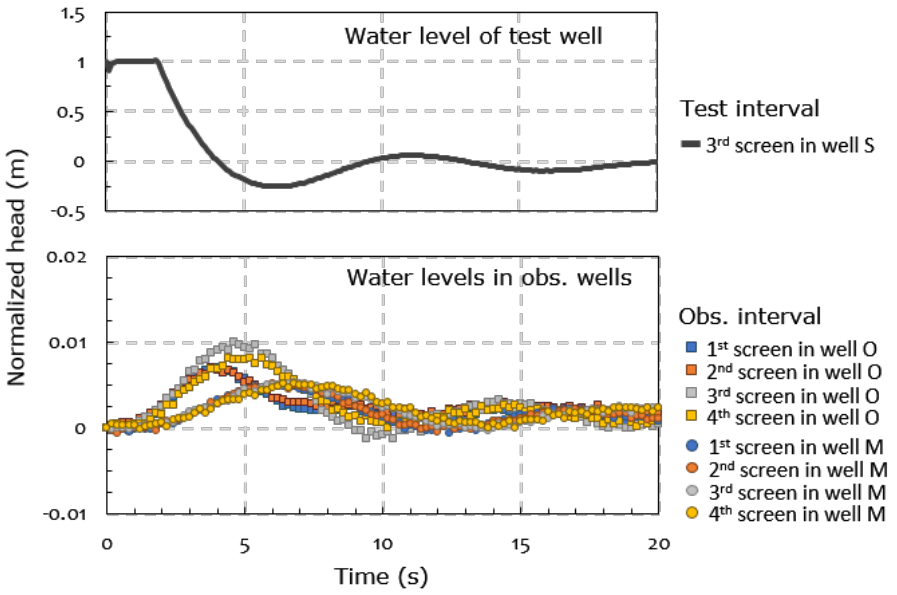

Figure A5.11: Slug test responses when testing at the 3rd screen interval in well S (24 m ~ 29 m shown in Figure 4.7).

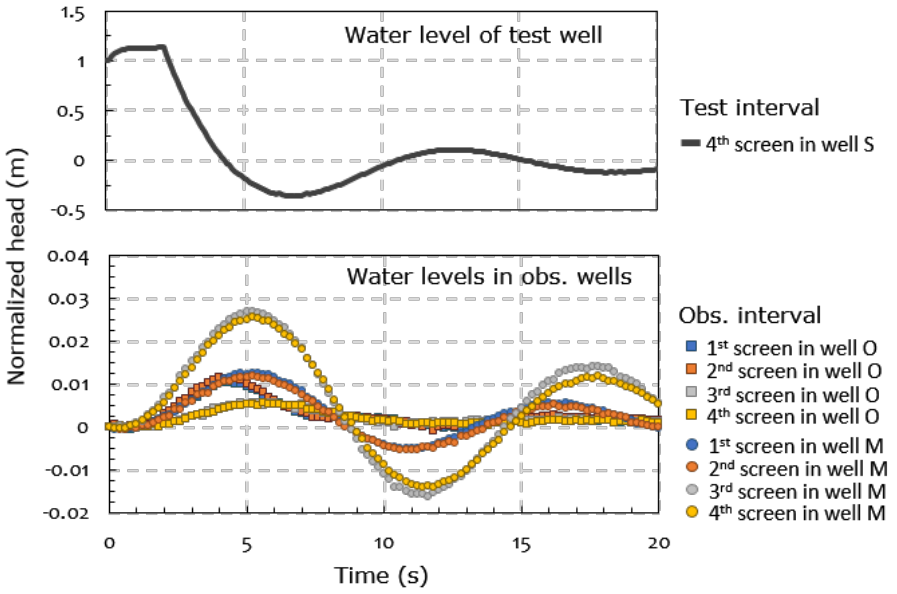

Figure A5.12: Slug test responses when testing at the 4th screen interval in well S (32 m ~ 37 m shown in Figure 4.7).

References

Alazmi, B., Vafai, K. (2001). Analysis of fluid flow and heat transfer interfacial conditions between a porous medium and a fluid layer. *International Journal of Heat and Mass Transfer, 44*(9), 1735-1749

Anderson, M.P. (2005). Heat as a ground water tracer. *Ground Water, 43*(6), 951-968, https://dx.doi.org/10.1111/j.1745-6584.2005.00052.x

Audouin, O., Bodin, J. (2008). Cross-borehole slug test analysis in a fractured limestone aquifer. *Journal of Hydrology, 348*(3-4), 510-523

Baetzel, K. (2017a). Hydrogeological Characterization of a Fratured Aquifer based on Modelling and Heat Tracer Experiments. *Faculity of Geoscience and Geography*

Baetzel, K. (2017b). Hydrogeological Characterization of a Fratured Aquifer based on Modelling and Heat Tracer Experiments. *Unpublished Master Thesis). University of Göttingen*

Bakker, M., Calje, R., Schaars, F., van der Made, K.J., de Haas, S. (2015). An active heat tracer experiment to determine groundwater velocities using fiber optic cables installed with direct push equipment. *Water Resources Research, 51*(4), 2760-2772, https://dx.doi.org/10.1002/2014wr016632

Basiricò, S., Crosta, G.B., Frattini, P., Villa, A., Godio, A. (2015). Borehole flowmeter logging for the accurate design and analysis of tracer tests. *Groundwater, 53*(S1), 3-9

Bayer, P. (2000). Aquifer-Analog-Studie in grobklastischen 'braided river'Ablagerungen: Sedimentäre/hydrogeologische Wandkartierung und Kalibrierung von Georadarmessungen—Diplomkartierung. *Diplomkartierung, Universitaet Tuebingen*

Bayer, P., Huggenberger, P., Renard, P., Comunian, A. (2011). Three-dimensional high resolution fluvio-glacial aquifer analog: Part 1: Field study. *Journal of Hydrology, 405*(1-2), 1-9

Bear, J. (2013). *Dynamics of fluids in porous media*: Courier Corporation.

Beckie, R., Harvey, C.F. (2002). What does a slug test measure: An investigation of instrument response and the effects of heterogeneity. *Water Resources Research, 38*(12), 26-21-26-14

Bodvarsson, G. (1969). On the temperature of water flowing through fractures. *Journal of Geophysical Research, 74*(8), 1987-1992

Braester, C., Thunvik, R. (1984). Determination of formation permeability by double-packer tests. *Journal of Hydrology, 72*(3-4), 375-389

Brauchler, R., Cheng, J.-T., Dietrich, P., Everett, M., Johnson, B., Liedl, R., Sauter, M. (2007). An inversion strategy for hydraulic tomography: Coupling travel time and amplitude inversion. *Journal of Hydrology, 345*(3-4), 184-198

Brauchler, R., Hu, R., Dietrich, P., Sauter, M. (2011). A field assessment of high-resolution aquifer characterization based on hydraulic travel time and hydraulic attenuation tomography. *Water Resources Research, 47*(3)

Brauchler, R., Hu, R., Hu, L., Jimenez, S., Bayer, P., Dietrich, P., Ptak, T. (2013). Rapid field application of hydraulic tomography for resolving aquifer heterogeneity in unconsolidated sediments. *Water Resources Research, 49*(4), 2013-2024, https://dx.doi.org/10.1002/wrcr.20181

Brauchler, R., Hu, R., Vogt, T., Al-Halbouni, D., Heinrichs, T., Ptak, T., Sauter, M. (2010). Cross-well slug interference tests: An effective characterization method for resolving aquifer heterogeneity. *Journal of Hydrology, 384*(1-2), 33-45

Brauchler, R., Liedl, R., Dietrich, P. (2003). A travel time based hydraulic tomographic approach. *Water Resources Research, 39*(12)

Bredehoeft, J.D., Cooper Jr, H.H., Papadopulos, I.S. (1966). Inertial and storage effects in well-aquifer systems:

An analog investigation. *Water Resources Research, 2*(4), 697-707

Brindt, N., Wallach, R. (2017). The moving-boundary approach for modeling gravity-driven stable and unstable flow in soils. *Water Resources Research, 53*(1), 344-360

Brodic, B., Malehmir, A., Juhlin, C. (2017). Delineating fracture zones using surface-tunnel-surface seismic data, P-S, and S-P mode conversions. *Journal of Geophysical Research: Solid Earth, 122*(7), 5493-5516

Butler, J.J. (2019). *The design, performance, and analysis of slug tests*: Crc Press.

Butler, J.J., Bohling, G.C., Hyder, Z., Mcelwee, C.D. (1994). The Use of Slug Tests to Describe Vertical Variations in Hydraulic Conductivity. *Journal of Hydrology, 156*(1-4), 137-162, https://dx.doi.org/Doi 10.1016/0022-1694(94)90075-2

Butler, J.J., Jr. (2002). A simple correction for slug tests in small-diameter wells. *Ground Water, 40*(3), 303-307, https://dx.doi.org/10.1111/j.1745-6584.2002.tb02658.x

Butler, J.J., Zhan, X.Y. (2004). Hydraulic tests in highly permeable aquifers. *Water Resources Research, 40*(12), https://dx.doi.org/Artn W12402
10.1029/2003wr002998

Butler Jr, J.J. (2002). A simple correction for slug tests in small-diameter wells. *Groundwater, 40*(3), 303-308

Butler Jr, J.J., Healey, J.M., McCall, G.W., Garnett, E.J., Loheide, S.P. (2002). Hydraulic tests with direct-push equipment. *Groundwater, 40*(1), 25-36

Butler Jr, J.J., Zhan, X. (2004). Hydraulic tests in highly permeable aquifers. *Water Resources Research, 40*(12)

Cardenas, M.B., Gooseff, M.N. (2008). Comparison of hyporheic exchange under covered and uncovered channels based on linked surface and groundwater flow simulations. *Water Resources Research, 44*(3)

Cardiff, M., Barrash, W., Kitanidis, P.K. (2013). Hydraulic conductivity imaging from 3-D transient hydraulic tomography at several pumping/observation densities. *Water Resources Research, 49*(11), 7311-7326

Cardiff, M., Barrash, W., Thoma, M., Malama, B. (2011). Information content of slug tests for estimating hydraulic properties in realistic, high-conductivity aquifer scenarios. *Journal of Hydrology, 403*(1-2), 66-82

Cardiff, M., Zhou, Y., Barrash, W., Kitanidis, P.K. (2020). Aquifer imaging with oscillatory hydraulic tomography: Application at the field scale. *Groundwater, 58*(5), 710-722

Castagna, M., Becker, M.W., Bellin, A. (2011). Joint estimation of transmissivity and storativity in a bedrock fracture. *Water Resources Research, 47*(9)

Chen, J., Hubbard, S., Peterson, J., Williams, K., Fienen, M., Jardine, P., Watson, D. (2006). Development of a joint hydrogeophysical inversion approach and application to a contaminated fractured aquifer. *Water Resources Research, 42*(6)

Chesnaux, R., Chapuis, R., Molson, J. (2006). A new method to characterize hydraulic short-circuits in defective borehole seals. *Groundwater, 44*(5), 676-681

Cimolin, F., Discacciati, M. (2013). Navier–Stokes/Forchheimer models for filtration through porous media. *Applied Numerical Mathematics, 72*, 205-224

Clemo, T. (2010). Coupled aquifer-borehole simulation. *Groundwater, 48*(1), 68-78

Coleman, T.I., Parker, B.L., Maldaner, C.H., Mondanos, M.J. (2015). Groundwater flow characterization in a fractured bedrock aquifer using active DTS tests in sealed boreholes. *Journal of Hydrology, 528*, 449-462

Commer, M., Finsterle, S., Hoversten, G.M. (2020). Three-dimensional fracture continuum characterization aided by surface time-domain electromagnetics and hydrogeophysical joint inversion—proof-of-concept. *Computational Geosciences, 24*, 1895-1909

Cooper, H.H., Jr., Bredehoeft, J.D., Papadopulos, I.S., Bennett, R.R. (1965). The response of well-aquifer systems to seismic waves. *Journal of Geophysical Research, 70*(16), 3915-3926

Dai, Y., Zhou, Z., Zhao, Y., Cui, Z. (2015). Evaluation of the effects of the radial constant-head boundary in slug tests. *Hydrogeology Journal, 23*(4), 807-818

Day-Lewis, F.D. (2001). *Using radar tomography, tracer experiments and hydraulic data to characterize fractured rock flow systems*: Stanford University.

Day-Lewis, F.D., Lane, J.W., Gorelick, S.M. (2006). Combined interpretation of radar, hydraulic, and tracer data from a fractured-rock aquifer near Mirror Lake, New Hampshire, USA. *Hydrogeology Journal, 14*(1-2), 1-14

Day-Lewis, F.D., Slater, L.D., Robinson, J., Johnson, C.D., Terry, N., Werkema, D. (2017). An overview of geophysical technologies appropriate for characterization and monitoring at fractured-rock sites. *Journal of environmental management, 204*, 709-720

Díaz-Curiel, J., Biosca, B., Arévalo-Lomas, L., Miguel, M.J., Caparrini, N. (2022). Advances in the hydraulic interpretation of water wells using flowmeter logs. *Hydrology and Earth System Sciences, 26*(10), 2617-2636

Dietrich, P., Helmig, R., Sauter, M., Hötzl, H., Köngeter, J., Teutsch, G. (2005). *Flow and transport in fractured porous media*: Springer.

Dijkstra, E.W. (1959). A note on two problems in connexion with graphs. *Numerische mathematik, 1*(1), 269-271

Doetsch, J., Krietsch, H., Schmelzbach, C., Jalali, M., Gischig, V., Villiger, L., . . . Maurer, H. (2020). Characterizing a decametre-scale granitic reservoir using ground-penetrating radar and seismic methods. *Solid Earth, 11*(4), 1441-1455

Donea, J., Huerta, A., Ponthot, J.-P., Rodriguez-Ferran, A. (2004). Arbitrary Lagrangian-Eulerian Methods, volume 1 of Encyclopedia of Computational Mechanics, chapter 14. *John Wiley & Sons Ltd, 3*, 1-25

Dong, Y.H., Fu, Y.M., Yeh, T.C.J., Wang, Y.L., Zha, Y.Y., Wang, L.H., Hao, Y.H. (2019). Equivalence of Discrete Fracture Network and Porous Media Models by Hydraulic Tomography. *Water Resources Research, 55*(4), 3234-3247, https://dx.doi.org/10.1029/2018wr024290

Dorn, C., Linde, N., Doetsch, J., Le Borgne, T., Bour, O. (2012). Fracture imaging within a granitic rock aquifer using multiple-offset single-hole and cross-hole GPR reflection data. *Journal of Applied Geophysics, 78*, 123-132

Doro, K.O., Cirpka, O.A., Leven, C. (2015). Tracer Tomography: Design Concepts and Field Experiments Using Heat as a Tracer. *Groundwater, 53*(S1), 139-148, https://dx.doi.org/10.1111/gwat.12299

Dougherty, D., Babu, D. (1984). Flow to a partially penetrating well in a double-porosity reservoir. *Water Resources Research, 20*(8), 1116-1122

Duarte, F., Gormaz, R., Natesan, S. (2004). Arbitrary Lagrangian–Eulerian method for Navier–Stokes equations with moving boundaries. *Computer Methods in Applied Mechanics and Engineering, 193*(45-47), 4819-4836

Ellefsen, K.J., Hsieh, P.A., Shapiro, A.M. (2002). Crosswell seismic investigation of hydraulically conductive, fractured bedrock near Mirror Lake, New Hampshire. *Journal of Applied Geophysics, 50*(3), 299-317

Faust, C.R., Mercer, J.W. (1984). Evaluation of slug tests in wells containing a finite-thickness skin. *Water Resources Research, 20*(4), 504-506

Fienen, M.N., Clemo, T., Kitanidis, P.K. (2008). An interactive Bayesian geostatistical inverse protocol for hydraulic tomography. *Water Resources Research, 44*(12)

Fischer, P., Jardani, A., Soueid Ahmed, A., Abbas, M., Wang, X., Jourde, H., Lecoq, N. (2017). Application of large-scale inversion algorithms to hydraulic tomography in an alluvial aquifer. *Groundwater, 55*(2), 208-218

Goraj, R. (2016). Transformation of the Navier-Stokes equation to the Cauchy Momentum equation using a novel

mathematical notation. *Applied Mathematics, 7*(10), 1068-1073

Grasmueck, M. (1996). 3-D ground-penetrating radar applied to fracture imaging in gneiss. *Geophysics, 61*(4), 1050-1064

Hanspal, N.S., Waghode, A.N., Nassehi, V., Wakeman, R.J. (2006). Numerical analysis of coupled Stokes/Darcy flows in industrial filtrations. *Transport in porous media, 64*(1), 73-101, https://dx.doi.org/10.1007/s11242-005-1457-3

Hanspal, N.S., Waghode, A.N., Nassehi, V., Wakeman, R.J. (2009). Development of a predictive mathematical model for coupled stokes/Darcy flows in cross-flow membrane filtration. *Chemical Engineering Journal, 149*(1-3), 132-142, https://dx.doi.org/10.1016/j.cej.2008.10.012

Houben, G.J. (2015). Hydraulics of water wells—flow laws and influence of geometry. *Hydrogeology Journal, 23*(8), 1633-1657

Hu, L.T., Chen, C.X., Chen, X.H. (2011). Simulation of groundwater flow within observation boreholes for confined aquifers. *Journal of Hydrology, 398*(1-2), 101-108, https://dx.doi.org/10.1016/j.jhydrol.2010.12.013

Hu, L.W., Doetsch, J., Brauchler, R., Bayer, P. (2017). Characterizing CO2 plumes in deep saline formations: Comparison and joint evaluation of time-lapse pressure and seismic tomography. *Geophysics, 82*(4), Id1-Id18, https://dx.doi.org/10.1190/Geo2016-0365.1

Hu, R., Brauchler, R., Herold, M., Bayer, P. (2011). Hydraulic tomography analog outcrop study: Combining travel time and steady shape inversion. *Journal of Hydrology, 409*(1-2), 350-362, https://dx.doi.org/10.1016/j.jhydrol.2011.08.031

Hu, R., Liu, Q., Xing, Y. (2018). Case study of heat transfer during artificial ground freezing with groundwater flow. *Water, 10*(10), 1322

Hu, R., Liu, Q., Xing, Y.X. (2018). Case Study of Heat Transfer during Artificial Ground Freezing with Groundwater Flow. *Water, 10*(10), 1322, https://dx.doi.org/10.3390/w10101322

Hyder, Z., Butler Jr, J.J., McElwee, C.D., Liu, W. (1994). Slug tests in partially penetrating wells. *Water Resources Research, 30*(11), 2945-2957

Illman. (2014). Hydraulic tomography offers improved imaging of heterogeneity in fractured rocks. *Groundwater, 52*(5), 659-684

Illman, W.A. (2014). Hydraulic tomography offers improved imaging of heterogeneity in fractured rocks. *Ground Water, 52*(5), 659-684, https://dx.doi.org/10.1111/gwat.12119

Illman, W.A., Berg, S.J., Zhao, Z. (2015). Should hydraulic tomography data be interpreted using geostatistical inverse modeling? A laboratory sandbox investigation. *Water Resources Research, 51*(5), 3219-3237

Illman, W.A., Liu, X., Takeuchi, S., Yeh, T.C.J., Ando, K., Saegusa, H. (2009). Hydraulic tomography in fractured granite: Mizunami Underground Research site, Japan. *Water Resources Research, 45*(1)

Jahr, T., Buntebarth, G., Sauter, M. (2020). Earth tides as revealed by micro-temperature measurements in the subsurface. *Journal of Geodynamics, 136*, 101718, https://dx.doi.org/10.1016/j.jog.2020.101718

Jin, Y., Holzbecher, E., Sauter, M. (2014). A novel modeling approach using arbitrary Lagrangian–Eulerian (ALE) method for the flow simulation in unconfined aquifers. *Computers & Geosciences, 62*, 88-94

Kabala, Z., Pinder, G., Milly, P. (1985). Analysis of well-aquifer response to a slug test. *Water Resources Research, 21*(9), 1433-1436

Karasaki, K., Freifeld, B., Cohen, A., Grossenbacher, K., Cook, P., Vasco, D. (2000). A multidisciplinary fractured rock characterization study at Raymond field site, Raymond, CA. *Journal of Hydrology, 236*(1-2), 17-34, https://dx.doi.org/10.1016/S0022-1694(00)00272-9

Karasaki, K., Long, J., Witherspoon, P. (1988). Analytical models of slug tests. *Water Resources Research, 24*(1),

115-126

Keys, W., Brown, R. (1978). The use of temperature logs to trace the movement of injected water. *Groundwater, 16*(1), 32-48

Kim, N. (2003). Remarks for the axisymmetric Navier–Stokes equations. *Journal of Differential Equations, 187*(2), 226-239

Kipp, K.L., Jr. (1985). Type curve analysis of inertial effects in the response of a well to a slug test. *Water Resources Research, 21*(9), 1397-1408

Kittilä, A., Jalali, M., Evans, K.F., Willmann, M., Saar, M.O., Kong, X.Z. (2019). Field comparison of DNA-labeled nanoparticle and solute tracer transport in a fractured crystalline rock. *Water Resources Research, 55*(8), 6577-6595

Klepikova, M., Brixel, B., Jalali, M. (2020). Transient hydraulic tomography approach to characterize main flowpaths and their connectivity in fractured media. *Advances in water resources, 136*, 103500, https://dx.doi.org/10.1016/j.advwatres.2019.103500

Klepikova, M.V., Le Borgne, T., Bour, O., Gallagher, K., Hochreutener, R., Lavenant, N. (2014). Passive temperature tomography experiments to characterize transmissivity and connectivity of preferential flow paths in fractured media. *Journal of Hydrology, 512*, 549-562, https://dx.doi.org/10.1016/j.jhydrol.2014.03.018

Knudby, C., Carrera, J. (2005). On the relationship between indicators of geostatistical, flow and transport connectivity. *Advances in water resources, 28*(4), 405-421

Koh, E.-H., Lee, E., Lee, K.-K. (2016). Impact of leaky wells on nitrate cross-contamination in a layered aquifer system: Methodology for and demonstration of quantitative assessment and prediction. *Journal of Hydrology, 541*, 1133-1144

Lacombe, S., Sudicky, E., Frape, S., Unger, A. (1995). Influence of leaky boreholes on cross-formational groundwater flow and contaminant transport. *Water Resources Research, 31*(8), 1871-1882

Lang, P.S., Paluszny, A., Nejati, M., Zimmerman, R.W. (2018). Relationship Between the Orientation of Maximum Permeability and Intermediate Principal Stress in Fractured Rocks. *Water Resources Research, 54*(11), 8734-8755, https://dx.doi.org/10.1029/2018wr023189

Le Borgne, T., Bour, O., De Dreuzy, J., Davy, P., Touchard, F. (2004). Equivalent mean flow models for fractured aquifers: Insights from a pumping tests scaling interpretation. *Water Resources Research, 40*(3)

Le Borgne, T., Bour, O., Paillet, F., Caudal, J.-P. (2006). Assessment of preferential flow path connectivity and hydraulic properties at single-borehole and cross-borehole scales in a fractured aquifer. *Journal of Hydrology, 328*(1-2), 347-359

Lee, J., Kokkinaki, A., Kitanidis, P.K. (2018). Fast Large-Scale Joint Inversion for Deep Aquifer Characterization Using Pressure and Heat Tracer Measurements. *Transport in Porous Media, 123*(3), 533-543, https://dx.doi.org/10.1007/s11242-017-0924-y

Leiss, B. (2011). *Neue Untersuchungen zur Geologie der Leinetalgrabenstruktur: Bausteine zur Erkundung des geothermischen Potentials der Region Göttingen*: Universitätsverlag Göttingen.

Lessoff, S.C., Schneidewind, U., Leven, C., Blum, P., Dietrich, P., Dagan, G. (2010). Spatial characterization of the hydraulic conductivity using direct-push injection logging. *Water Resources Research, 46*(12)

Liang, X., Zhan, H., Zhang, Y.K. (2018). Aquifer recharge using a vadose zone infiltration well. *Water Resources Research, 54*(11), 8847-8863

Liu, Q., Hu, L., Bayer, P., Xing, Y., Qiu, P., Ptak, T., Hu, R. (2020). A numerical study of slug tests in a three-dimensional heterogeneous porous aquifer considering well inertial effects. *Water Resources Research, 56*(11), e2020WR027155

Lo, H.-C., Chen, P.-J., Chou, P.-Y., Hsu, S.-M. (2014). The combined use of heat-pulse flowmeter logging and packer testing for transmissive fracture recognition. *Journal of Applied Geophysics, 105*, 248-258

Ma, R., Zheng, C.M. (2010). Effects of Density and Viscosity in Modeling Heat as a Groundwater Tracer. *Ground Water, 48*(3), 380-389, https://dx.doi.org/10.1111/j.1745-6584.2009.00660.x

Maji, R., Sudicky, E. (2008). Influence of mass transfer characteristics for DNAPL source depletion and contaminant flux in a highly characterized glaciofluvial aquifer. *Journal of contaminant hydrology, 102*(1-2), 105-119

Malama, B., Kuhlman, K.L., Barrash, W., Cardiff, M., Thoma, M. (2011). Modeling slug tests in unconfined aquifers taking into account water table kinematics, wellbore skin and inertial effects. *Journal of Hydrology, 408*(1-2), 113-126

Malama, B., Kuhlman, K.L., Brauchler, R., Bayer, P. (2016). Modeling cross-hole slug tests in an unconfined aquifer. *Journal of Hydrology, 540*, 784-796

Maldaner, C.H., Munn, J.D., Coleman, T.I., Molson, J.W., Parker, B.L. (2019). Groundwater flow quantification in fractured rock boreholes using active distributed temperature sensing under natural gradient conditions. *Water Resources Research, 55*(4), 3285-3306

Malvern, L.E. (1969). *Introduction to the Mechanics of a Continuous Medium*. Englewood Cliffs: Prentice-Hall.

Maréchal, J.-C., Dewandel, B., Subrahmanyam, K. (2004). Use of hydraulic tests at different scales to characterize fracture network properties in the weathered-fractured layer of a hard rock aquifer. *Water Resources Research, 40*(11)

Marschall, P., Barczewski, B. (1989). The analysis of slug tests in the frequency domain. *Water Resources Research, 25*(11), 2388-2396

Massiot, C., Townend, J., Nicol, A., McNamara, D.D. (2017). Statistical methods of fracture characterization using acoustic borehole televiewer log interpretation. *Journal of Geophysical Research: Solid Earth, 122*(8), 6836-6852

McElwee, C. (2002). Improving the analysis of slug tests. *Journal of Hydrology, 269*(3-4), 122-133

McElwee, C., Bohling, G., Butler Jr, J. (1995a). Sensitivity analysis of slug tests. Part 1. The slugged well. *Journal of Hydrology, 164*(1-4), 53-67

McElwee, C., Butler, J.J., Jr, Bohling, G., Liu, W. (1995b). Sensitivity analysis of slug tests Part 2. Observation wells. *Journal of Hydrology, 164*(1-4), 69-87

McElwee, C., Zenner, M. (1998). A nonlinear model for analysis of slug-test data. *Water Resources Research, 34*(1), 55-66

Melville, J.G., Molz, F.J., Güven, O., Widdowson, M.A. (1991). Multilevel slug tests with comparisons to tracer data. *Groundwater, 29*(6), 897-907

Michalski, A., Klepp, G.M. (1990). Characterization of transmissive fractures by simple tracing of in-well flow. *Groundwater, 28*(2), 191-198

Moench, A.F. (1984). Double-porosity models for a fissured groundwater reservoir with fracture skin. *Water Resources Research, 20*(7), 831-846

Munn, J.D., Maldaner, C.H., Coleman, T.I., Parker, B.L. (2020). Measuring Fracture Flow Changes in a Bedrock Aquifer Due to Open Hole and Pumped Conditions Using Active Distributed Temperature Sensing. *Water Resources Research, 56*(10), e2020WR027229, https://dx.doi.org/10.1029/2020WR027229

Munoz, G. (2014). Exploring for geothermal resources with electromagnetic methods. *Surveys in geophysics, 35*(1), 101-122

National Research Council. (1996). *Rock Fractures and Fluid Flow: Contemporary Understanding and Applications*. Washington, DC: The National Academies Press.

Oberdorfer, P., Holzbecher, E., Hu, R., Ptak, T., Sauter, M. (2013). *A five spot well cluster for hydraulic and thermal tomography.* Paper presented at the Proceedings, 38th Workshop on Geothermal Reservoir Engineering.

Paradis, D., Gloaguen, E., Lefebvre, R., Giroux, B. (2015). Resolution analysis of tomographic slug test head data: Two-dimensional radial case. *Water Resources Research, 51*(4), 2356-2376

Paradis, D., Gloaguen, E., Lefebvre, R., Giroux, B. (2016). A field proof-of-concept of tomographic slug tests in an anisotropic littoral aquifer. *Journal of Hydrology, 536*, 61-73

Pehme, P.E., Greenhouse, J.P., Parker, B.L. (2007). The active line source temperature logging technique and its application in fractured rock hydrogeology. *Journal of Environmental and Engineering Geophysics, 12*(4), 307-322

Pehme, P.E., Parker, B.L., Cherry, J.A., Greenhouse, J.P. (2010). Improved Resolution of Ambient Flow through Fractured Rock with Temperature Logs. *Ground Water, 48*(2), 191-205, https://dx.doi.org/10.1111/j.1745-6584.2009.00639.x

Piecha, B. (2008). *Untersuchungen zur Wärmeleitfähigkeit des Göttinger Untergrunds im Rahmen der Nutzung oberflächennaher Erdwärme.*

Qiu, P. (2020). *Automated data processing and numerical methods for travel-time based hydraulic tomography.* Georg-August-Universität Göttingen.

Quinn, P., Cherry, J.A., Parker, B.L. (2015). Combined use of straddle packer testing and FLUTe profiling for hydraulic testing in fractured rock boreholes. *Journal of Hydrology, 524*, 439-454

Quinn, P., Klammler, H., Cherry, J., Parker, B. (2018). Insights from unsteady flow analysis of underdamped slug tests in fractured rock. *Water Resources Research, 54*(8), 5825-5840

Ramey, H.J., Agarwal, R.G., Martin, I. (1975). Analysis of"Slug Test"or DST Flow Period Data. *Journal of Canadian Petroleum Technology, 14*(03)

Read, Bour, O., Bense, V., Le Borgne, T., Goderniaux, P., Klepikova, M.V., . . . Boschero, V. (2013). Characterizing groundwater flow and heat transport in fractured rock using fiber-optic distributed temperature sensing. *Geophysical Research Letters, 40*(10), 2055-2059, https://dx.doi.org/10.1002/grl.50397

Read, T., Bour, O., Selker, J., Bense, V., Le Borgne, T., Hochreutener, R., Lavenant, N. (2014). Active-distributed temperature sensing to continuously quantify vertical flow in boreholes. *Water Resources Research, 50*(5), 3706-3713

Ringel, L.M., Jalali, M., Bayer, P. (2021). Stochastic Inversion of Three-Dimensional Discrete Fracture Network Structure With Hydraulic Tomography. *Water Resources Research, 57*(12), e2021WR030401

Ringel, L.M., Somogyvári, M., Jalali, M., Bayer, P. (2019). Comparison of Hydraulic and Tracer Tomography for Discrete Fracture Network Inversion. *Geosciences, 9*(6), 274

Robinson, Slater, L., Johnson, T., Shapiro, A., Tiedeman, C., Ntarlagiannis, D., . . . Imbrigiotta, T. (2016). Imaging pathways in fractured rock using three-dimensional electrical resistivity tomography. *Groundwater, 54*(2), 186-201

Robinson, J., Slater, L., Johnson, T., Shapiro, A., Tiedeman, C., Ntarlagiannis, D., . . . Lane, J. (2016). Imaging Pathways in Fractured Rock Using Three-Dimensional Electrical Resistivity Tomography. *Groundwater, 54*(2), 186-201, https://dx.doi.org/10.1111/gwat.12356

Rücker, C., Günther, T., Wagner, F.M. (2017). pyGIMLi: An open-source library for modelling and inversion in geophysics. *Computers & Geosciences, 109*, 106-123

Sarris, T.S., Close, M., Abraham, P. (2018). Using solute and heat tracers for aquifer characterization in a strongly heterogeneous alluvial aquifer. *Journal of Hydrology, 558*, 55-71, https://dx.doi.org/10.1016/j.jhydrol.2018.01.032

Schmelzbach, C., Horstmeyer, H., Juhlin, C. (2007). Shallow 3D seismic-reflection imaging of fracture zones in crystalline rock. *Geophysics, 72*(6), B149-B160

Schöniger, A., Nowak, W., Hendricks Franssen, H.J. (2012). Parameter estimation by ensemble Kalman filters with transformed data: Approach and application to hydraulic tomography. *Water Resources Research, 48*(4)

Schuster, V. (2015). Untersuchungen zur hydraulischen Durchlässigkeit und kluftbedingter Durchlässigkeitsanisotropie von Bohrkernmaterial aus einem Geothermietestfeld. *Bachelorarbeit, Universität Göttingen*

Schwede, R.L., Li, W., Leven, C., Cirpka, O.A. (2014). Three-dimensional geostatistical inversion of synthetic tomographic pumping and heat-tracer tests in a nested-cell setup. *Advances in water resources, 63*, 77-90, https://dx.doi.org/10.1016/j.advwatres.2013.11.004

Shapiro, A.M., Hsieh, P.A. (1998). How good are estimates of transmissivity from slug tests in fractured rock? *Groundwater, 36*(1), 37-48

Somogyvári, M., Bayer, P. (2017). Field validation of thermal tracer tomography for reconstruction of aquifer heterogeneity. *Water Resources Research, 53*(6), 5070-5084

Somogyvári, M., Bayer, P., Brauchler, R. (2016). Travel-time-based thermal tracer tomography. *Hydrology and Earth System Sciences, 20*(5), 1885-1901

Somogyvári, M., Kühn, M., Reich, S. (2019). Reservoir-scale transdimensional fracture network inversion.

Springer, R., Gelhar, L. (1991). Characterization of large-scale aquifer heterogeneity in glacial outwash by analysis of slug tests with oscillatory response, Cape Cod, Massachusetts. *US Geol. Surv. Water Res. Invest. Rep, 91*, 36-40

Tiedeman, C.R., Barrash, W. (2020). Hydraulic tomography: 3D hydraulic conductivity, fracture network, and connectivity in mudstone. *Groundwater, 58*(2), 238-257

Tsoflias, G.P., Halihan, T., Sharp Jr, J.M. (2001). Monitoring pumping test response in a fractured aquifer using ground-penetrating radar. *Water Resources Research, 37*(5), 1221-1229

Van der Kamp, G. (1976). Determining aquifer transmissivity by means of well response tests: The underdamped case. *Water Resources Research, 12*(1), 71-77

Vasco, D., Keers, H., Karasaki, K. (2000). Estimation of reservoir properties using transient pressure data: An asymptotic approach. *Water Resources Research, 36*(12), 3447-3465

Vasco, D.W. (2018). An Extended Trajectory Mechanics Approach for Calculating the Path of a Pressure Transient: Derivation and Illustration. *Water Resources Research, 54*(4), 2642-2660, https://dx.doi.org/10.1002/2017wr021360

Vasco, D.W., Datta-Gupta, A. (1999). Asymptotic solutions for solute transport: A formalism for tracer tomography. *Water Resources Research, 35*(1), 1-16, https://dx.doi.org/10.1029/98wr02742

Vasco, D.W., Doetsch, J., Brauchler, R. (2019). An extended trajectory-mechanics approach for calculating the path of a pressure transient: travel-time tomography. *Hydrology and Earth System Sciences, 23*(11), 4541-4560

Vollbrecht, A., Tanner, D.C. (2011). Der Leinetalgraben als Teil einer regionalen Pull-Apart-Struktur. *Neue Untersuchungen zur Geologie der Leinetalgrabenstruktur.-Universitätsdrucke, Göttingen*, 9-15

Wagner, V., Li, T., Bayer, P., Leven, C., Dietrich, P., Blum, P. (2014). Thermal tracer testing in a sedimentary aquifer: field experiment (Lauswiesen, Germany) and numerical simulation. *Hydrogeology Journal, 22*(1), 175-187, https://dx.doi.org/10.1007/s10040-013-1059-z

Wang, X., Jourde, H., Aliouache, M., Massonnat, G. (2018). Characterization of horizontal transmissivity anisotropy using cross-hole slug tests. *Journal of Hydrology, 564*, 89-98

Wang, X.G., Jardani, A., Jourde, N. (2017). A hybrid inverse method for hydraulic tomography in fractured and karstic media. *Journal of Hydrology, 551*, 29-46, https://dx.doi.org/10.1016/j.jhydrol.2017.05.051

Werner, H. (2013). *Strukturgeologische Charakterisierung eines Geothermietestfeldes auf der Basis bohrlochgeophysikalischer Messdaten und Bohrkerngefügen auf dem Göttinger Nordcampus.* Universität Göttingen, GZG.

Widdowson, M.A., Molz, F.J., Melville, J.G. (1990). An analysis technique for multilevel and partially penetrating slug test data. *Groundwater, 28*(6), 937-945

Xu, M.H., Liu, Y.Q., Huang, Q.L., Zhang, Y.X., Luan, G.F. (2007). An improved Dijkstra's shortest path algorithm for sparse network. *Applied Mathematics and Computation*, *185*(1), 247-254, https://dx.doi.org/10.1016/j.amc.2006.06.094

Yang, H., Hu, R., Qiu, P., Liu, Q., Xing, Y., Tao, R., Ptak, T. (2020). Application of wavelet de-noising for travel-time based hydraulic tomography. *Water, 12*(6), 1533

Yang, H.C., Hu, R., Qiu, P.X., Liu, Q., Xing, Y.X., Tao, R., Ptak, T. (2020). Application of Wavelet De-Noising for Travel-Time Based Hydraulic Tomography. *Water, 12*(6), 1533, https://dx.doi.org/10.3390/w12061533

Yang, L., Wang, X.S., Jiao, J.J. (2015). Numerical modeling of slug tests with MODFLOW using equivalent well blocks. *Groundwater, 53*(1), 158-163

Zenner, M.A. (2008). Experimental evidence of the applicability of Colebrook and Borda Carnot-type head loss formulas in transient slug test analysis. *Journal of Hydraulic Engineering*, *134*(5), 644-651

Zha, Y., Yeh, T.C.J., Illman, W.A., Zeng, W., Zhang, Y., Sun, F., Shi, L. (2018). A reduced-order successive linear estimator for geostatistical inversion and its application in hydraulic tomography. *Water Resources Research, 54*(3), 1616-1632

Zhao, A.H., Zhang, Z.J., Teng, J.W. (2004). Minimum travel time tree algorithm for seismic ray tracing: improvement in efficiency. *Journal of Geophysics and Engineering*, *1*(4), 245-251, https://dx.doi.org/10.1088/1742-2132/1/4/001

Zhao, H., Luo, N., Illman, W.A. (2021). The importance of fracture geometry and matrix data on transient hydraulic tomography in fractured rocks: Analyses of synthetic and laboratory rock block experiments. *Journal of Hydrology, 601*, 126700

Zhu, J., Yeh, T.-C.J. (2005). Characterization of aquifer heterogeneity using transient hydraulic tomography. *Water Resources Research, 41*(7)

Zlotnik, V.A., McGuire, V.L. (1998). Multi-level slug tests in highly permeable formations: 1. Modification of the Springer-Gelhar (SG) model. *Journal of Hydrology, 204*(1-4), 271-282

Zurbuchen, B.R., Zlotnik, V.A., Butler Jr, J.J. (2002). Dynamic interpretation of slug tests in highly permeable aquifers. *Water Resources Research, 38*(3), 7-1-7-18